SOME PROPERTIES OF THE IONOSPHERE AT LOW RADIO FREQUENCIES

Thesis by

Robert Smith Macmillan

In Partial Fulfillment of the Requirements

for the Degree of

Doctor of Philosophy

California Institute of Technology

Pasadena, California

1954

ACKNOWLEDGMENTS

I wish to express my deepest appreciation to Professor William H. Pickering who directed this research work. I am especially grateful for his many valuable suggestions, encouragement, and continued enthusiastic interest throughout the course of this research.

I should like to express my gratitude and appreciation to all of those who have helped in carrying on this research program:

To Robert C. Serviss and Robert H. Jones for assisting in the construction and operation of the transmitting and receiving equipment; to Arthur S. Hicks for supervising the construction of the transmitting antenna and for attending to the maintenance of the transportation and power generating equipment; and to Oscar Rudnick for permitting us to erect the transmitting antenna on his property.

My appreciation is also extended to the Office of Naval Research for their financial support which enabled us to carry on this study.

Robert S. Macmillan

ABSTRACT

Low-frequency ionospheric polarization, relative virtual height, and relative reflection coefficient measurements were made at near vertical incidence during October 1952. These measurements were made at a frequency of 50 kc/s.

A new, continuous-wave, phase-measuring technique was employed. The essential features of the system are (1) a horizontal transmitting antenna near the surface of the ground which is resonant at the operating frequency and which radiates no ground wave in the direction of the receiver and (2) a receiving station located within line-of-sight of the transmitter at which the phase of the low-frequency sky wave is directly compared with a reference phase transmitted over a very-high-frequency link. The transmitting antenna is considered in detail, and the electronics system is briefly described.

Some of the general features of the earth's atmosphere and the ionosphere are presented. The magneto-ionic theory is developed, and the propagation of electromagnetic waves in an ionized atmosphere is discussed. This material is presented in order that the 50-kc/s ionospheric data may be properly interpreted. The applicability of the quasi-homogeneous, magneto-ionic theory to low-frequency-propagation problems is considered.

The virtual height of the E-layer was found to change

by approximately 7.5 km during the sunrise and sunset periods. Rapid fluctuations in the virtual height and reflection coefficients of the E-layer are attributed to (1) strong magneto-ionic splitting, (2) fluctuating ionization gradients in the lower nighttime E-region, (3) interference effects due to the presence of two or more partially reflecting layers (i. e. the fine structure of the E-layer), and (4) interference effects due to the interaction of the two magneto-ionic components. Not all of the polarization results are consistent with the predictions of the quasi-homogeneous, magneto-ionic theory.

Low-frequency noise measurements were also made during October 1952. The 50-kc/s atmospheric noise field strength reached a maximum value during the middle of the night. The atmospheric noise received in the east-west direction reached a much higher maximum value than that received in the north-south direction.

TABLE OF CONTENTS

I. INTRODUCTION

The ionosphere is necessary for the propagation of medium- and high-frequency radio waves around the curved surface of the earth. Without its presence, long-distance, medium-frequency, and high-frequency radio communication would be impossible. For this reason, the ionosphere has been the subject for a considerable amount of research during the past twenty years. Our state of knowledge regarding the ionosphere is still far from complete. At present, ionospheric research constitutes one of the most important phases of research in the field of radio propagation.

The ionosphere is produced by ultraviolet radiation from the sun which ionizes the constituent gases of the earth's atmosphere (Refs. 1, 2, 3). The ionization begins at a height of about 60 kilometers and extends to the outer limits of the atmosphere. The density of the ionization is not uniform throughout, but there are regions or layers of maximum ionization. These ionized layers are known collectively as the ionosphere. Figure 1 gives the nomenclature and approximate heights of the various ionized layers. In addition to the layers shown, another layer E_2 is sometimes formed, during the daytime, immediately above the E-layer. At night, the D-region disappears, and the F_1- and F_2-layers coalesce to form a single F-region.

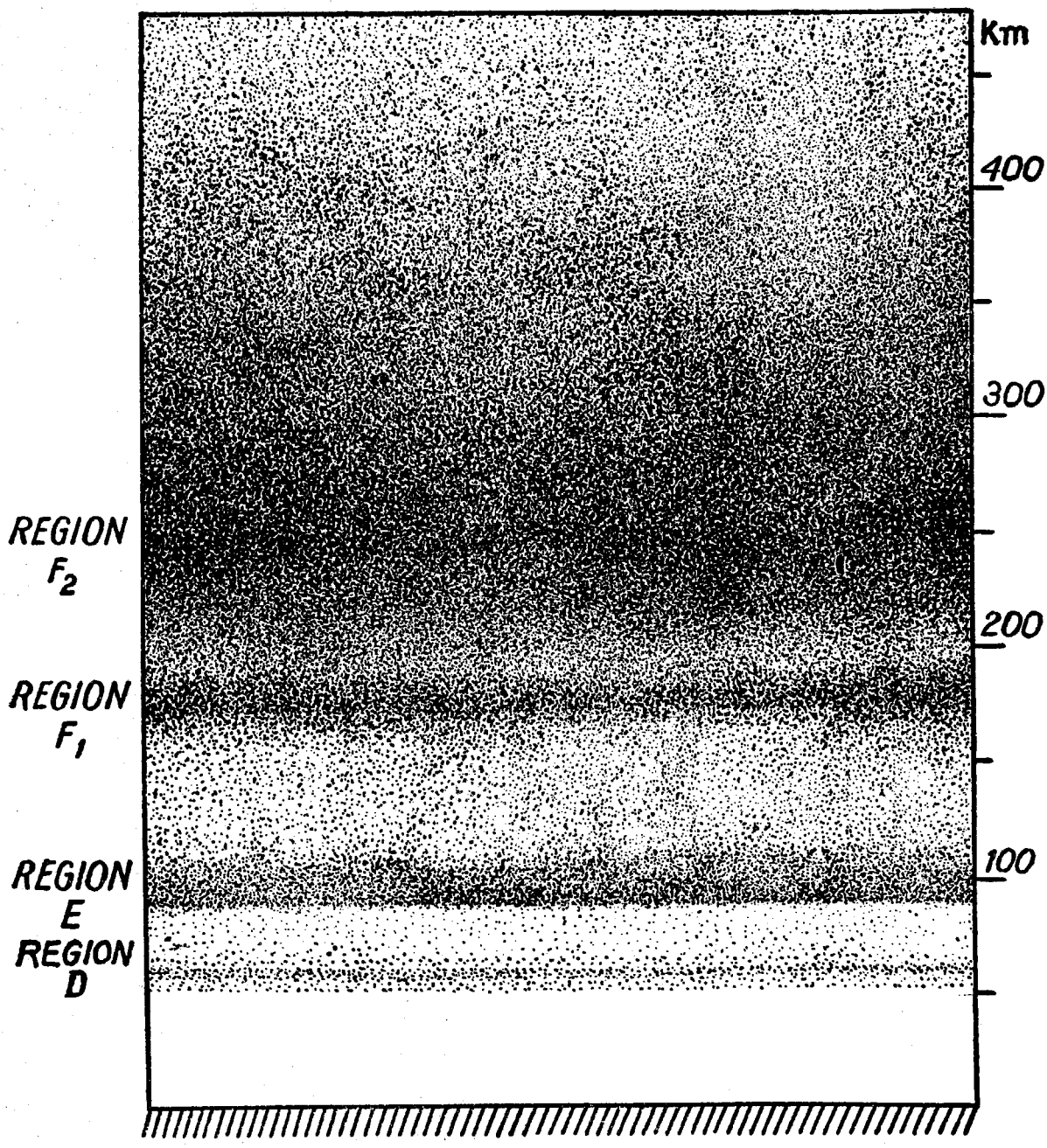

Figure I. Ionized Regions of the Upper Atmosphere
The relative density of ionization is roughly indicated by the depth of shading (after S. K. Mitra).

The characteristics of the ionosphere are different in different geographic locations. Its characteristics change with season and with sunspot cycle. The various factors which are responsible for the changes are not independent in their effects. There are also random fluctuations in the ionosphere which are not yet completely explained. The variations of the ionosphere present a complicated geophysical phenomenon which must be understood in order to make the best use of radio.

A number of radio methods have been developed for exploring the ionospheric regions. However, most of the investigations have been conducted by using radio frequencies in the range of 0.5 to 30 megacycles per second. During the past several years, a few stations have been established for investigating the properties of the ionosphere in the frequency range of 100 to 350 kilocycles per second. There are very few ionospheric data available at frequencies below 100 kc/s. Nearly all the work below 50 kc/s has been done in England, where use was made of the 16-kc/s GBR transmitter at Rugby. At 16 kc/s, the English investigators observed sudden phase anomalies which were strongly correlated with the appearance of solar flares and the fadeout of short radio waves.

During the past few years, there has been increasing interest in the properties of the ionosphere at very-low and low radio frequencies. Data of this type are needed for the design and establishment of low-frequency, high-precision

navigational systems. Data on very-low-frequency propagation are needed by the United States Navy, which is using frequencies in this range to communicate with the fleet and submerged submarines. There are many unsolved problems regarding the constitution, circulation, and ionization processes in the lower regions of the ionosphere. It is expected that very-low-frequency and low-frequency radio measurements will help solve some of these problems.

The aim of the research program being conducted at the California Institute of Technology has been to design a practical, flexible, and inexpensive system for investigating the ionosphere at very-low and low radio frequencies. This research program is being supported by the Office of Naval Research.

Two graduate theses are being presented at this time which describe the work that has been accomplished. One thesis describes the electronics system in detail* and discusses the design considerations. The present thesis is chiefly concerned with an analysis of the data which have been taken. Some of the properties of the earth's atmosphere and the ionosphere are presented. The electronics system is defined and discussed briefly, and some of the general principles of ionospheric radio propagation are considered. All of this material is necessary for the proper interpretation of the data.

---

* Thesis submitted by C. William Bergman in partial fulfillment of the requirements for the degree of Electrical Engineer, California Institute of Technology, 1953.

II. THE EARTH'S ATMOSPHERE

Some of the general physical features of the earth's atmosphere are shown in Figure 2. The atmosphere is generally divided into two regions: the troposphere (or lower atmosphere) and the upper atmosphere. The troposphere extends from sea level to about 15 km above sea level. The height of the troposphere varies between 8 km over polar regions to about 18 km over equatorial regions. The upper atmosphere extends from the top of the troposphere (or tropopause) to the outer limits of the atmosphere.

The troposphere is indirectly heated by the earth's surface, after which convective mixing takes place. Since the major gases of the atmosphere are very transparent to visible and near-infrared radiation, the troposphere is little heated by direct absorption. Instead, the solar radiation reaching the earth heats the ground surface, and the surface radiates energy in the far-infrared region of the spectrum. Water vapor, carbon dioxide, and ozone have strong absorption bands in the far-infrared region. Thus the outgoing radiation from the ground suffers great absorption by these gases. The strong surface heating gives rise to an unstable distribution of density with height. Convective motions are set up which establish a stable temperature lapse rate of approximately $6^{o}C/km$.

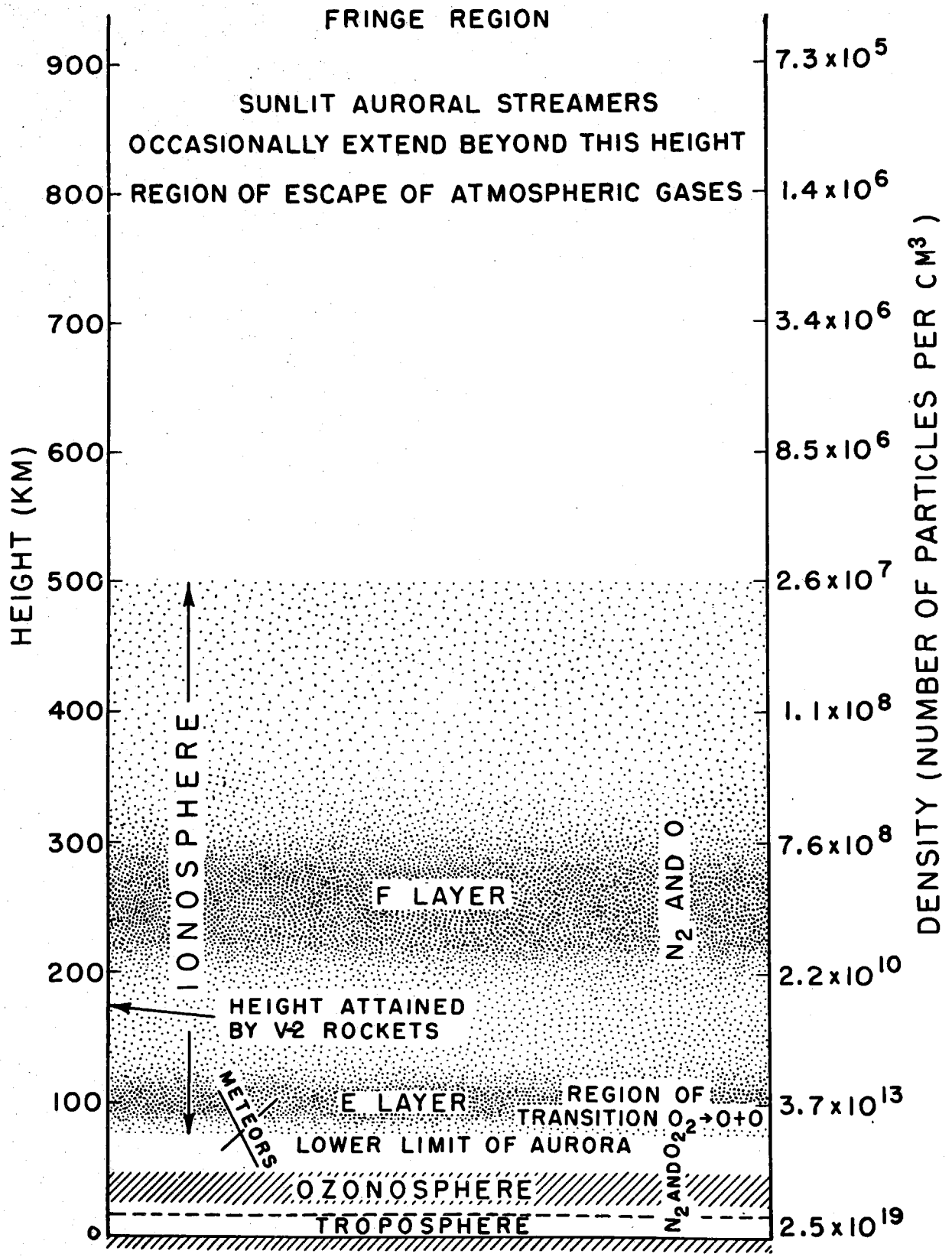

Figure 2. Some of the Physical Features of the Upper Atmosphere (after S. K. Mitra)

Thus the troposphere is approximately in adiabatic or convective equilibrium. Winds keep the gases thoroughly mixed, so that except for water vapor the composition of the atmosphere is the same throughout the troposphere.

In the stratosphere, which is the region of the atmosphere immediately above the troposphere, the temperature is controlled by radiation processes. The temperature of the stratosphere remains nearly constant with a diurnal variation of less than $1^{\circ}C$.

The temperature of the atmosphere as a function of height is shown in Figure 3. The rocket data are from the flight on 7 March 1947 at White Sands Proving Ground, New Mexico. The sounding data were obtained within an hour of the rocket flight. For comparison, temperature distributions as deduced from abnormal-sound-propagation experiments and from meteoric data are also given.

The constituent gases of the upper atmosphere are subject to solar heating, photo-dissociation, allotropic modification, photo-excitation, and ionization. The solar radiation responsible for these effects is the entire ultraviolet region of wavelength less than 3,000 Angstrom units. The temperature rise in the middle atmospheric region (30 to 50 km) is due to the absorption of ultraviolet radiation by ozone. In the region from 60 to 80 km, there is no strong absorption of solar radiation. Thus there is observed a falling of temperature. Above 80 km, there are absorptions

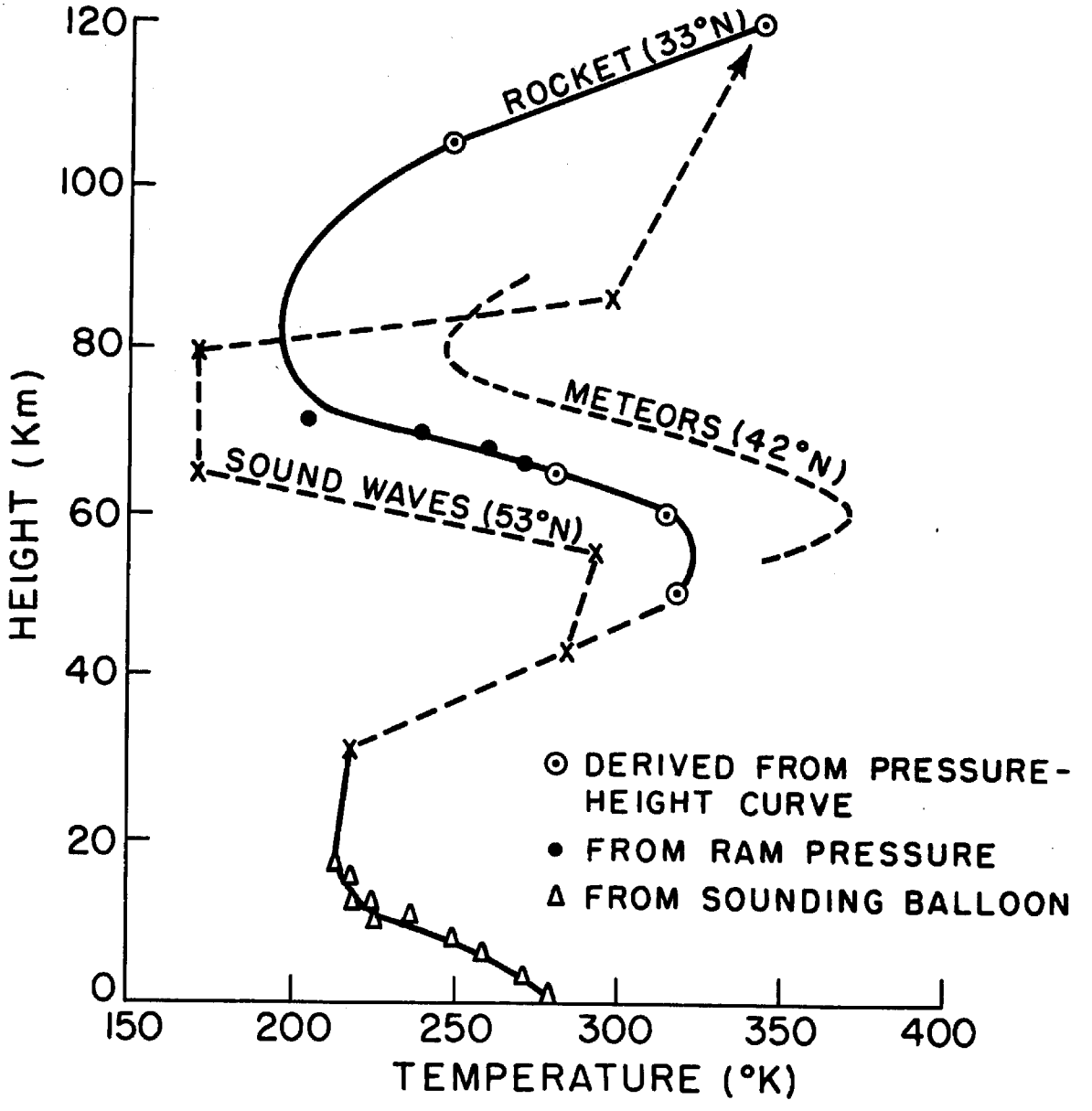

Figure 3. Temperature of the Atmosphere as a Function of Height (after S. K. Mitra and Sheppard)

leading to the ionization of the atmospheric gases and to the dissociation of molecular oxygen into atomic oxygen.

Experiments made with samples of air collected by V-2 rockets have shown that the composition of the atmosphere remains practically the same up to a height of 70 km. Above 80 km, the composition changes because of the dissociation of molecular oxygen into atomic oxygen. The region of 80 to 135 km is a transition region from an atmosphere consisting of N_2 and O_2 to one of N_2 and O. The spectra of auroral streamers extending up to 1,000 km demonstrate the existence of N_2 and O in the high regions of the atmosphere.

The upper atmosphere is subject to winds due partly to temperature gradients and partly to tidal effects. Air movements have been deduced from meteor trails and observations of sounding balloons, smoke shells, and noctilucent clouds. Tentative curves for the variation of wind speed with height are shown in Figure 4 (Refs. 2, 4). The motions of the lower regions of the ionosphere (D- and E-regions) form worldwide current systems. The magnetic field of these current systems probably produces the quiet-day variations of the terrestrial magnetic field.

As was mentioned in the introduction, the atmosphere from 60 km upward is more or less ionized by solar ultraviolet radiation. The density of the ionization is not uniform throughout, but there are layers of maximum ionization. It is easy to understand the mechanism of layer formation in a qualitative sort of way. Consider an atmosphere

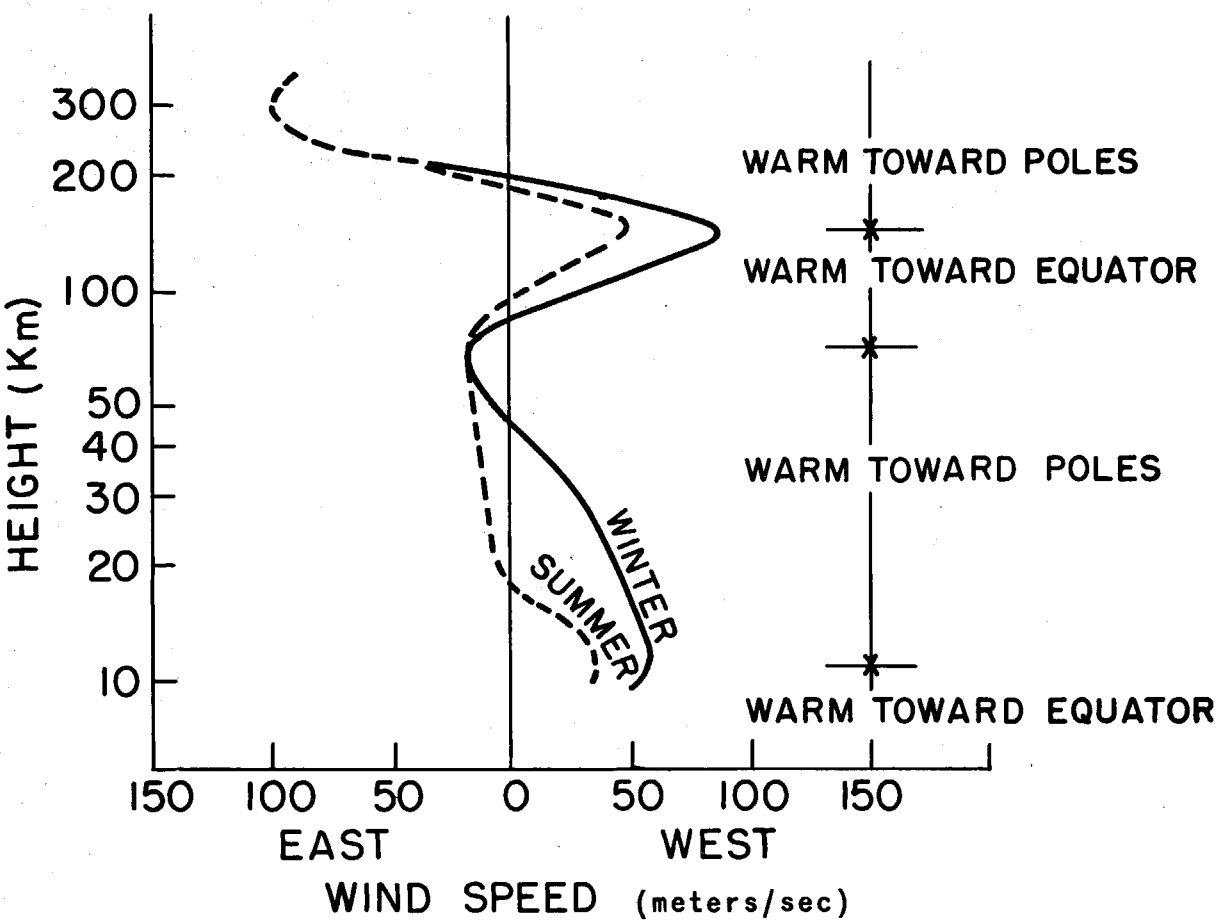

Figure 4. Probable Variation of the Wind Speed (East and West Components) with Height in Middle Latitudes (after S. K. Mitra and Sheppard)

of a single gaseous element whose density decreases exponentially upward. If a beam of monochromatic radiation enters the atmosphere from above and is absorbed in producing ionization, the rate of ion production will be a maximum at a certain level. This situation results because the rate of ion production at any height is controlled by the intensity of the incident radiation and the density of the absorbing gas. As the radiation passes through the atmosphere from above, the intensity decreases, and the density of the gas increases. These two factors combine to produce a level of maximum ionization, the height of which is determined by the coefficient of absorption of the gas for the particular radiation and by the rate of decrease of density upward.

According to some of the most recent theories regarding the origin of the ionospheric regions, the F_1- and F_2-layers result from the ionization of N_2 and atomic oxygen, the E-layer results from the ionization of molecular oxygen, and the D-layer most probably results from the ionization of molecular oxygen and possibly sodium and nitric oxide (NO).

In Section III, some of the properties of the ionospheric layers are considered. We are concerned only with the lower regions of the ionosphere in the low-frequency radio experiments; thus most emphasis is placed on the description of the D- and E-layers.

III. THE IONOSPHERE

A. The Propagation of Electromagnetic Waves in an Ionized Gas

Before the general physical properties of the ionospheric layers are presented, some basic principles of electromagnetic-wave propagation in an ionized gas are discussed.

The magneto-ionic theory has been developed to describe the propagation of electromagnetic waves in an ionized medium in the presence of a static magnetic field. This theory, together with optical-ray theory, has been very useful in describing the ionospheric propagation and reflection of high-frequency radio waves (Refs. 1, 5). At low and very-low frequencies, the application of any optical-ray theory to describe ionospheric propagation or reflection is open to some question (Ref. 6).

The derivation of the magneto-ionic equations has been given in a number of papers during the last twenty years. However, the basic physical assumptions underlying the theory are seldom given. These assumptions are important in the interpretation and application of the theory. For this reason, a brief outline of the derivation, together with the basic physical assumptions involved in the derivation, are presented here.

The magneto-ionic theory is based upon the electron theory of Lorentz and his dispersion theory. In Maxwell's theory, the properties of material bodies in electromagnetic

fields are described by the capacitivity ϵ, the conductivity σ, and the magnetic permeability μ. These quantities are found to be dependent on the physical condition of the medium (its temperature, etc.) and the frequency of the electromagnetic fields. Lorentz developed his electron theory in an effort to show how ϵ and σ depend on the structure and physical condition of the material body. The dispersion theory accounts for the variation of the capacitivity with frequency of the electromagnetic fields.

In the electron theory, it is assumed that the material body consists of a large number of charged particles separated from one another by free space. The material is assumed to be electrically neutral, there being equal numbers of positively and negatively charged particles. In the present discussion, it is assumed that there are no elastic forces between the particles. In the magneto-ionic theory, it is assumed that only electrons, because of their greater mobility, take part in the electromagnetic actions. These electrons are free to move throughout the medium at random without experiencing any restoring forces. At sufficiently low frequencies, magneto-hydrodynamic waves can occur because of the motion of ions in the earth's magnetic field. (It may be that magneto-hydrodynamic waves are responsible for the audio-frequency tweeks, whistlers, and rumbles that are received on long-wire antennae.)

In the Lorentz theory, the average values of all quantities are used. Thus, for example, the electric field is

defined as

$$\bar{E} = \frac{1}{v}\int_{v} E\, dv \tag{1}$$

where v is a physically small volume. That is, v is small in comparison with the wavelength and the size of the body, but it contains a large number of particles. This definition is necessary since E varies greatly as we pass from one particle through the free space between particles to another particle.

In any medium, the Maxwell displacement current is the sum of the free-space displacement current

$$\epsilon_v \frac{\partial \vec{E}}{\partial t} \tag{2}$$

and the displacement current due to the dielectric

$$\epsilon' \frac{\partial \vec{E}}{\partial t} \tag{3}$$

Thus the displacement current in the medium is

$$\left(\epsilon_v + \epsilon'\right) \frac{\partial \vec{E}}{\partial t} = \epsilon \frac{\partial \vec{E}}{\partial t} = \frac{\partial \vec{D}}{\partial t} \tag{4}$$

In the electron theory, the free-space displacement current is assumed to exist not only in the free space between particles but also within the particles themselves. The action of the material medium is introduced through the motion of the charged particles. If N is the number of particles of charge e and velocity u per cubic meter, the instantaneous value of the average convection current density may be written

$$\text{Neu} = \rho u \tag{5}$$

By using the mean values of all quantities, Maxwell's equations may be written

$$\nabla \times \vec{H} = \vec{i} + \epsilon \frac{\partial \vec{E}}{\partial t} = \rho \vec{u} + \epsilon_v \frac{\partial \vec{E}}{\partial t} \tag{6}$$

$$\nabla \times \vec{E} = -\mu_v \frac{\partial \vec{H}}{\partial t} \tag{7}$$

$$\nabla \cdot \vec{H} = 0 \tag{8}$$

$$\nabla \cdot \vec{E} = \frac{1}{\epsilon_v} \rho \tag{9}$$

In order to derive the magneto-ionic equations, let us choose a coordinate system with x in the direction of propagation. The static magnetic field may be separated into two components, H_L in the direction of propagation and H_T normal to the direction of propagation. No generality is lost by taking H_T in the z direction. The coordinate system is shown in Figure 5.

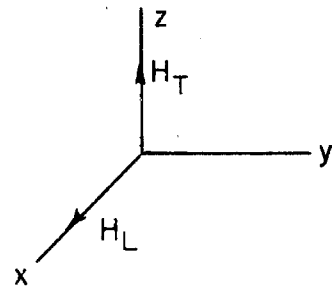

Figure 5.
Coordinate System for the
Magneto-Ionic Equations

For plane waves propagating in the x direction, the partial derivatives with respect to y and z are zero. Maxwell's equations may now be written in component form

$$0 = -\mu_v \frac{\partial H_x}{\partial t} \tag{10}$$

$$-\frac{\partial E_z}{\partial x} = -\mu_v \frac{\partial H_y}{\partial t} \tag{11}$$

$$\frac{\partial E_y}{\partial x} = -\mu_v \frac{\partial H_z}{\partial t} \tag{12}$$

$$0 = \epsilon_v \frac{\partial E_x}{\partial t} + \rho u_x \tag{13}$$

$$-\frac{\partial H_z}{\partial x} = \epsilon_v \frac{\partial E_y}{\partial t} + \rho u_y \tag{14}$$

$$\frac{\partial H_y}{\partial x} = \epsilon_v \frac{\partial E_z}{\partial t} + \rho u_z \tag{15}$$

We notice that there is no forward component of the magnetic field of the wave. In general, a forward component of the electric field exists because of the forward component in the motion of the electrons. For this reason, it is best to describe the polarization of the wave in terms of the magnetic-field components. Four wave equations may be easily derived from Equations 14, 12, 11, and 15

$$\left(\frac{\partial^2}{\partial x^2} - \frac{1}{c^2}\frac{\partial^2}{\partial t^2}\right) E_z = -\mu_v Ne \frac{\partial^2 z}{\partial t^2} \tag{16}$$

$$\left(\frac{\partial^2}{\partial x^2} - \frac{1}{c^2}\frac{\partial^2}{\partial t^2}\right) E_y = -\mu_v Ne \frac{\partial^2 y}{\partial t^2} \tag{17}$$

$$\left(\frac{\partial^2}{\partial x^2} - \frac{1}{c^2}\frac{\partial^2}{\partial t^2}\right) H_z = Ne \frac{\partial^2 y}{\partial x \partial t} \tag{18}$$

$$\left(\frac{\partial^2}{\partial x^2} - \frac{1}{c^2}\frac{\partial^2}{\partial t^2}\right) H_y = -Ne \frac{\partial^2 z}{\partial x \partial t} \tag{19}$$

Let us assume that the field components and displacements are represented by expressions containing the factor $e^{(j\omega t - \Gamma x)}$. These solutions are valid when $\frac{d\Gamma}{dx}$ is very small and can be neglected. This approximation is equivalent to assuming the variation of the propagation constant to be so gradual that the medium may be considered as homo-

geneous throughout a distance of a few wavelengths. Equations 16 through 19 become

$$\left(\Gamma^2 + \frac{\omega^2}{c^2}\right) E_z = \mu_v \omega^2 Nez \tag{20}$$

$$\left(\Gamma^2 + \frac{\omega^2}{c^2}\right) E_y = \mu_v \omega^2 Ney \tag{21}$$

$$\left(\Gamma^2 + \frac{\omega^2}{c^2}\right) H_z = -j\omega Ney\, \Gamma \tag{22}$$

$$\left(\Gamma^2 + \frac{\omega^2}{c^2}\right) H_y = j\omega Nez\, \Gamma \tag{23}$$

From Equation 13, we obtain the expression

$$E_x = \frac{Ne}{\epsilon_v} x \tag{24}$$

All of the equations have been written for a negative charge; i.e., $\rho = -Ne$. From Equations 20 through 23, we see that

$$\frac{H_y}{H_z} = -\frac{E_z}{E_y} \tag{25a}$$

or

$$\vec{H} \cdot \vec{E} = 0 \tag{25b}$$

Thus the electric and magnetic vectors in the wave front are normal.

In order to solve Equations 20 through 24 for the propagation constant Γ, the relations between the components

of current, electric field, earth's magnetic field, and ionization must be found. Let us write the equations of motion of an electron in the magnetic field, subject to a periodically changing electromagnetic field and to a resistance due to collisions with molecules. The coordinate system is shown in Figure 5. The force due to radiation pressure is small. Thus the effect of the time-varying magnetic field of the electro-magnetic field is neglected. It is assumed that the movement of positive and negative charges in opposite directions does not produce a net polarization in the region. The equations of motion are

$$m\frac{d^2x}{dt^2} = -eE_x - g\frac{dx}{dt} - e\mu_v H_T \frac{dy}{dt} \tag{26}$$

$$m\frac{d^2y}{dt^2} = -eE_y - g\frac{dy}{dt} + e\mu_v H_T \frac{dx}{dt} - e\mu_v H_L \frac{dz}{dt} \tag{27}$$

$$m\frac{d^2z}{dt^2} = -eE_z - g\frac{dz}{dt} + e\mu_v H_L \frac{dy}{dt} \tag{28}$$

where g is a damping factor which arises from the collision of the electron with ions and with neutral gas atoms and molecules. Chapman (Ref. 7) has shown that g is equal to $m\nu$, where ν is the electronic collisional frequency. By assuming sinusoidal solutions, Equations 26 through 28 may be written in the form, respectively

$$E_x = \left(\frac{\omega^2 m}{e} - j\frac{\omega m\nu}{e}\right)x - j\omega\mu_v H_T y \tag{29a}$$

$$E_y = \left(\frac{\omega^2 m}{e} - j\,\frac{\omega m \upsilon}{e}\right) y + j\omega\mu_v H_T x - j\omega\mu_v H_L z \tag{30a}$$

$$E_z = \left(\frac{\omega^2 m}{e} - j\,\frac{\omega m \upsilon}{e}\right) z + j\omega\mu_v H_L y \tag{31a}$$

In order to simplify Equations 29a through 31a, let

$$\gamma_T = \frac{\omega\mu_v \epsilon_v H_T}{Ne} \tag{32}$$

$$\gamma_L = \frac{\omega\mu_v \epsilon_v H_L}{Ne} \tag{33}$$

$$p = -\frac{\omega^2 m \epsilon_v}{Ne^2} \tag{34}$$

$$q = \frac{\omega m \upsilon \epsilon_v}{Ne^2} \tag{35}$$

Equations 29a through 31a become, respectively,

$$E_x = -\frac{Ne}{\epsilon_v}(p+jq)x - j\gamma_T \frac{Ney}{\epsilon_v} \tag{29b}$$

$$E_y = -\frac{Ne}{\epsilon_v}(p+jq)y + j\gamma_T \frac{Nex}{\epsilon_v} - j\gamma_L \frac{Nez}{\epsilon_v} \tag{30b}$$

$$E_z = -\frac{Ne}{\epsilon_v}(p+jq)z + j\gamma_L \frac{Ney}{\epsilon_v} \tag{31b}$$

Equations 20, 21, 24, 29b, 30b, and 31b may be easily solved for the propagation constant

$$\frac{c^2\Gamma^2}{\omega^2} = -1 - \left[(p+jq) - \frac{\gamma_T^2}{2(1+p+jq)} \pm \sqrt{\frac{\gamma_T^4}{4(1+p+jq)^2} + \gamma_L^2}\right]^{-1} \tag{36}$$

The polarization of the wave may be defined as

$$R = \frac{H_z}{H_y} = \frac{j}{\gamma_L}\left[\left(\frac{c^2\Gamma^2}{\omega^2} + 1\right)^{-1} + (p+jq)\right] \tag{37}$$

$$R = \frac{j}{\gamma_L}\left[\frac{\gamma_T^2}{2(1+p+jq)} \pm \sqrt{\frac{\gamma_T^4}{4(1+p+jq)^2} + \gamma_L^2}\right] \tag{38}$$

Equation 36 was first derived by Appleton (Ref. 8) and independently by Hartree. It is known as the Appleton-Hartree equation. An inspection of Equation 36 shows that the propagation constant may assume two values. Thus the interaction of the electrons with the earth's magnetic field causes a wave incident on the ionosphere to be split into two components of different phase velocity, polarization, and absorption. One of these components is called the ordinary ray, whereas the other is called the extraordinary ray. Equations 36 and 38 are discussed in more detail later in this thesis.

B. The D-Layer of the Ionosphere

The derivation of the magneto-ionic equations has served to introduce the parameters which are necessary for describing the various ionospheric layers. Let us now consider the D-layer.

The D-layer is present during the daytime and extends from a height of about 60 to 90 km where it merges with the E-layer. At these heights, recombination of the ions takes place rapidly; thus the D-layer disappears during the night.

The D-layer is probably formed by the ionization of O_2 at its first ionization potential (12.2 electron volts). This process, first suggested by Mitra, Bahr, and Ghosh (Ref. 9), is now widely accepted. However, there is experimental and theoretical evidence that other ionization processes also take place. Nicolet (Ref. 10) has suggested that there are three elements which are important in the formation of the D-region:

(a) A normal layer formed by the ionization of O_2 at its first ionization potential.

(b) A more or less sporadic layer produced by the ionization of sodium.

(c) A layer produced by the ionization of NO by radiation at λ = 1,300 Angstrom units. This process is probably important during periods of intense ionization when the fadeout of medium- and high-frequency radio waves is observed.

It is probable that the ionization processes described in items (a) and (b) normally occur.

Very little information is available regarding the ionization distribution with height. Budden, Ratcliffe, and Wilkes (Ref. 11) have performed a number of propagation experiments at 16 kc/s. They have estimated the density of

electrons at the reflection level to be between 2 x $10^2/cm^3$ and 2.5 x $10^2/cm^3$. The reflection height at 16 kc/s was found to vary between 70 and 80 km. At 16 kc/s, the reflection coefficient is about 0.1, whereas at 100 kc/s, the reflection coefficient is less than 0.001. It is likely that the electron density increases monotonically with height and trails off into the E-layer without showing any well-defined maximum.

A. P. Mitra (Ref. 12) has made a theoretical study of the structure of the layer. He calculated the densities of electrons and ions at various heights by assuming that the D-layer is produced by ionization of O_2 at the first ionization potential. His calculations indicate that the electron density increases continuously with height, making it difficult to separate the D-layer from the E-layer. However, the ion density which he calculated has a maximum value at nearly the same height as that at which the rate of ion production is a maximum.

C. The E- and F-Regions of the Ionosphere

The E- and F-regions are the two main regions of maximum ionization in the ionosphere. They are located at average heights of 100 and 275 km, respectively. A considerable number of the experimental and theoretical data describing the properties of these regions is available (Ref. 1).

The E-layer extends from a height of about 90 to 110 km. It is probably formed by the ionization of excited or pre-

ionized O_2 molecules (Ref. 13). Radio measurements indicate that the maximum E-layer ionization is located at about 100 km. The maximum electron density is approximately 1.5 x $10^5/cm^3$ at noon and 1 x $10^4/cm^3$ at midnight.

In addition to the E-layer, a subsidiary E_2-layer sometimes appears during the daytime. The maximum ionization of the E_2-layer is located at approximately 140 km. An abnormality of the E-region is known as sporadic E, which exists at heights of 90 to 120 km. It is caused in part by meteor ionization.

During the daytime, the F-region splits into two layers, F_1 and F_2. These two layers are located at heights of approximately 200 and 300 km, respectively. The F_2-layer is absent at night. According to one rather widely accepted hypothesis, the F_2-layer is produced by ionization of atomic oxygen, and the F_1-layer is produced by ionization of N_2.

In order to apply the magneto-ionic equations, it is necessary to know the values of the electronic collisional frequencies. Collisional frequencies have been calculated by George (Ref. 14). His calculations are based on the most recent estimates of temperature and pressure in the upper atmosphere. The collisional frequencies for the E-region are given in Table I.

Table I. Electronic Collisional Frequencies

Daytime		Nighttime	
Height (km)	Frequency (collisions/sec)	Height (km)	Frequency (collisions/sec)
80	1.08×10^7	80	7.00×10^6
90	3.58×10^6	90	1.56×10^6
100	1.38×10^6	100	3.60×10^5
120	2.74×10^5	120	1.99×10^4
140	6.72×10^4	140	1.16×10^3

IV. THE LOW-FREQUENCY IONOSPHERIC STATION

A complete low-frequency ionospheric sounding station has been constructed and successfully operated. The station is located in the Mojave Desert of California. The transmitting site is 10 miles southwest of Randsburg, California, and the receiving site is 15 miles northwest of Victorville, Calif. The distance between the sites is approximately 64 km. This location for the station was chosen because the characteristics of the ground are very favorable, and the noise level is relatively low.

The objective of the research project has been to design a practical, flexible, and inexpensive system for obtaining low-frequency and very-low-frequency sky-wave amplitude, sky-wave polarization, and virtual-height data as a continuous function of time. A continuous-wave technique was chosen as being most satisfactory at very-low frequencies. The essen-

tial features of the system are (1) a horizontal transmitting antenna near the surface of the ground which is resonant at the operating frequency and which radiates no ground wave in the direction of the receiver and (2) a receiving station located within line-of-sight of the transmitter at which the phase of the low-frequency sky wave is directly compared with a reference phase transmitted over a very-high-frequency link. The system employs a low-power transmitter and a highly selective receiver. Amplitude, polarization, and virtual-height data are recorded on Esterline-Angus recorders.

A. The Principles of Operation of the System

The principles of operation of the system are illustrated in Figures 6 and 7. The transmitting antenna is a horizontal, resonant dipole placed near the surface of the earth. The properties of this antenna are such that no ground wave is propagated in the direction normal to the antenna. The receiving site is located in this direction, off the side of the transmitting antenna. A very-high-frequency, line-of-sight link is established between the transmitting and receiving stations. In principle, the very-high-frequency signal is modulated by the low-frequency transmitter, and a phase comparison is made between the low-frequency sky wave and the modulation of the very-high-frequency signal.

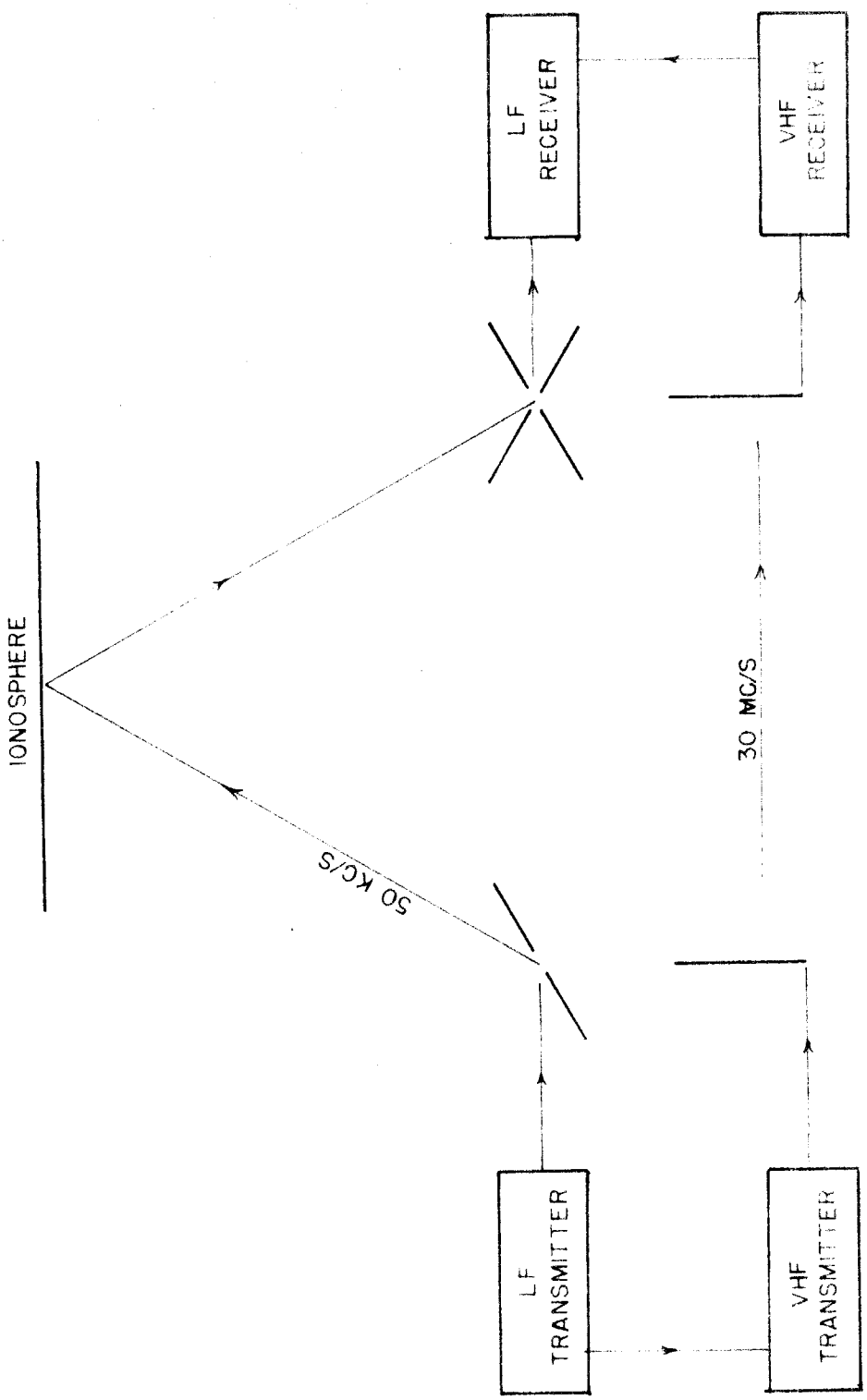

FIGURE 6. BLOCK DIAGRAM OF 50-KC/S IONOSPHERIC STATION

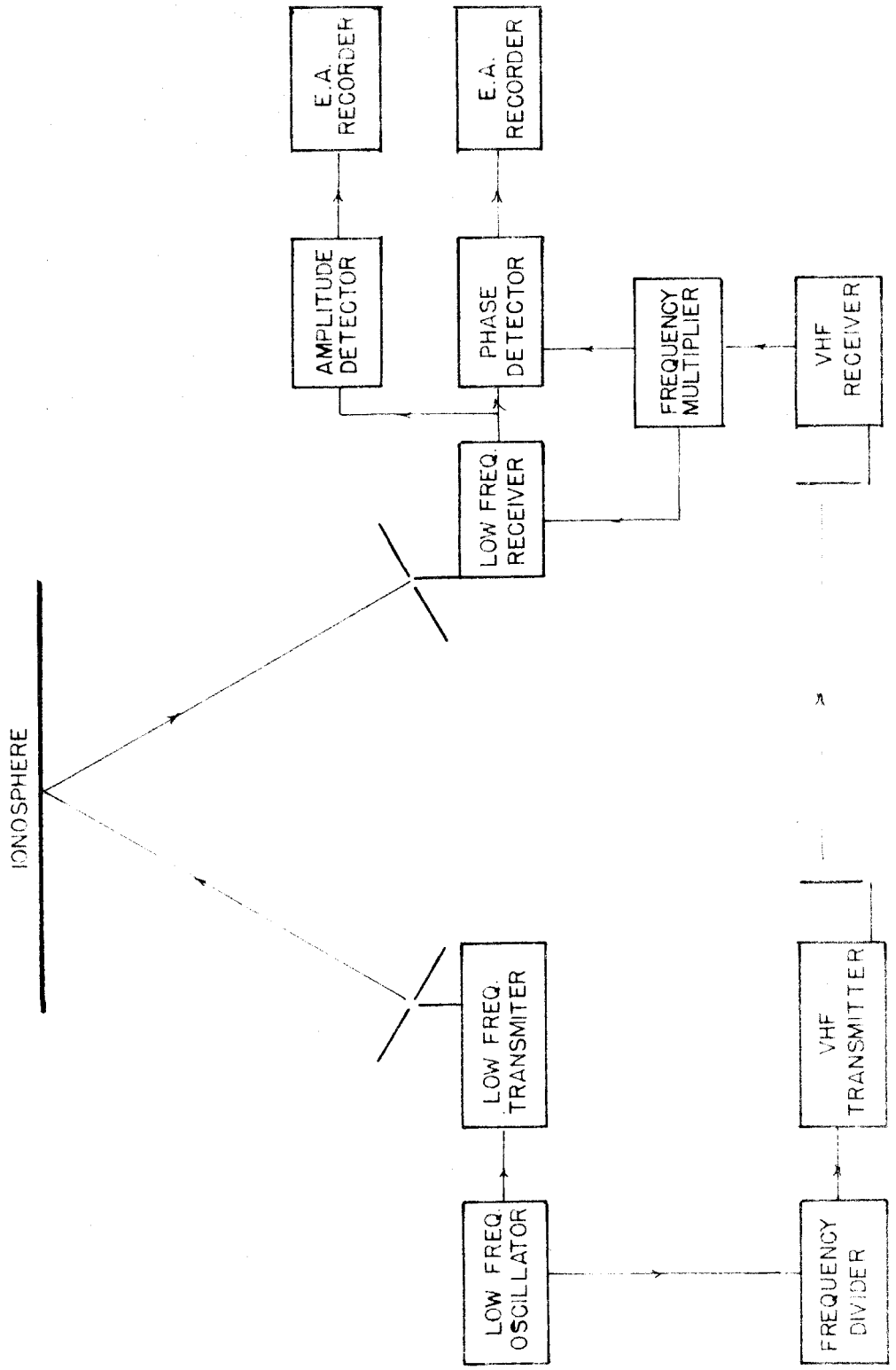

FIGURE 7. BLOCK DIAGRAM OF THE TRANSMITTING AND RECEIVING SYSTEM

B. The Transmitting Antenna

The transmitting antenna consists of a wire 26,000 feet long supported about 11 feet above the ground. The antenna may be sectioned by switches which are located every 1,000 feet along the antenna. The antenna is tuned to the proper frequency by opening the appropriate switches. The antenna can be operated as a resonant dipole in the frequency range of 18 to 250 kc/s.

The field pattern in the plane normal to the length of the antenna is obtained by considering the direct and reflected waves radiated by the antenna. The two waves are added in order to obtain the total radiation field of the antenna. The magnitude and phase of the reflected wave are determined by the characteristics of the ground. When the reflected wave is added to the direct wave, a pattern such as that shown in Figure 8 is obtained.

The field strength above the antenna is a maximum when the ground conductivity and relative capacitivity are low. For this reason, a site for the transmitting antenna was chosen in the Mojave Desert, which is an arid region. The transmitting antenna is located on a long, high, granite ridge. The ridge is about 10 miles long and several miles wide. The cracks in the granite are dry to a depth probably in excess of 1,200 feet.

In addition to the pattern shown in Figure 8, the antenna excites a ground wave whose pattern is shown in

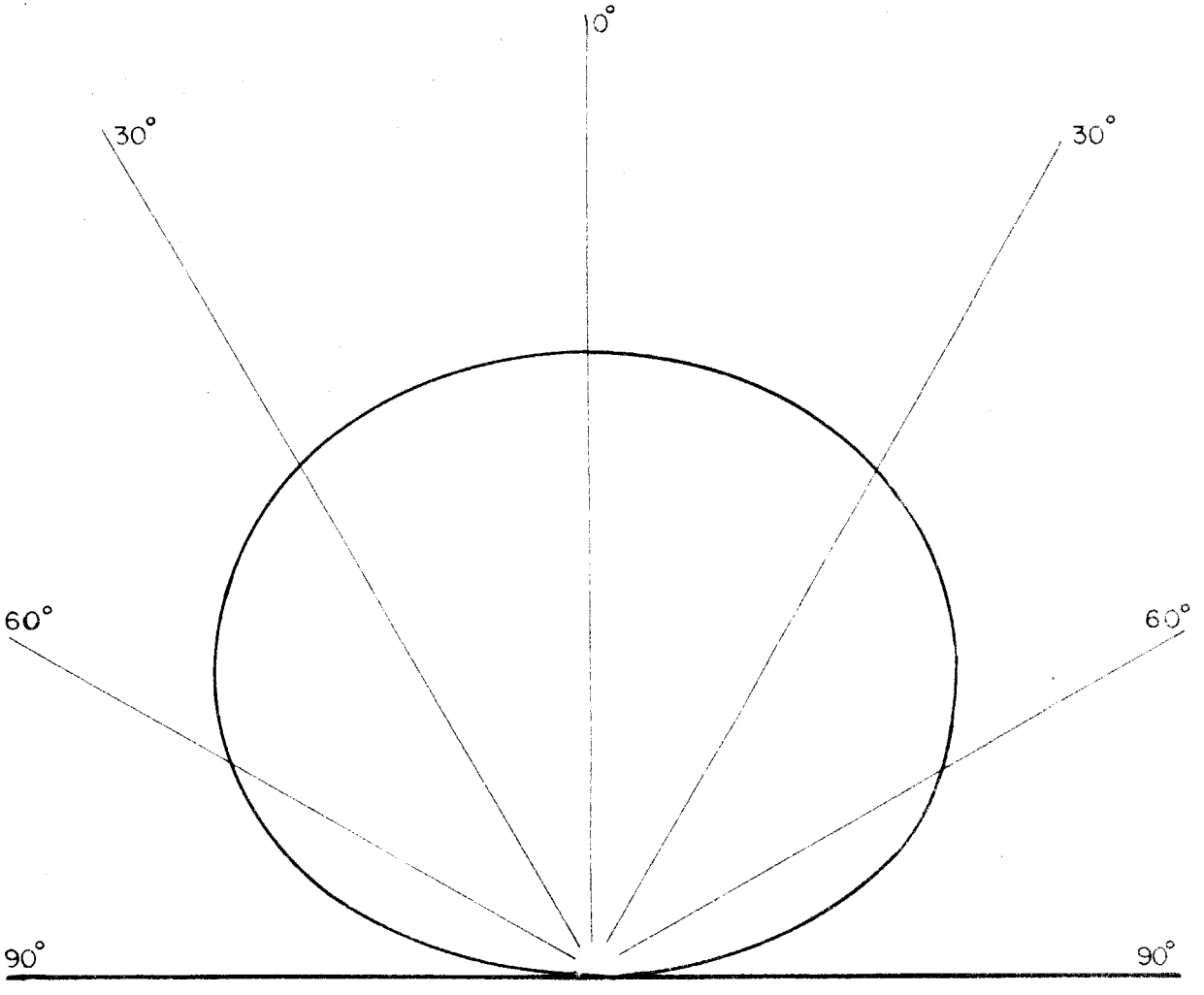

FIGURE 8. FIELD PATTERN IN THE PLANE NORMAL TO THE LENGTH OF THE DIPOLE

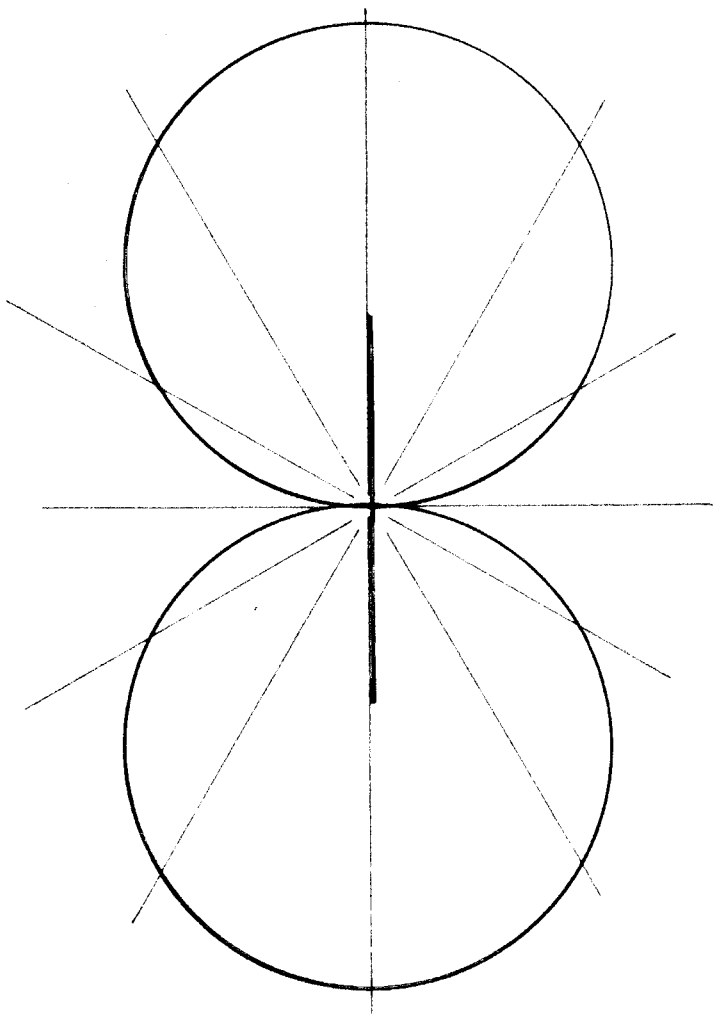

FIGURE 9. GROUND WAVE PATTERN OF A HORIZONTAL DIPOLE OVER THE EARTH

Figure 9. It is important to note that there is no ground wave in the direction normal to the length of the antenna. As with the field strength above the antenna, the ground-wave intensity is determined by the ground constants.

The system has been operated at a frequency of 50 kc/s. At 50 kc/s, the resonant length of the antenna is 8,600 feet. In order to match the 100-ohm output impedance of the transmitter, the antenna was fed at a point 1,700 feet from the center. The center-fed antenna has an input impedance of 65 ohms, resistive. The measured quality factor Q of the antenna is 12.

A detailed analysis of the transmitting antenna is given in Section V.

C. The Transmitting-Receiving System

The transmitting and receiving antennae are oriented as shown in Figure 10. The bearing of the transmitter from the receiver is 347°, whereas the magnetic north pole has a bearing of 16°. The altitude of both sites is about 3,500 feet, and they are within line-of-sight of each other.

The transmitter feeding the low-frequency antenna is a supersonic generator capable of delivering 800 watts in the frequency range of 14 to 70 kc/s. Since there is no ground wave in the direction of the receiver, the field strength as measured is due entirely to the wave reflected from the ionosphere. Although there is the distinct advantage in not

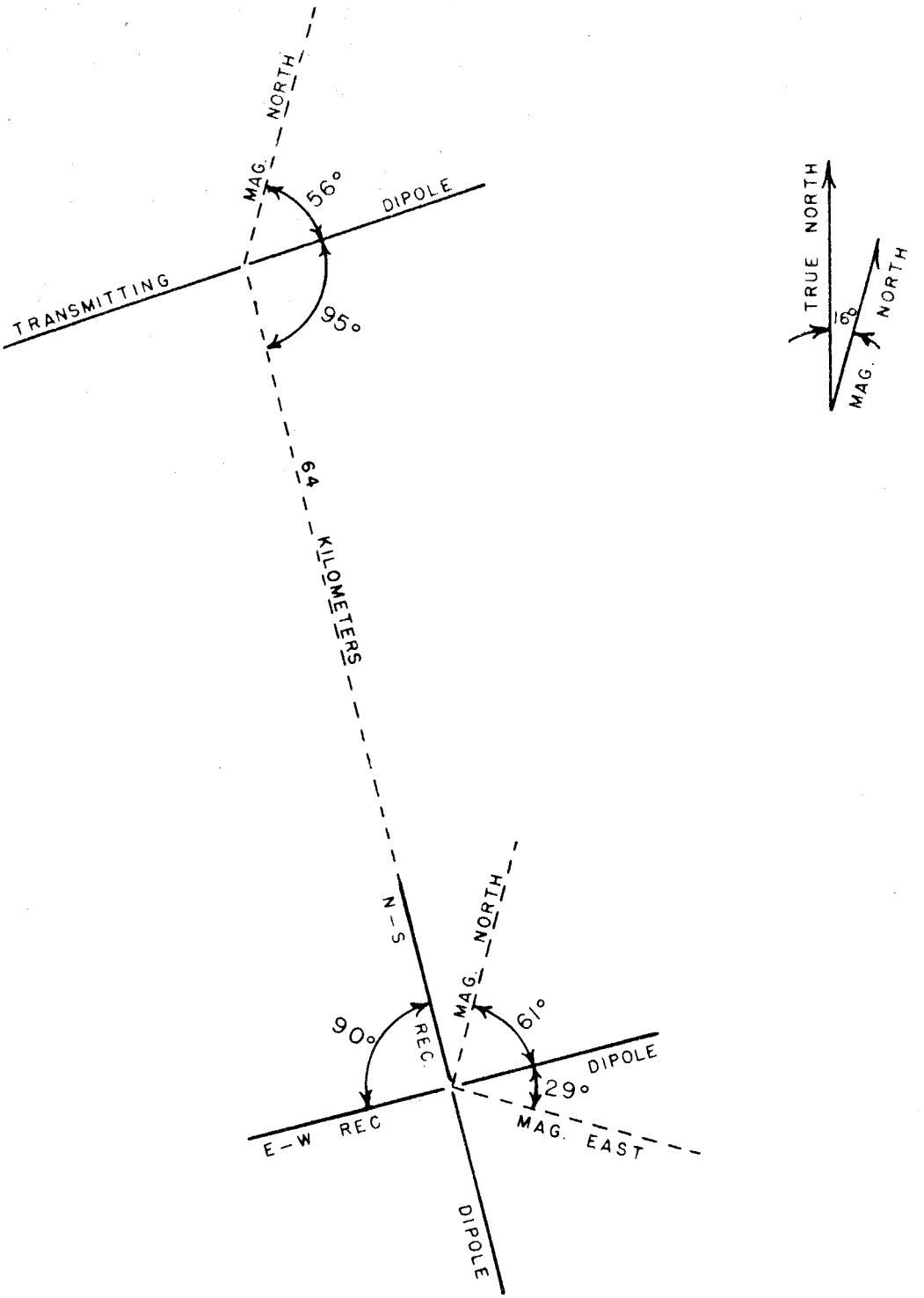

Figure 10. Geometry of the Transmitting and Receiving Antennae

having to separate the ground wave from the received signal, the fact that there is no ground wave means that some other method must be used to obtain a reference signal for the phase measurements. This reference is supplied by use of a 50-watt, very-high-frequency transmitter which is in line-of-sight of the receiver.

A crystal oscillator provides a stable frequency source for the low-frequency transmitter. It is also the reference for the modulation of the very-high-frequency transmitter. Since the modulating frequency is limited to less than 3,000 cycles per second because of the design of the equipment, the 50-kc/s oscillator output is divided by 31. A 1,612-c/s signal is sent to the receiving site as the reference signal. The division is accomplished by the use of a scaling circuit employing the proper feedback between stages in order to realize the factor of 31.

The 50-kc/s receiving antennae consist of crossed dipoles 100 feet in length. By switching the receiver from one antenna to the other, it is possible to determine the polarization of the received wave. The receiving dipoles have essentially the same pattern as the transmitting antenna but have a high impedance. A 50-kc/s pre-amplifier is used to convert the double-ended signal from the antennae into a single-ended signal for use in the receiver. The receiver is a double-conversion superheterodyne using the twenty-fifth and the seventh harmonics of the 1,612-c/s reference signal as local oscillator frequencies. These frequencies were

chosen so that the second intermediate frequency would be exactly 1,612 c/s. The received signal is thus reduced in frequency to equal that of the reference signal. A direct comparison of phase is possible by means of a phase meter.

Atmospheric noise was one of the main considerations in the design of the entire system. The 1,612-c/s intermediate frequency made a very narrow bandwidth of 30 c/s easy to realize. The over-all system required the bandwidth to be of this order of magnitude, since the phase meter would not function properly for signal-to-noise ratios which were too low. The noise bandwidth at the output of the phase meter is also 30 c/s; for recording purposes, additional filtering to limit the bandwidth of the system to 1 c/s is employed. For a reasonable signal-to-noise ratio, the resolution of the phase-measuring system is equivalent to a change of 0.05 km in virtual height. This resolution is much superior to that of the conventional pulse techniques.

The amplitude of the reflected wave is recorded by using a Navy AN/URM-6 field-strength meter. The bandwidth of this receiver at 50 kc/s is 350 c/s. The recorded output is the resultant of signal plus noise. By automatically turning the low-frequency transmitter off for 45 seconds of each 5-minute interval, a record of the atmospheric noise level is obtained.

In the Appendix, circuit diagrams for the electronic equipment are given. Figures 11 through 13 are photographs showing the transmitting and receiving equipment.

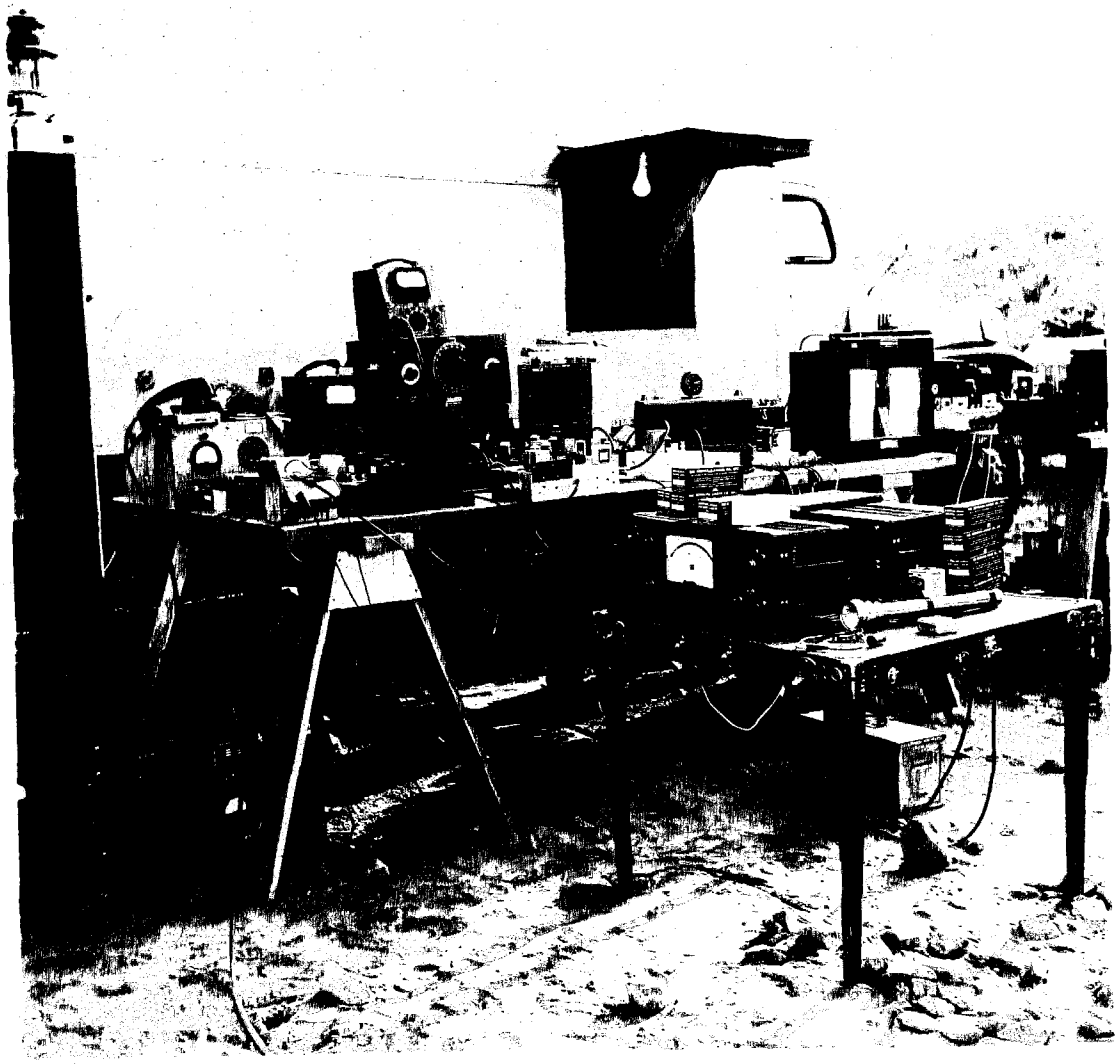

Figure 11. The Receiving Equipment

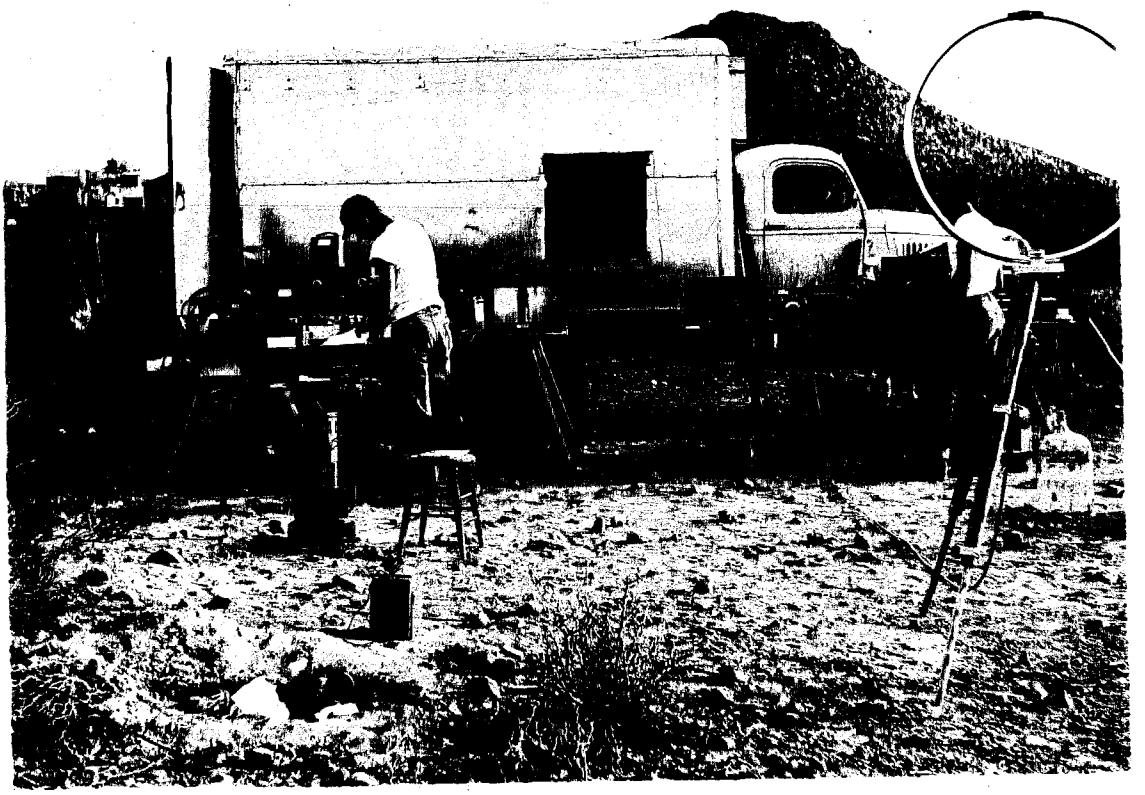

Figure 12. The Receiving Equipment

Figure 13. The Transmitting Station

In Section V, a detailed analysis of the transmitting antenna is given.

V. THE LOW-FREQUENCY TRANSMITTING ANTENNA*

In order to investigate the D- and E-regions of the ionosphere, it was necessary to design a transmitting antenna for use in the frequency range of 14 to 75 kc/s. Conventional antenna systems were found to be undesirable because of the excessive cost, which amounts to one million dollars, on the average, for each 10 per cent of efficiency achieved. The cost of low-frequency antenna systems is high because they usually require tall towers, extensive ground systems, and either high-voltage tuning capacitors or large tuning coils. Tuning coils or tuning capacitors can be eliminated by using a resonant antenna such as a half-wave linear dipole, and it was with the idea of using a resonant antenna that an investigation of ground antennae was started. A ground antenna is, in this case, a half-wave linear dipole (or resonant loop) a full wavelength in circumference, placed directly on the ground or a very small fraction of a wavelength above the ground. A half-wave linear dipole at 14 kc/s would be 10.7 km (35,000 feet) long. The greater part of the material in this section deals directly with the dipole antenna; however, the theory is readily extended to the loop

* This section was written jointly by the author and C. Wm. Bergman. It was jointly written because the authors intend to submit this material to one of the technical journals for publication.

antenna.

A. Sommerfeld's Integral Equations

In order to determine whether or not it is practical to use such a ground antenna, we refer to the work of Sommerfeld (Refs. 15, 16), who treated the problem of a horizontal Hertz dipole (Ref. 17) over an arbitrary plane earth. Sommerfeld has derived rigorous integral equations for the Hertz vector of such a dipole antenna. For completeness, his derivation is briefly outlined here.

The Hertz vector $\vec{\Pi}$ for the Hertz dipole of Figure 14, which is located at (0,0,h), is

$$\vec{\Pi} = \vec{i}\,\Pi_x = \frac{\vec{i}\, I\ell e^{j(kR-\omega t)}}{4\pi\omega\epsilon R} \tag{39}$$

where k is the wave number $\sqrt{\omega^2\mu\epsilon - j\sigma\mu\omega}$ of the medium of capacitivity ϵ, magnetic permeability μ, and conductivity σ; j is the usual imaginary notation, and

$$R^2 = x^2 + y^2 + (z-h)^2 = r^2 + (z-h)^2$$

The electric current in the dipole is $i = I \cos \omega t$ amperes. The Hertz vector satisfies the wave equation

$$\nabla^2\vec{\Pi} = \mu\epsilon \frac{\partial^2\vec{\Pi}}{\partial t^2} + \mu\sigma \frac{\partial \Pi}{\partial t} \tag{40a}$$

as do the electromagnetic-field components. First of all, the time dependence can be removed, and the wave equation becomes

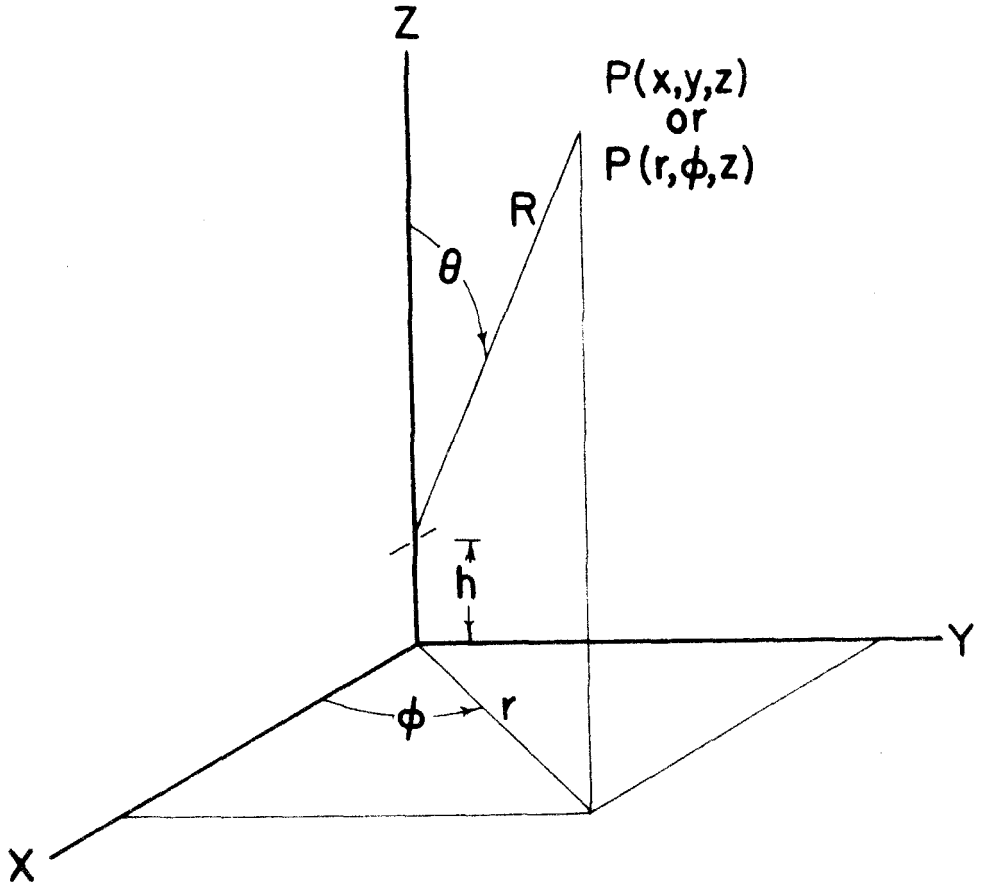

Figure 14.
Hertz dipole in free space

$$\nabla^2\vec{\Pi} = -(\omega^2\epsilon\mu + j\sigma\mu\omega)\vec{\Pi} = -k^2\vec{\Pi} \tag{40b}$$

If the dipole is oriented in the x direction, the Hertz vector, at any point in space, has an x component only. In the plane z = 0, the magnitude of the Hertz vector is a function of r only.

The electric and magnetic intensity vectors $\vec{E}$ and $\vec{H}$ of the radiation field can be obtained from $\vec{\Pi}$ as follows:

$$\vec{E} = k^2\vec{\Pi} + \nabla(\nabla\cdot\vec{\Pi}) \tag{41}$$

$$\vec{H} = \frac{k^2}{j\omega\mu}\nabla \times \vec{\Pi} \tag{42}$$

Equations 41 and 42 may be derived from Maxwell's equations.

The horizontal dipole above an arbitrary plane earth, at z = 0, may be represented by the total Hertz vector $\vec{\Pi}_1$: $\vec{\Pi}_1$ is made up of a primary excitation $\vec{\Pi}_{prim}$ due to the dipole only and a secondary excitation $\vec{\Pi}_{sec}$ due to the perturbation effect of the plane earth. The Hertz vector in the earth $\vec{\Pi}_2$ is completely determined by the boundary conditions imposed upon $\vec{\Pi}$ by $\vec{E}$ and $\vec{H}$. These boundary conditions for the two components of $\vec{\Pi}$ (Π_x and Π_z) are

$$\Pi_{x_1} = n^2\Pi_{x_2} \tag{43}$$

$$\frac{\partial\Pi_{x_1}}{\partial z} = n^2\frac{\partial\Pi_{x_2}}{\partial z} \tag{44}$$

$$\Pi_{z_1} = n^2 \Pi_{z_2} \tag{45}$$

$$\frac{\partial \Pi_{z_1}}{\partial z} - \frac{\partial \Pi_{z_2}}{\partial z} = \frac{\partial \Pi_{x_2}}{\partial x} - \frac{\partial \Pi_{x_1}}{\partial x} \tag{46}$$

where $n^2 = k_2^2/k_1^2$. The constants for the earth are ϵ_2, μ_2, σ_2; and the constants for air are $\epsilon_1 = \epsilon_v$, $\mu_1 = \mu_v$, $\sigma_1 = 0$.

In order to apply these boundary conditions, Equation 39 must be put in the form of a superposition of eigenfunctions. By making use of the Fourier-Bessel integral theorem, Equation 39 may be written in cylindrical coordinates as follows:

$$\vec{\Pi} = \vec{\Pi}_{prim} = \frac{\vec{i}\, I\ell}{4\pi\omega\epsilon_v} \frac{e^{jkR}}{R}$$

$$= \frac{\vec{i}\, I\ell}{4\pi\omega\epsilon_v} \int_0^\infty J_0(\lambda r) e^{-a(z-h)} \frac{\lambda d\lambda}{a} \tag{47}$$

where λ, the eigenvalue of the eigenfunction, has a continuous spectrum $0 \le \lambda \le \infty$ and $a_n = \sqrt{\lambda^2 - k_n^2}$.

Sommerfeld's integral equations for Π_1 and Π_2 may now be written for the horizontal dipole at a height h above an arbitrary earth (Figure 15).

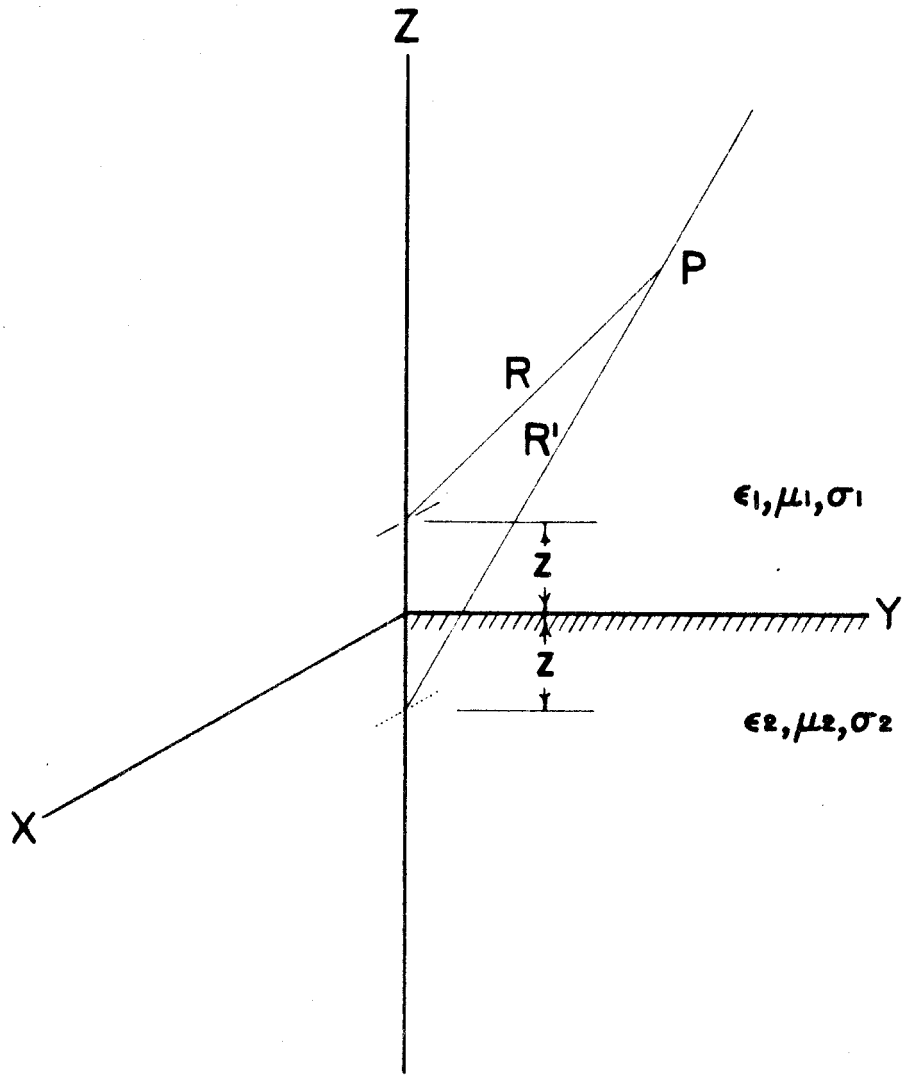

Figure 15.

Hertz dipole over a plane earth

$$\Pi_{x_1} = \frac{I\ell}{4\pi\omega\epsilon_1}\int_0^\infty J_0(\lambda r)\frac{\lambda}{a_1}\left[e^{-a_1(z-h)} - e^{-a_1(z+h)}\left(1-\frac{2a_1}{a_1+a_2}\right)\right]d\lambda$$

$$= \frac{I\ell}{4\pi\omega\epsilon_1}\left[\frac{e^{jk_1R}}{R} - \frac{e^{jk_1R'}}{R'} + 2\int_0^\infty J_0(\lambda r)e^{-a_1(z+h)}\frac{\lambda d\lambda}{a_1+a_2}\right] \tag{48}$$

$$\Pi_{x_2} = \frac{I\ell}{4\pi\omega\epsilon_1}\frac{2}{n^2}\int_0^\infty J_0(\lambda r)e^{a_2z-a_1h}\frac{\lambda d\lambda}{a_1+a_2} \tag{49}$$

$$\Pi_{z_1} = \frac{I\ell}{4\pi\omega\epsilon_1}\frac{2\cos\phi}{k_1^2}\frac{\partial}{\partial r}\int_0^\infty J_0(\lambda r)e^{-a_1(z+h)}\frac{a_1-a_2}{n^2a_1+a_2}\lambda d\lambda$$

(50)

$$= \frac{-I\ell}{4\pi\omega\epsilon_1}\frac{2\cos\phi}{k_1^2}\int_0^\infty J_1(\lambda r)e^{-a_1(z+h)}\frac{a_1-a_2}{n^2a_1+a_2}\lambda^2 d\lambda$$

$$\Pi_{z_2} = \frac{I\ell}{4\pi\omega\epsilon_1}\frac{2\cos\phi}{k_2^2}\frac{\partial}{\partial r}\int_0^\infty J_0(\lambda r)e^{a_2z-a_1h}\frac{a_1-a_2}{n^2a_1+a_2}\lambda d\lambda$$

$$= \frac{-I\ell}{4\pi\omega\epsilon_1}\frac{2\cos\phi}{k_2^2}\int_0^\infty J_1(\lambda r)e^{a_2z-a_1h}\frac{a_1-a_2}{n^2a_1+a_2}\lambda^2 d\lambda \tag{51}$$

where $R^2 = x^2 + y^2 + (z-h)^2$ and $R'^2 = x^2 + y^2 + (z+h)^2$.

It is believed that Equations 48 through 51 are valid for the radiation field; however, the techniques that various people have used on these equations in order to find Poynting's vector or the electric and magnetic field strengths invariably involve approximations which are not valid for all values of k_2. It can be seen that the evaluation of these integrals involves integration of an equation having

a Riemann surface of four sheets with branch points at $\lambda = k_1$ and $\lambda = k_2$. Care must be taken that the path of integration lies in the proper sheet. Equations 50 and 51 have an additional complexity of a pole at $\lambda = p$, where $1/p^2 = (1/k_1^2) + (1/k_2^2)$ because of the fact that $n^2 a_1 + a_2$ is zero for $\lambda = p$. The significance which Sommerfeld places upon the solution obtained by integration around this pole is discussed in Section V-D.

The appearance of a component of the Hertz vector in the z direction is worth noting, because the primary excitation had no such component. The Π_z values of Equations 50 and 51 are brought about by the perturbation effect of the plane earth, and we see from Equation 41 that a vertically polarized wave results. This wave has a maximum value in the $\pm$ x direction and a zero value in the $\pm$ y direction. This property will be extremely important in the consideration of the antenna as an instrument for ionospheric research.

In Equation 48, we can see that the solution for Π_x is the sum of the solutions of two dipoles, one at $z = h$ and another at $z = -h$, plus the expression

$$\frac{I\ell}{4\pi\omega\epsilon_1}\left[2\int_0^\infty J_0(\lambda r)e^{-a_1(z+h)}\frac{\lambda d\lambda}{a_1+a_2}\right]$$

We know from physical reasoning that for $k_2 = k_1$ this term must be equal to

$$\frac{I\ell}{4\pi\omega\epsilon_1}\frac{e^{jk_1R'}}{R'}$$

and that for $k_2 = \infty$ the term must equal zero. Furthermore, for finite current I and with $k_2 = \infty$, Π_{x_2}, Π_{z_1}, and Π_{z_2} must also be zero. In addition, Π_{z_1} and Π_{z_2} are, of course, zero for $k_2 = k_1$.

B. Ground Losses

It is interesting to note that the determination of power output from Equations 48 through 51 is not unduly complicated. We shall not go through the development, which is available in References 15 and 16, but shall merely write the expression for radiation resistance

$$R_{rad} = \frac{k_1^2 \ell^2}{4\pi} \sqrt{\frac{\mu_v}{\epsilon_v}} \left(\frac{2}{3} - \frac{\sin \zeta}{\zeta} + \frac{\sin \zeta - \zeta \cos \zeta}{\zeta^3} + L \right) \tag{52}$$

where

$$L = \frac{1}{k_1^3} \mathcal{R}e \left[j \int_0^\infty e^{-2a_1 h} \frac{2a_1 a_2 - \lambda^2}{n^2 a_1 + a_2} \lambda \, d\lambda \right] \tag{53}$$

and $\zeta = 2 k_1 h$. Thus R_{rad} is a function of the height h above the ground. L vanishes for $k_2 = \infty$. This special case is plotted in Figure 16. The scale is changed so that the resistance of the antenna for infinite height is 70 ohms. If one wishes to evaluate L for finite values of k_2, again approximations must be made which will not be valid in general. The solution assumes an infinitesimal source, and at this source the fields must, of necessity, be infinite. Thus it seems plausible that, if h is allowed to approach zero, and if σ_2 is not zero, the radiation resistance R_{rad} goes toward an infinite value. It follows that an infinite

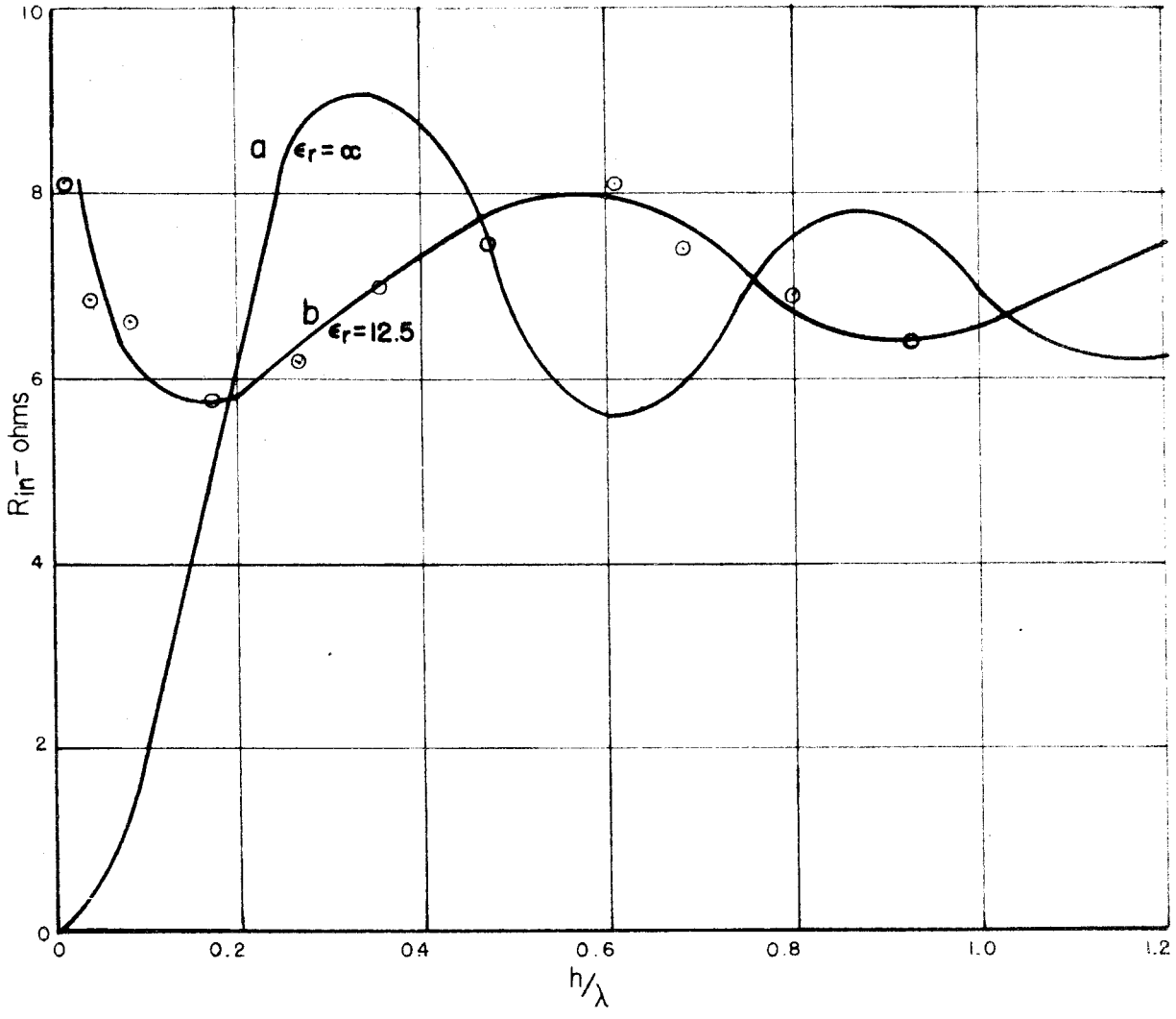

Figure 16.

Input resistance of a half wave dipole above a plane earth. a) Calculated for $\epsilon_r = \infty$ b) Experimental for $\epsilon_r = 12.5$

field causes infinite loss for a finite current in the antenna. This physical reasoning agrees with the result which Sommerfeld obtained on evaluating L for a partially conductive earth. It is important to note that, although the total resistance is infinite, this fact is due entirely to absorption in the ground, and only a finite amount of the loss is radiated into the air for a finite driving current. Therefore the efficiency of the dipole would be zero.

If we consider an actual antenna, we find that because of the finite dimensions of a physical antenna infinite fields do not exist. The fields are high enough, however, to cause considerable losses if the antenna is actually laid on the ground. We are able to reduce the losses to a reasonable value by raising the antenna several feet above the ground. At low frequencies, it is apparent that the actual height above the ground is the determining factor for reducing losses, not the ratio h/λ .

C. The Reflection Method

For an ionospheric-research antenna, one would be most interested in the field-strength pattern in two planes (the x-z plane and the y-z plane) for all angles of θ (Figure 15), for in these two planes the wave incident on the ionosphere is polarized either in the plane of incidence or normal to the plane of incidence. We can obtain this field pattern by developing a reflection method whose validity has been checked by experiment. In this method, we assume that

the fields radiated directly from the antenna are related to the current flowing in the antenna and are independent of the presence of the earth. In order to find the field at a point P (Figure 17) due to a dipole an arbitrary distance h above the plane earth, the wave leaving the antenna at an angle θ is added to the reflected wave which left the antenna at an angle $180^\circ - \theta$. For this condition to be valid, ℓ_3/d must be much less than 1. A complex dielectric constant introduces a change in the phase of the reflected wave. However, this change need not be considered here, and the earth is assumed to be a perfect dielectric.

The reflection coefficient for an electromagnetic wave polarized perpendicular to the plane of incidence is

$$\rho_{\perp} = \frac{\cos\theta_1 - \sqrt{n^2 - \sin^2\theta_1}}{\cos\theta_1 + \sqrt{n^2 - \sin^2\theta_1}} = \frac{E_3}{E_1} \tag{54}$$

and for the wave polarized in the plane of incidence, it is

$$\rho_{\parallel} = \frac{\epsilon_2\cos\theta_1 - \epsilon_1\sqrt{n^2 - \sin^2\theta_1}}{\epsilon_2\cos\theta_1 + \epsilon_1\sqrt{n^2 - \sin^2\theta_1}} = \frac{E_3}{E_1} \tag{55}$$

$$\mu_1 = \mu_2 = \mu_v$$

Since the reflected wave travels a path which is longer by an amount $\ell = \ell_1 - \ell_2 = 2h\cos\theta_1$ (Figure 17), it is delayed in phase by an angle

$$\delta = \frac{2h\cos\theta_1\, 360^\circ}{\lambda} \tag{56}$$

Thus, if the reflected field intensity is E_3, the total field at point P is

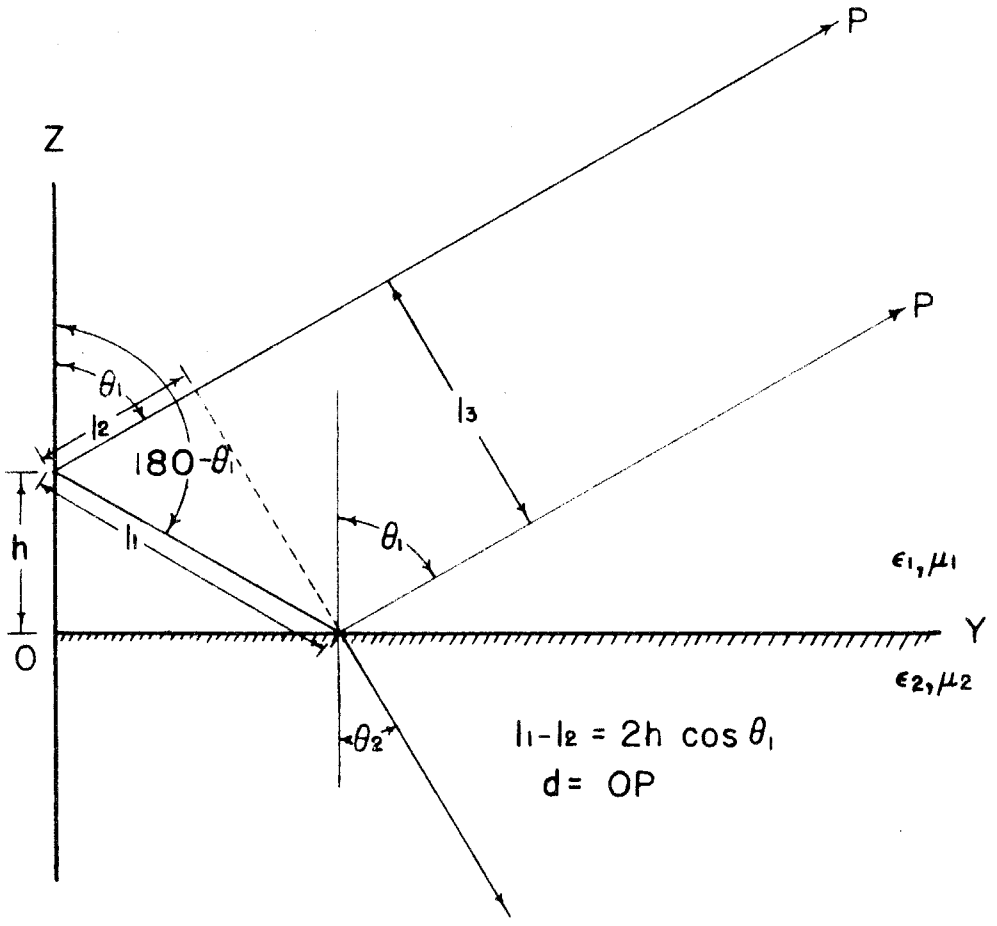

Figure 17.

Geometry of the reflection method

$$E_P = E_1 + E_3 e^{-j\delta} = E_1\left(1 + \rho e^{-j\delta}\right) \tag{57}$$

In the y-z plane, for h = 0, Equation 57 becomes

$$E_P = \frac{2E_1 \cos\theta_1}{\cos\theta_1 + \sqrt{n^2 - \sin^2\theta_1}} \tag{58}$$

Figure 18 shows the result of such a computation, in the y-z plane of Figure 17, for various heights h with $\epsilon_2/\epsilon_1 = \epsilon_r = 10$. The antenna current in each case is held constant, and unity field strength is assumed for a dipole in free space. For this calculation $\rho_\perp$ was used, whereas $\rho_{||}$ would be needed in order to find the fields in the x-z plane. The pattern for the x-z plane can be approximated for small angles of θ by multiplying the value in Figure 18 by the directivity factor D_θ shown in Figure 19.

$$D_\theta = \cos\theta \qquad \text{for the Hertz dipole} \tag{59a}$$

$$D = \frac{\cos(90\sin\theta)}{\cos\theta} \qquad \text{for the half-wave dipole} \tag{59b}$$

For our low-frequency, ionospheric-research antenna, h/λ is essentially zero, but it is of interest to consider the radiation patterns for several heights above the ground. It is possible to see how the radiation resistance varies with height by noting the relative areas contained within each pattern of Figure 18. Figure 18 also shows the calculated pattern of the E-field within the lossless dielectric.

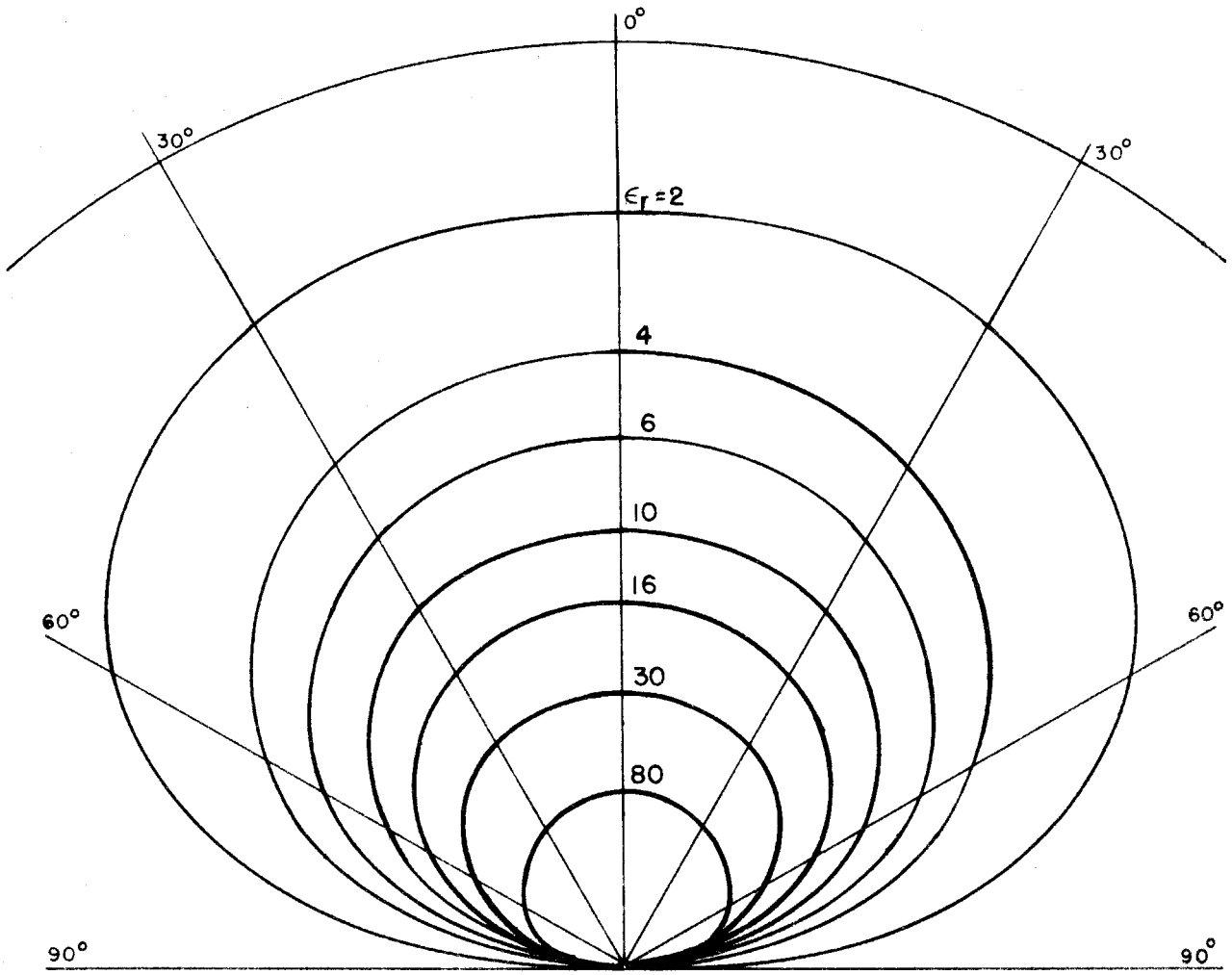

Figure 18.

Pattern in y,z plane of a dipole over a plane dielectric earth with h = 0.

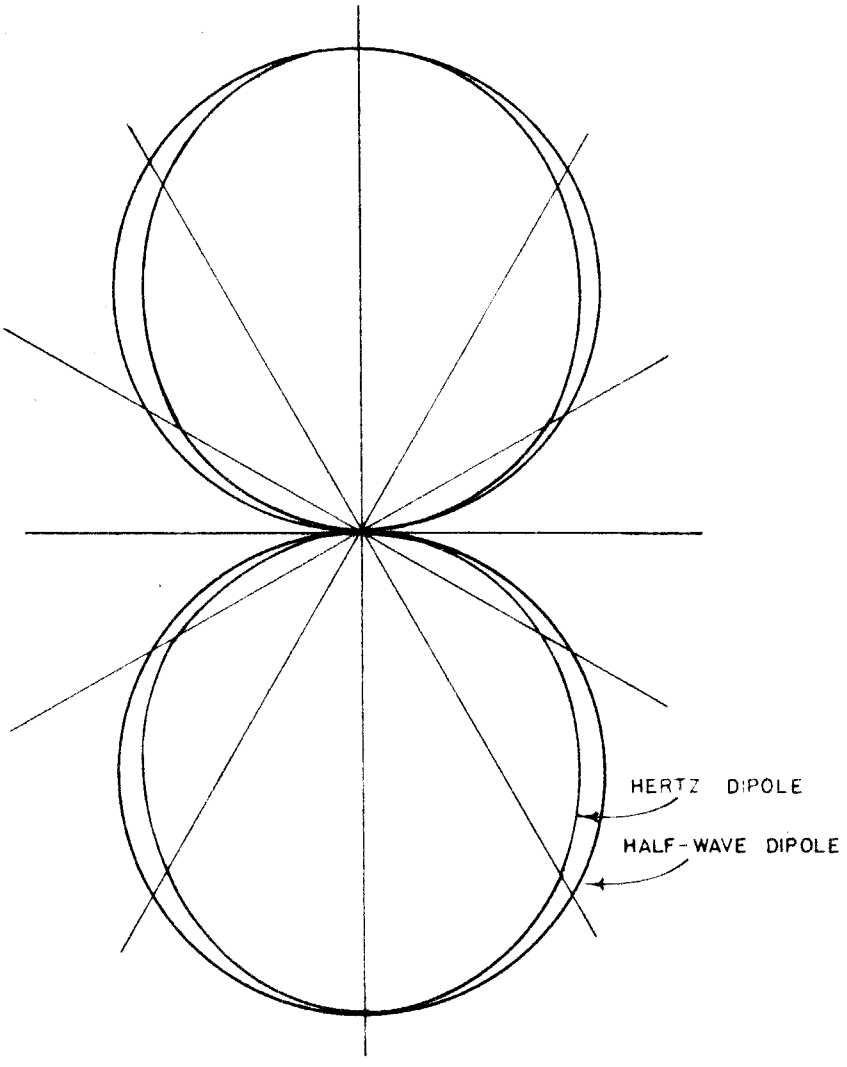

Figure 19.
Pattern in the x,z plane of a Hertz dipole and of a half-wave dipole.

This pattern remains the same for various heights of the antenna above the ground. Note that, when h is equal to zero, the field has the same maximum value below the antenna as above. Moreover, in the dielectric, the entire pattern is confined to a cone of revolution whose central angle is

$$\beta = \sin^{-1}\frac{k_2}{k_1} = \sin^{-1}\sqrt{\epsilon_r} \qquad (60)$$

where $\epsilon_r = \epsilon_2/\epsilon_1$.

Figure 20 shows how the pattern, for h = 0, varies for different values of the relative capacitivity, and we can observe how the radiation resistance decreases with increasing relative capacitivity. As before, constant driving current is assumed. The pattern of the antenna has a maximum value in the $\theta = 0^\circ$ direction and has decreased by only 10 per cent at $\theta = 30^\circ$. Figure 21 is a plot of the normalized maximum field as a function of ϵ_r . The fact that there is zero field strength in the $\theta = 90^\circ$ direction is useful, because the problem of separating ground wave from sky wave is eliminated in the y or $\phi = 90^\circ$ direction. The ground wave in the x or $\phi = 0^\circ$ direction is considered shortly.

It is possible to compare the results obtained by the reflection method for h = 0 with Sommerfeld's results at a point directly above the antenna, $\theta = 0$, and at a point off the side of the antenna, $\theta = \pi/2$, $\phi = \pi/2$. For the latter case, $\theta = \pi/2$, $\phi = \pi/2$, both methods give zero

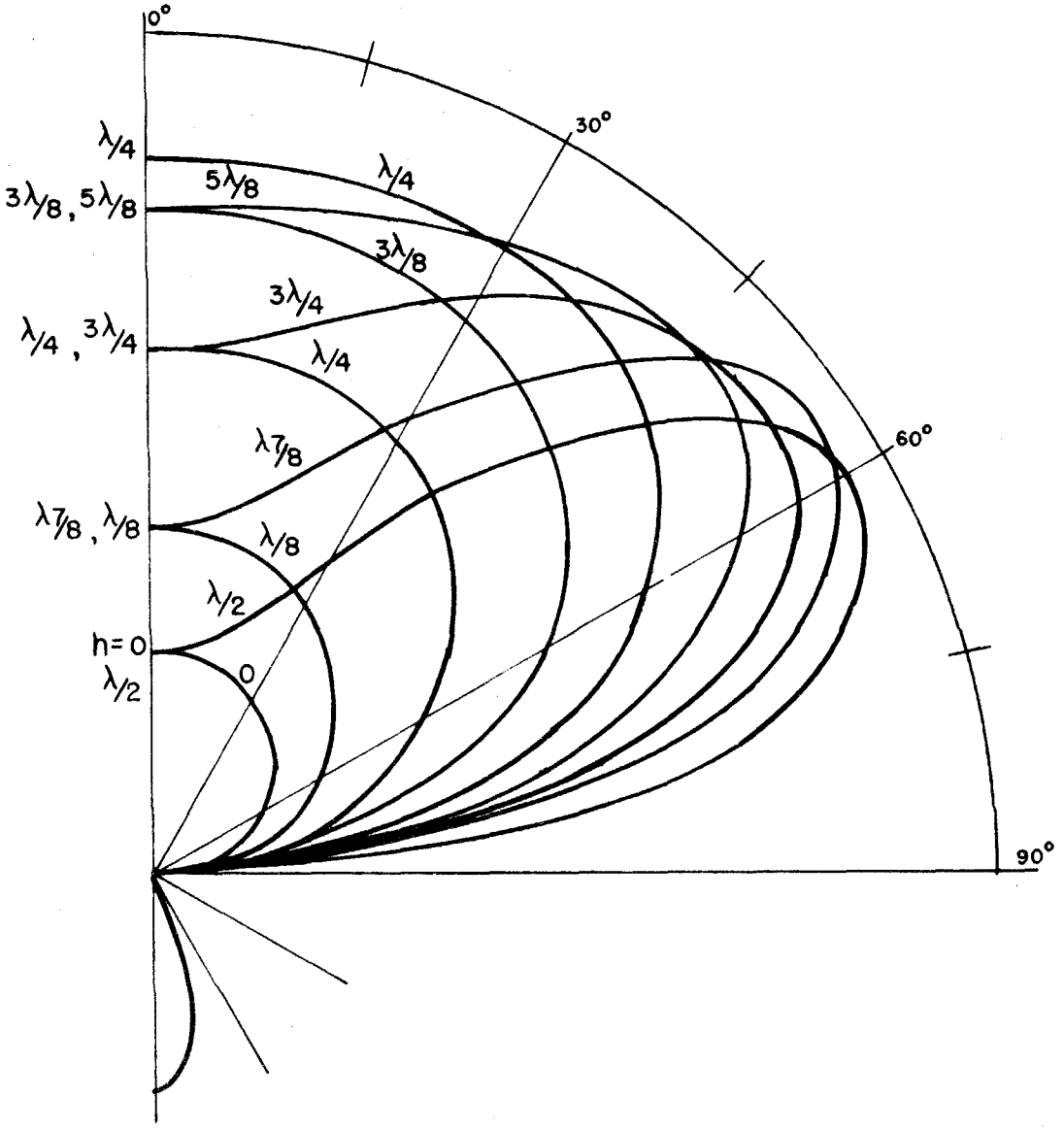

Figure 20.

Field pattern in y,z plane for a dipole at height h above the ground ($\epsilon_r = 10$).

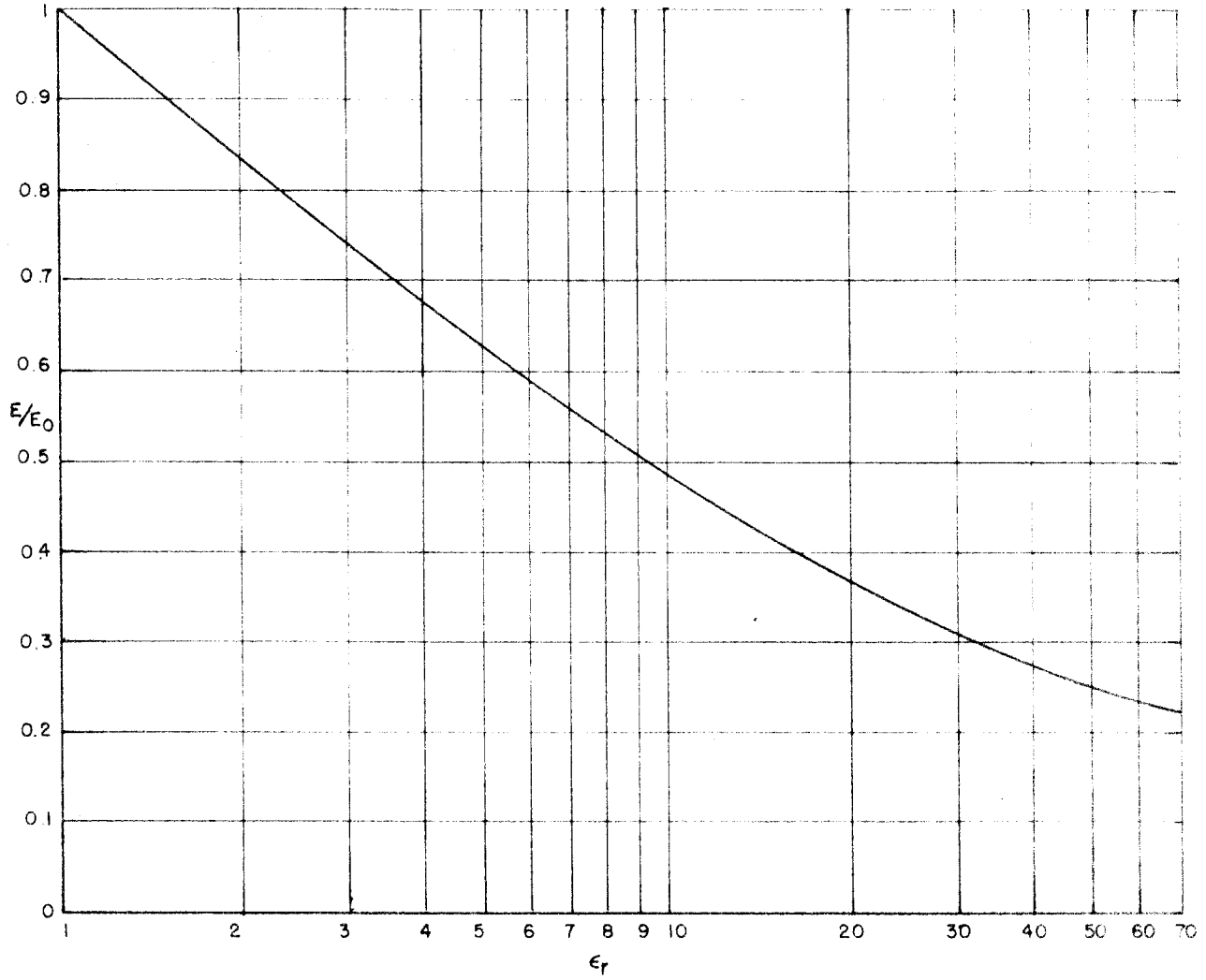

Figure 21.

Maximum field strength of a dipole over a plane dielectric earth ($h=0, \theta=0$) as a function of ϵ_r.

field strength. At $\theta = 0$, according to Equation 58 the field strength is $2\sqrt{\epsilon_1}/(\sqrt{\epsilon_1}+\sqrt{\epsilon_2})$ times the field strength of an equivalent dipole in free space. At $\theta = 0$, $r = 0$, Equation 48 for Π_x becomes

$$\Pi_x\Big|_{r=0} = \frac{I\ell}{4\pi\omega\epsilon_1}\left[\int_0^\infty e^{-a_1(z+h)}\frac{2\lambda d\lambda}{a_1+a_2} + \frac{e^{jk_1(z-h)}}{z-h} - \frac{e^{jk_1(z+h)}}{z+h}\right] \qquad (61)$$

The integral in this case can be evaluated for large values of z, and Π_x becomes

$$\Pi_x\Big|_{r=0} = \frac{I\ell}{4\pi\omega\epsilon_1}\left[\frac{e^{jk_1(z-h)}}{z-h} - \frac{e^{jk_1(z+h)}}{z+h} + \frac{2\sqrt{\epsilon_1}}{\sqrt{\epsilon_1}+\sqrt{\epsilon_2}}\,\frac{e^{jk_1(z+h)}}{(z+h)}\right] \qquad (62)$$

For $h = 0$, Π_x is $2\sqrt{\epsilon_1}/(\sqrt{\epsilon_1}+\sqrt{\epsilon_2})$ times the free-space value; thus the two methods give the same result.

D. The Ground Wave

The radiation field of the horizontal dipole, over an arbitrary earth, consists of a horizontally polarized sky wave and a vertically polarized ground wave. The reflection method does not give rise to a solution corresponding to a vertically polarized ground wave. For the case of a horizontal dipole at the surface of a perfect dielectric earth, the ground wave may be easily calculated from Sommerfeld's integral equation (Equation 50). This equation may be written in the form

$$\Pi_{z_1} = \frac{-I\ell}{4\pi\omega\epsilon_1}\,\frac{2\cos\phi}{k_1^2}\int_0^\infty J_1(\lambda r)e^{-a_1 z}\,\frac{(a_1-a_2)}{n^2a_1+a_2}\,\lambda^2 d\lambda = P+Q \qquad (63)$$

The integrand has branch points at $\lambda = k_1$ and $\lambda = k_2$ and a pole at $\lambda = p$, where p is given by the equation

$$n^2\sqrt{p^2+k_1^2} + \sqrt{p^2-k_2^2} = 0 \qquad (64a)$$

or

$$p^2 = k_1^2 k_2^2 / (k_1^2+k_2^2) \qquad (64b)$$

The term P of Equation 63 is the contribution of the pole to the value of the integral. Sommerfeld has shown that this portion of the solution for Π_{z_1} gives rise to a ground wave. P may be calculated by applying the residue theorem of complex-variable theory. The integral of Equation 63 may be transformed into one involving the Hankel function H_1^1

$$\Pi_{z_1} = \frac{-I\ell}{4\pi\omega\epsilon_1}\frac{\cos\phi}{k_1^2}\int_{-\infty}^{\infty} H_1^1(\lambda r)e^{-\alpha_1 z}\frac{\alpha_1-\alpha_2}{n^2\alpha_1+\alpha_2}\lambda^2\, d\lambda \qquad (65)$$

The residue of the integrand at the pole $\lambda = p$ is

$$Res = \frac{-I\ell}{4\pi\omega\epsilon_1}\frac{\cos\phi}{K}H_1^1(pr)e^{-\sqrt{p^2-k_1^2}\,z}\, p\left(\sqrt{p^2-k_1^2}-\sqrt{p^2-k_2^2}\right) \qquad (66)$$

where $K = \frac{k_2^2}{\sqrt{p^2-k_1^2}} + \frac{k_1^2}{\sqrt{p^2-k_2^2}}$ Thus P is

$$P = j2\pi\, Res \qquad (67)$$

For large r, the asymptotic expression for the Hankel function may be used, and P becomes

$$P = -j\frac{I\ell}{z\omega\epsilon_1}\frac{\cos\phi}{K}p\left(\sqrt{p^2-k_1^2}-\sqrt{p^2-k_2^2}\right)\sqrt{\frac{2}{\pi p}}e^{j\left[pr-\frac{3\pi}{4}\right]}\frac{e^{-\sqrt{p^2-k_1^2}\,z}}{\sqrt{r}} \qquad (68a)$$

The magnitude of P, at $\phi = 0$, $z = 0$, is

$$|P| = \frac{I\ell}{2\omega\epsilon_1}\sqrt{\frac{2p}{\pi}}\,\frac{\left(\sqrt{p^2-k_1^2}-\sqrt{p^2-k_2^2}\right)}{K}\,\frac{1}{\sqrt{r}} \tag{68b}$$

E. The Experimental Results

A half-wave antenna, at 197 mc/s, was used in order to investigate further the problem of a dipole over a dielectric earth. The field strength in the plane normal to the length of the antenna was measured, and the results are plotted in Figure 22. The pattern of the antenna agrees very well with the calculated values.

If the field strength above the antenna is found for the two heights of the antenna h which give a maximum and a minimum value, it is possible to calculate the relative capacitivity ϵ_r . We have from Equation 57

$$E_{min} = \frac{2\sqrt{\epsilon_1}}{\sqrt{\epsilon_1}+\sqrt{\epsilon_2}}\,E_1 = \frac{2}{\sqrt{\epsilon_r}+1}\,E_1 \tag{69}$$

$$E_{max} = \frac{2\sqrt{\epsilon_r}}{\sqrt{\epsilon_r}+1}\,E_1 \tag{70}$$

The ratio of the two, E_{max}/E_{min}, is $\sqrt{\epsilon_r}$; ϵ_r was found to be 12.5.

We have not yet tried to determine the losses in the earth when the ratio h/λ_v is small. The 200-mc/s experiment provided a measurement of input resistance as a function of height, and the results are plotted in Figure 16.

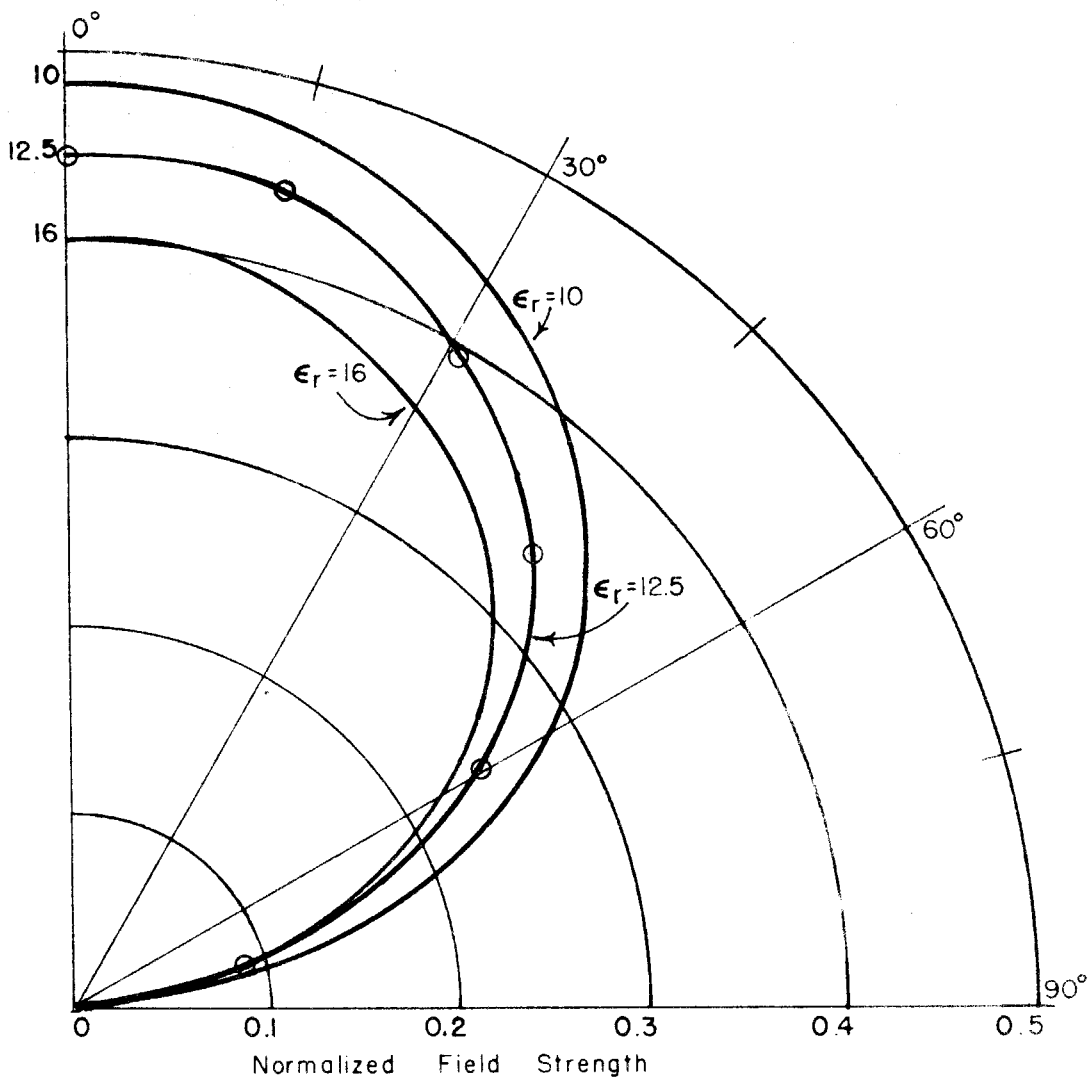

Figure 22.

Field pattern for a dipole over a plane earth h=o (calculated results for ϵ_r = 16,10 and measured values for ϵ_r = 12.5.)

Figure 16 shows fluctuations about 70 ohms for h greater than $\lambda/4$, but as h approaches zero, the input resistance increases instead of decreasing. This rise is attributed to higher field strengths in the dielectric that cause additional losses. With the antenna about 1.5 centimeters above the ground, the input resistance was found to be 80 ohms.

The resonant length of a half-wave dipole in this dielectric, at 197 mc/s, would be $\lambda_v/2\sqrt{\epsilon_r}$, or about $0.14\,\lambda_v$. As the antenna is brought near the earth, a change in the resonant length is observed; it is plotted in Figure 23. When the field strength from a dipole, whose length is shortened, is calculated, the correction factor λ'/λ_v must be used, where λ' is twice the actual length of the dipole, and λ_v is the wavelength in free space. The pattern of a half-wave dipole, with sinusoidal current distribution, changes only in magnitude with decreasing antenna length.

A 60-kc/s antenna, approximately 2,000 meters long, was built over dry granite with a relative capacitivity ϵ_r of about 6 or 7 and very low loss. This was a pilot model for the 16-kc/s antenna. The average height of the antenna above the earth was 1 meter, and the value of λ'/λ_v was 0.8. The input resistance of the dipole was 127 ohms, 39 ohms of which is attributed to copper losses. The remaining 88 ohms consists of radiation and absorption losses.

The maximum field of a half-wave dipole in free space is

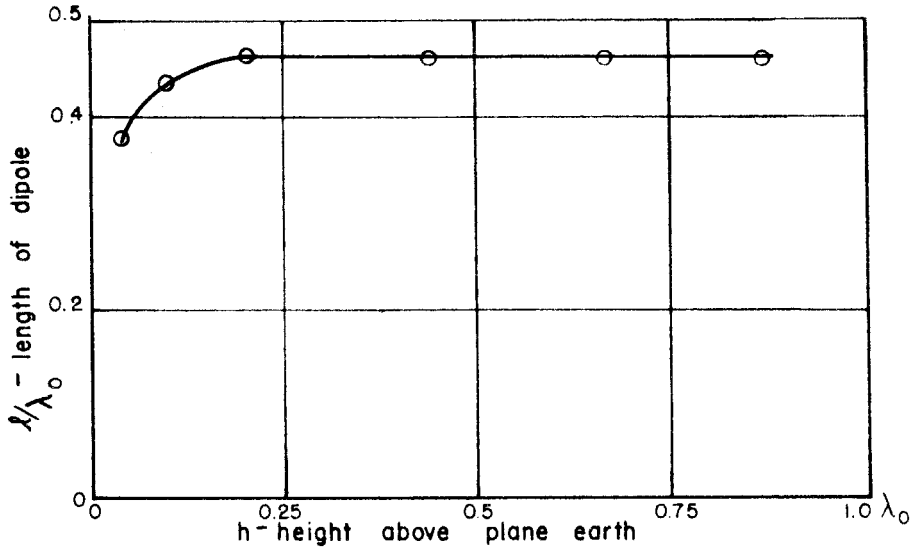

Figure 23.

The resonant length of a dipole as a function of height above the plane earth. $f_0 = 197$mc.

$$E_{rms} = \frac{60\, I_{rms}}{d} \qquad \text{volts/meter} \qquad (71)$$

Therefore the field strength at a distance d directly above a ground dipole antenna is

$$E_{rms} = \frac{2}{1+\sqrt{\epsilon_r}} \frac{\lambda'}{\lambda_v} \frac{60\, I_{rms}}{d} \qquad \text{volts/meter} \qquad (72)$$

which we see depends upon the relative capacitivity and current. If we use $\epsilon_r = 6$ for our 60-kc/s antenna, we obtain

$$E_{rms} = 0.46 \frac{60\, I_{rms}}{d} \qquad \text{volts/meter} \qquad (73)$$

One can obtain the effective* efficiency from Equations 71 and 72

$$\mathcal{E}_{eff} = \left(\frac{2}{1+\sqrt{\epsilon_r}} \frac{\lambda'}{\lambda_v}\right)^2 \frac{72}{R} \times 100\% \qquad (74)$$

where R is the input resistance of the ground antenna. Neglecting the copper losses, the 60-kc/s antenna has an effective efficiency of 17 per cent.

In order to find the magnitude of signal that can be expected at the receiver site, let us assume that d in the reflection from the D-layer is 180 km and that the reflection coefficient is about 0.1. Equation 73 gives the result of 15 μ volts/meter for each ampere of current in the antenna.

---

* The effective efficiency is defined as the ratio of the power required to set up a unity field strength at a height h_o over the earth to the power required to set up the same unity field strength at a distance h_o from a dipole in free space.

A receiving site was set up about 55 km from the transmitter, in a direction normal to the transmitting antenna, and the sky-wave signal came in quite clearly. Except for the fact that the receiving antenna need not be resonant, its characteristics are identical with those of the transmitting antenna. It improves the signal-to-noise ratio by virtue of its discrimination against vertically polarized waves.

Experimentation was also carried out with a resonant loop. The radiated signal from this antenna was received at a distance of 160 km from the transmitting site. This antenna has zero field strength above it and a maximum field strength at low angles of elevation. With this antenna we found that, by raising the wire off the ground by about 1/2 meter, the resonant frequency is increased by a factor of 1.7, and the loss is reduced by a factor of 2. The loop antenna was abandoned temporarily in favor of the dipole which had the desired properties necessary for ionospheric measurements near vertical incidence. The cost of either antenna is small, a fact which was, of course, a prime factor in making it possible for the authors to carry on the ionospheric research program.

F. The 16-kc/s Transmitting Antenna

The 16-kc/s transmitting antenna has been described in Section IV-B. Figures 24 through 26 are photographs showing operations in the construction of the antenna.

Figure 24. Drilling a Hole for an Antenna Pole

Figure 25. Withdrawing the Pneumatic Post Hole Digger

Figure 26. Erecting an Antenna Pole

VI. THE PROPAGATION OF ELECTROMAGNETIC WAVES IN THE IONOSPHERE

A. Ray Treatment

Certain problems involving the propagation of an electromagnetic wave in the ionosphere may be solved by a ray treatment similar to that used in geometrical optics. In the ionosphere, the ionization density increases gradually with height, reaches a maximum, and then diminishes. Depending on conditions, there may be several such ionization maxima which are called layers. If the change in ionization is small in the space of a wavelength, the amount of energy reflected as a wave penetrates the medium is small and can be neglected. In such a case, the medium is termed slowly varying, and it is sufficient to consider only the refraction that takes place.

In Section III, the complete magneto-ionic equations were derived. It is important to remember that in the derivation $\frac{d\Gamma}{dx}$ was assumed to be negligible. This approximation is equivalent to assuming the variation of the propagation constant to be so gradual that the medium may be considered as homogeneous throughout a distance of a few wavelengths. The magneto-ionic equations (Equations 36 and 38) are complicated and sometimes difficult to apply to specific problems without making simplifying assumptions. In order to illustrate the principles of the ray treatment, let us

consider a very simple example. Let us neglect the earth's magnetic field H_T and H_L and the damping factor g due to collisions of the electrons with other particles. The equation of motion for the electrons is simply

$$m \frac{d^2\zeta}{dt^2} = -e E_\zeta \tag{75a}$$

or

$$m \frac{dv_\zeta}{dt} = -e E_\zeta \tag{75b}$$

If E_ζ is given by the expression $E_\zeta = E_0 \sin \omega t$, then

$$m \frac{dv_\zeta}{dt} = -e E_0 \sin \omega t \tag{76}$$

Integrating, we obtain

$$v_\zeta = \frac{eE_0}{m\omega} \cos \omega t \tag{77}$$

This motion of the electrons produces a convection current, the density of which is given by

$$\rho v_\zeta = -Nev_\zeta = -\frac{Ne^2 E_0}{m\omega} \cos \omega t \tag{78}$$

The displacement current in the medium is

$$\epsilon \frac{\partial E}{\partial t} = \epsilon E_0 \omega \cos \omega t \tag{79}$$

For the ionosphere, the free-space value of capacitivity ϵ_v may be used. Thus the total current in the medium is

$$i_T = \left(\epsilon_v - \frac{Ne^2}{m\omega^2}\right) E_0 \omega \cos \omega t \tag{80}$$

The presence of the electrons has the effect of reducing the capacitivity of the medium from ϵ_v to

$$\left(\epsilon_v - \frac{Ne^2}{m\omega^2}\right)$$

Thus the index of refraction of the medium is less than 1, and the phase velocity of the waves is greater than that for free space. The refractive index of the medium is

$$n = \sqrt{\frac{\epsilon}{\epsilon_v}} = \sqrt{1 - \frac{Ne^2}{\epsilon_v m\omega^2}} \qquad (81)$$

The electron density of the ionized layer increases from the bottom upward; thus an electromagnetic wave incident obliquely on the layer is gradually bent down. If i is the angle of incidence, then according to Snell's law the condition for total reflection is

$$\sin i = n = \sqrt{1 - \frac{Ne^2}{\epsilon_v m\omega^2}} \qquad (82)$$

At vertical incidence, the condition for total reflection is $n = 0$.

In applying the magneto-ionic theory and ray treatment to E-layer propagation problems at low frequencies, the assumption may be made that the absorption due to collisions is negligible. This assumption is suggested by the fact that at night the reflection coefficient often approaches unity. The propagation is then of the quasi-transverse type (the terms quasi-transverse and quasi-longitudinal were introduced by Booker in Ref. 18). The author of this thesis believes that, under average conditions at low and very-low

frequencies in the range of 16 to 70 kc/s, this assumption results in a great oversimplification of the problem. In the lossless case (q = 0), Equation 36 may be written in the form

$$n^2 = 1 - \frac{x}{1 - \frac{y_T^2}{2(1-x)} \pm \sqrt{\frac{y_T^4}{4(1-x)^2} + y_L^2}} \qquad (83)$$

where

n = refractive index

$x = -\frac{1}{p} = \frac{KN}{f^2}$

$K = \frac{e^2}{4\pi^2 m \epsilon_v}$

N = ionization density

$y_T = -\frac{\gamma_T}{p} = \frac{f_T}{f}$

$y_L = -\frac{\gamma_L}{p} = \pm\frac{f_L}{f}$ (Plus sign used when the positive direction of the earth's magnetic field makes an acute angle with the direction of propagation)

f_T = transverse gyro frequency

f_L = longitudinal gyro frequency

f = wave frequency

At vertical incidence, reflection occurs when the refractive index is reduced to zero. At frequencies below the gyro frequency, n = 0 for

$x = 1$ (ordinary component of wave, given by plus sign before radical)

$x = 1 + y$ (extraordinary component of wave, given by minus sign before radical)

where

$$y = \frac{f_H}{f}$$

f_H = gyro frequency

In this case, the propagation of the ordinary wave is not affected by the earth's magnetic field. The terms ordinary wave and extraordinary wave have been derived from the optical analogy. In double refraction in optics, the ray which follows the ordinary laws of refraction is called the ordinary ray, and the other is called the extraordinary ray.

For the conditions of our experiments, the electronic gyro frequency f_H = 1,416 kc/s. The ionization density required for reflection of the extraordinary component at 50 kc/s is $\frac{1,416}{50} + 1$, or 29.3 times that necessary for reflection of the ordinary component. On entering an ionized region, an electromagnetic wave is split into two components. In our 50-kc/s experiments, the extraordinary component is reflected from a higher region of greater ionization density. The path length of the extraordinary wave in the ionized region is longer; thus, this wave will suffer greater attenuation.

If losses are neglected, the polarizations of the waves may be determined from the expression

$$R = \frac{j}{y_L}\left[\pm\sqrt{\frac{y_T^4}{4(1-x)^2} + y_L^2} - \frac{y_T^2}{2(1-x)}\right] \qquad (84)$$

B. Wave Treatment

Helliwell (Ref. 19) has made measurements for determining the vertical ionization gradient of the lower nighttime E-region. He obtained height versus frequency data on 21 April 1949. Measurements were made in 50-kc/s steps from 100 to 400 kc/s. A measurable increase in height occurred between 100 and 400 kc/s. This increase amounted to not more than 2 km. He assumed that the time variation is negligible; that the ionization density increases exponentially with height; that, at the level of reflection, the ionization density is proportional to the square of the frequency; and that the true height change is the same as the virtual height change. The scale height of the layer was determined by using the relation

$$N = N_0 e^{\frac{h-h_0}{H}} \tag{85}$$

where

N_0 = ionization density at height h_0

N = ionization density at height h

H = scale height of the layer

Helliwell found the scale height to be $H = 0.7$ km. Thus, in a distance of 0.7 km, the ionization density increased by a factor of 2.7. Helliwell believes that this scale height is typical for the lower sides of the layers in the nighttime E-region. For such layers, it is clear that the slowly varying conditions do not exist at low frequencies, where the wavelength is greater than 1 km. Thus, at low

frequencies, the applicability of the magneto-ionic theory and ray treatment is open to serious question. This fact suggests the use of a wave treatment in which the slowly varying approximations are not made.

In a wave treatment, we wish to find solutions to the wave equations when the propagation constant varies appreciably in the space of a wavelength. As yet there is no satisfactory wave treatment that may be applied to low-frequency ionospheric propagation problems. There are several reasons for this fact. In order to develop a wave theory, the ionization gradients in the lower ionospheric regions must be known. There is still considerable question as to the exact nature of these gradients. They cannot be deduced with confidence from theoretical considerations, because there is disagreement as to the exact ionization processes that take place in these regions. Also, there is some doubt as to the proper values of recombination coefficients, collisional frequencies, and temperatures to use. The ionization gradients have not been determined by radio measurements, because the measurements are difficult to make at low frequencies, and because they cannot be properly interpreted without initially having a suitable wave theory.

Another difficulty lies in the mathematical complexity of the nonlinear wave equations. Exact solutions to these equations may be obtained when the ionization gradients are represented by certain mathematical functions. However, these functions do not represent the ionized layers with

sufficient accuracy. As an example, the Epstein layer may be treated exactly; however, it does not satisfactorily represent an ionospheric layer.

Approximate solutions to the wave equations may be found by applying the Wentzel-Kramers-Brillouin (WKB) method of quantum mechanics (Ref. 20). Care must be used in applying the WKB method, because the solutions obtained are not valid if the propagation constant changes appreciably in the space of a wavelength. However, an approximate solution can be found by properly matching slowly varying solutions of neighboring regions.

An additional complexity arises when the wave-equation solutions are not independent. In this case, coupled wave equations must be solved. This condition arises when the geomagnetic dip angle assumes large values or when the ionization gradients are very steep. The coupled wave equations predict a third wave component. This phenomenon, termed ionospheric triple splitting, has been observed and treated by Eckersley (Ref. 21).

Several workers have made contributions toward the development of a wave theory. Booker (Ref. 22) has shown that the ray or slowly varying treatment is a true first-order approximation to the wave solution. Fösterling (Ref. 23) has adapted the WKB method to include coupling terms. He considered general values of the geomagnetic dip angle. His results generally confirm those of Booker, namely, that the significant results of the quasi-homogeneous treatment,

such as polarization, are approximately correct. Wilkes (Ref. 24) has obtained a formal solution for the coupled wave equations in the case of a linear variation of electron density, but he does not go beyond the formal solution. Feinstein (Ref. 25) has treated the case of a linear variation of electron density for a general angle of geomagnetic dip. He finds that with high electron-density gradients the ellipticity of the polarization ellipse is greater than that predicted by the slowly varying treatment.

Mallinckrodt (Ref. 26) has considered the problem of propagation in an inhomogeneous medium. His treatment is confined to the case of vertical incidence with a general tilt of the earth's magnetic field. For this case, he has shown that any linear medium has two and only two characteristic waves. The polarizations and complex reflection (or transmission) coefficients of the characteristic waves serve to define completely the effect of the medium on any incident wave. The characteristic waves (of either transmission or reflection) are defined as those waves which suffer no change in polarization on transmission or reflection. In the quasi-homogeneous treatment of the magneto-ionic theory, the characteristic waves are the ordinary and extraordinary wave components.

In the magneto-ionic theory, a very simple relationship exists between the polarizations of the ordinary and extraordinary components. In order to find this relationship, let us write Equation 38 in the form

$$R = \frac{j}{\gamma_L}\left(a \pm \sqrt{a^2 + \gamma_L^2}\right) \tag{86}$$

where

$$a = \frac{\gamma_T^2}{2(1+p+jq)} \tag{87}$$

It is now apparent that $R_o R_x = 1$ or $R_x = 1/R_o$, where R_o and R_x are the polarizations of the ordinary and extraordinary components. Unfortunately, on the basis of Mallinckrodt's treatment, there is no reason to expect that this reciprocal relationship applies to the inhomogeneous case.

All of the work toward development of a wave treatment has contributed to our qualitative understanding of the properties of rapidly varying ionospheric layers. At present, the quantitative results of this work cannot be readily applied to particular propagation problems. There are no simple equations by which one can find a wave solution corresponding to a particular set of constants. As a result of this fact, the ray treatment must be used in situations in which it is not strictly applicable. Its use is partially justified by the fact that the results of the quasi-homogeneous treatment give a solution which is at least approximately correct.

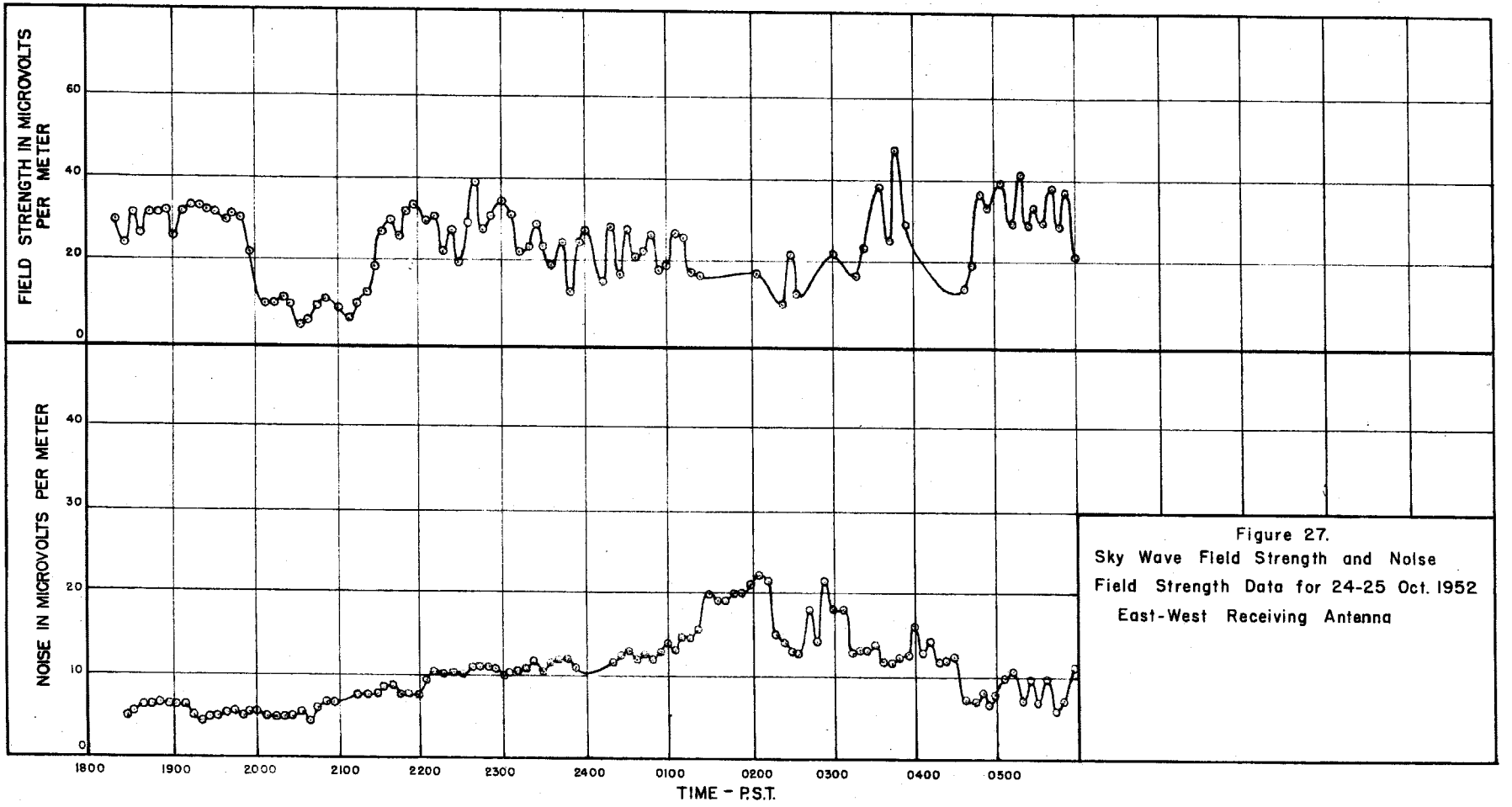

Figure 27.
Sky Wave Field Strength and Noise Field Strength Data for 24-25 Oct. 1952
East-West Receiving Antenna

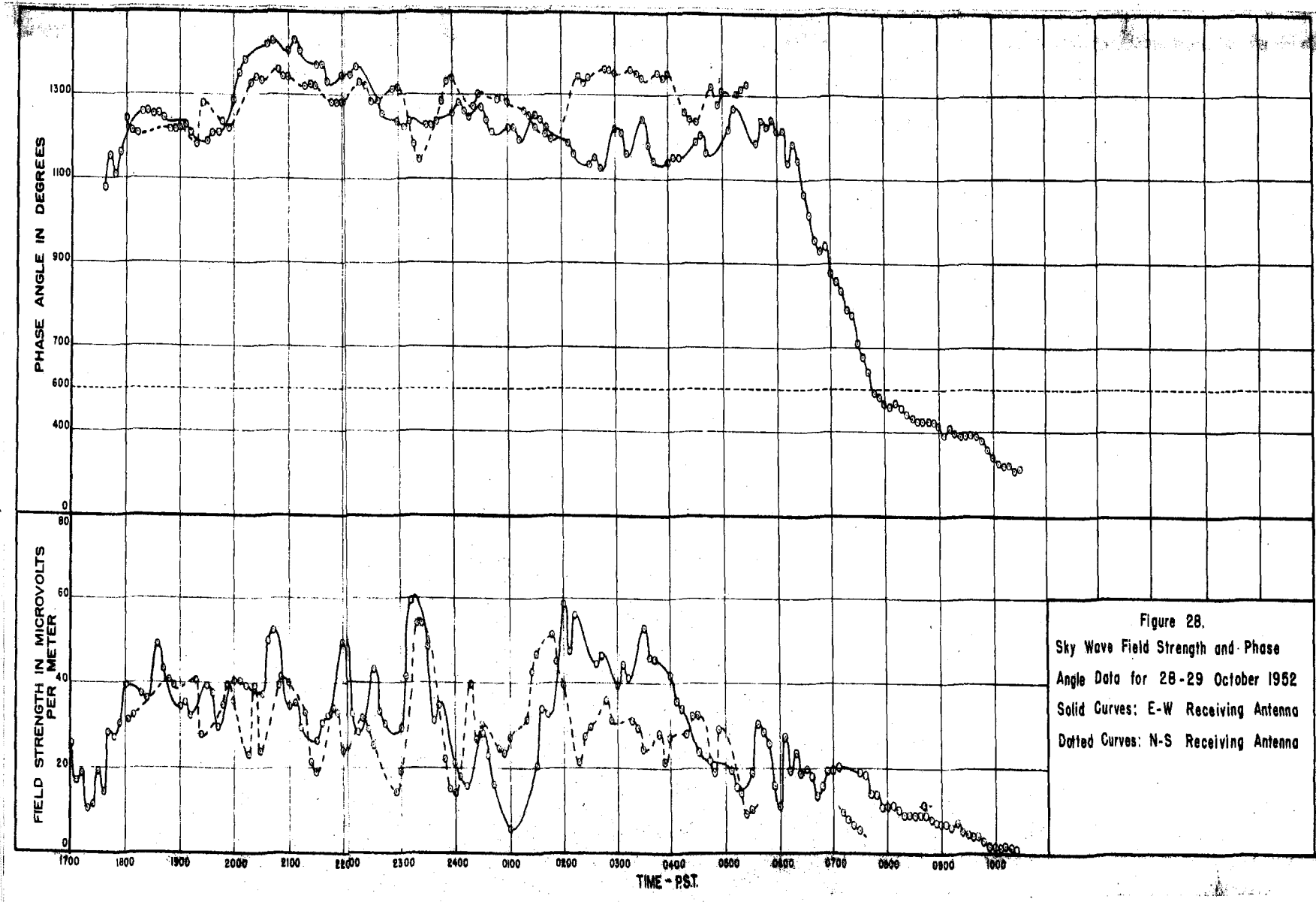

Figure 28.
Sky Wave Field Strength and Phase Angle Data for 28-29 October 1952
Solid Curves: E-W Receiving Antenna
Dotted Curves: N-S Receiving Antenna

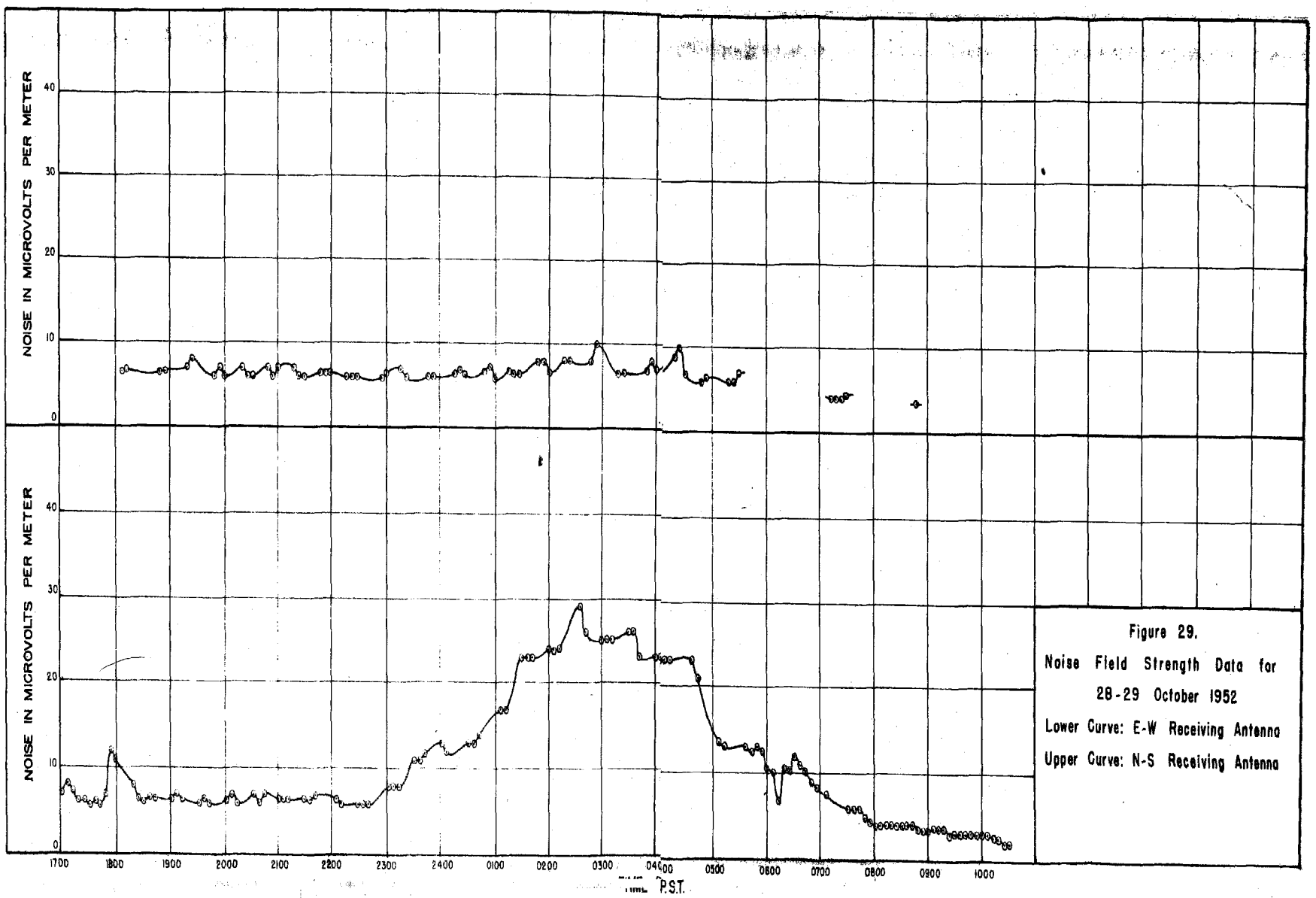

Figure 29.
Noise Field Strength Data for
28-29 October 1952
Lower Curve: E-W Receiving Antenna
Upper Curve: N-S Receiving Antenna

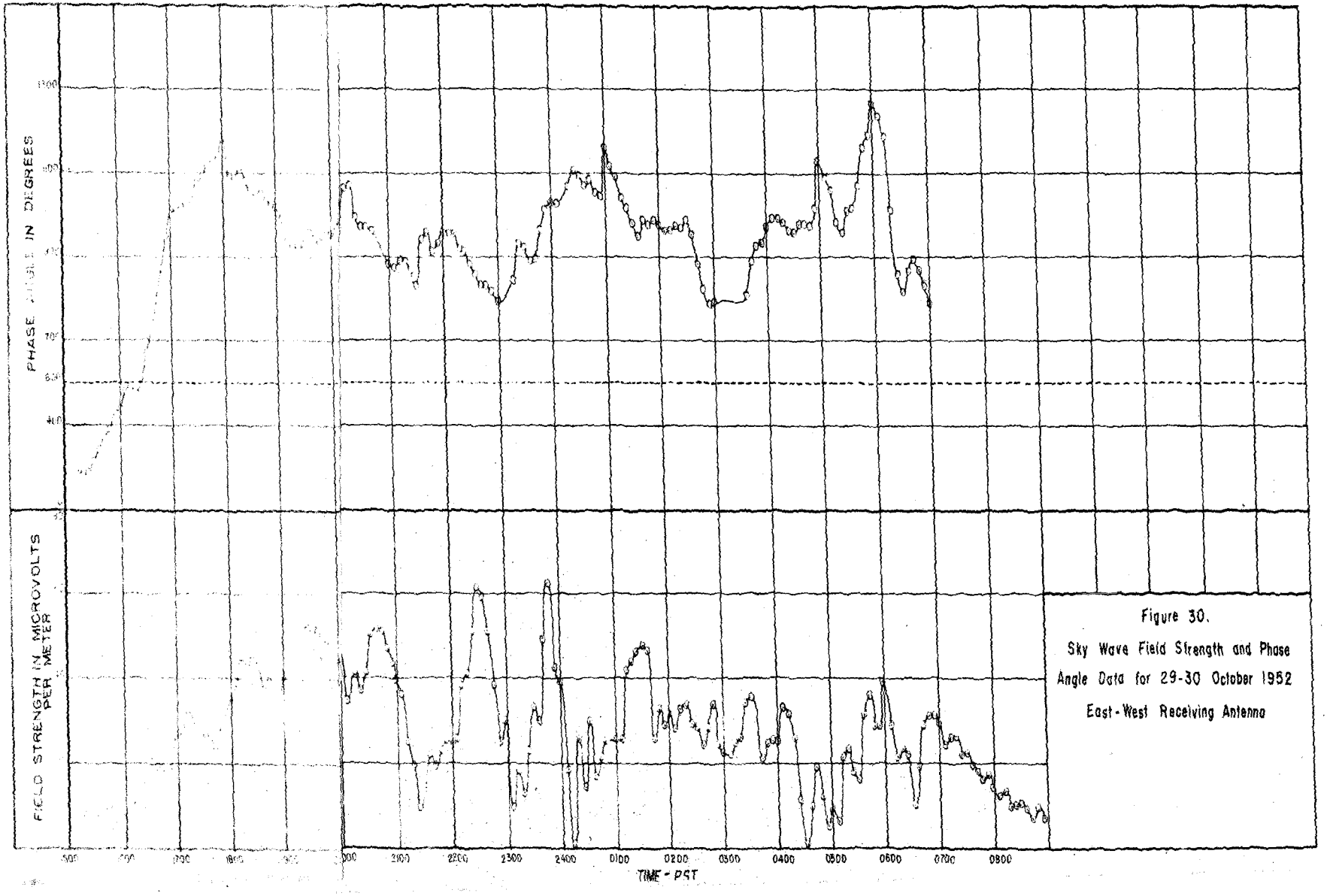

Figure 30.

Sky Wave Field Strength and Phase Angle Data for 29-30 October 1952 East-West Receiving Antenna

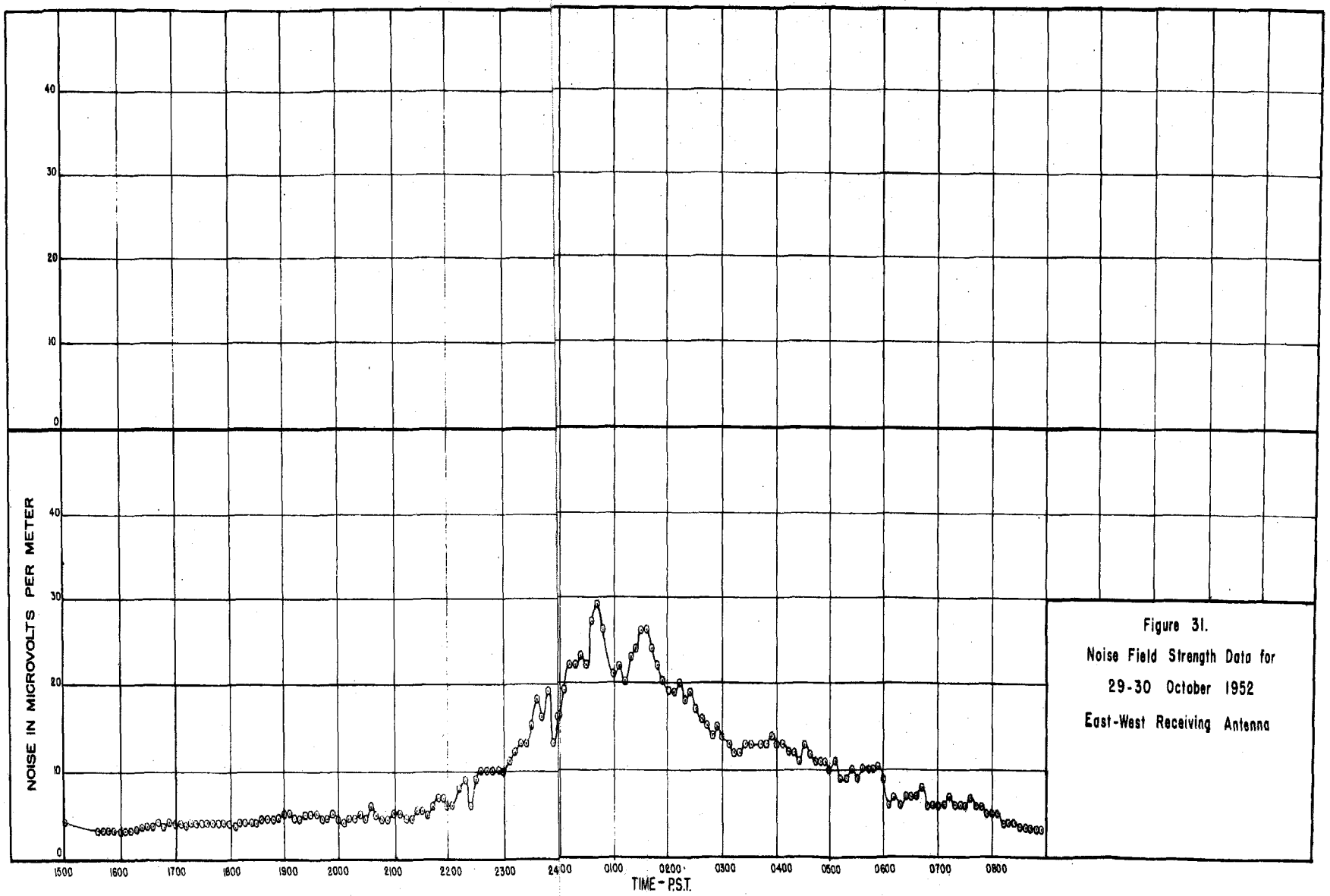

Figure 31.
Noise Field Strength Data for
29-30 October 1952
East-West Receiving Antenna

VII. THE 50-kc/s IONOSPHERIC DATA

Some 50-kc/s relative virtual-height and sky-wave-polarization measurements were made during several nights in October 1952. These data are presented in Figures 27 through 31. The measuring technique and system employed are briefly described in Section IV. The measurements of sky-wave field strength and noise field strength were obtained by using a Stoddart AN-URM-6 field-strength meter. This receiver has a bandwidth of 350 cycles per second at a frequency of 50 kc/s. The large loop antenna which is furnished with this instrument was used. Our own 50-kc/s, dual-conversion superheterodyne receiver was used in making the phase-angle measurements. In these measurements, the phase of the sky wave was compared with a reference phase transmitted over a very-high-frequency link. The orientations of the transmitting and receiving antennae are shown in Figure 10.

Some 100-kc/s and 310-kc/s ionospheric data obtained during the same nights are presented in Figures 32 through 39 for purposes of comparison. These data were obtained by Helliwell of Stanford University, who employed a pulse technique in making these measurements. As will be seen upon examining the data, the time (PST) is marked below the trace on every hour. The receiver frequency alternates between 100 and 310 kc/s, remaining on each frequency for 5 minutes. Except during the first 30-second period in which the height marks are displayed, the receiver is connected alternately

Figure 32. 100-kc/s and 310-kc/s Pulse Data

Figure 33. 100-kc/s and 310-kc/s Pulse Data

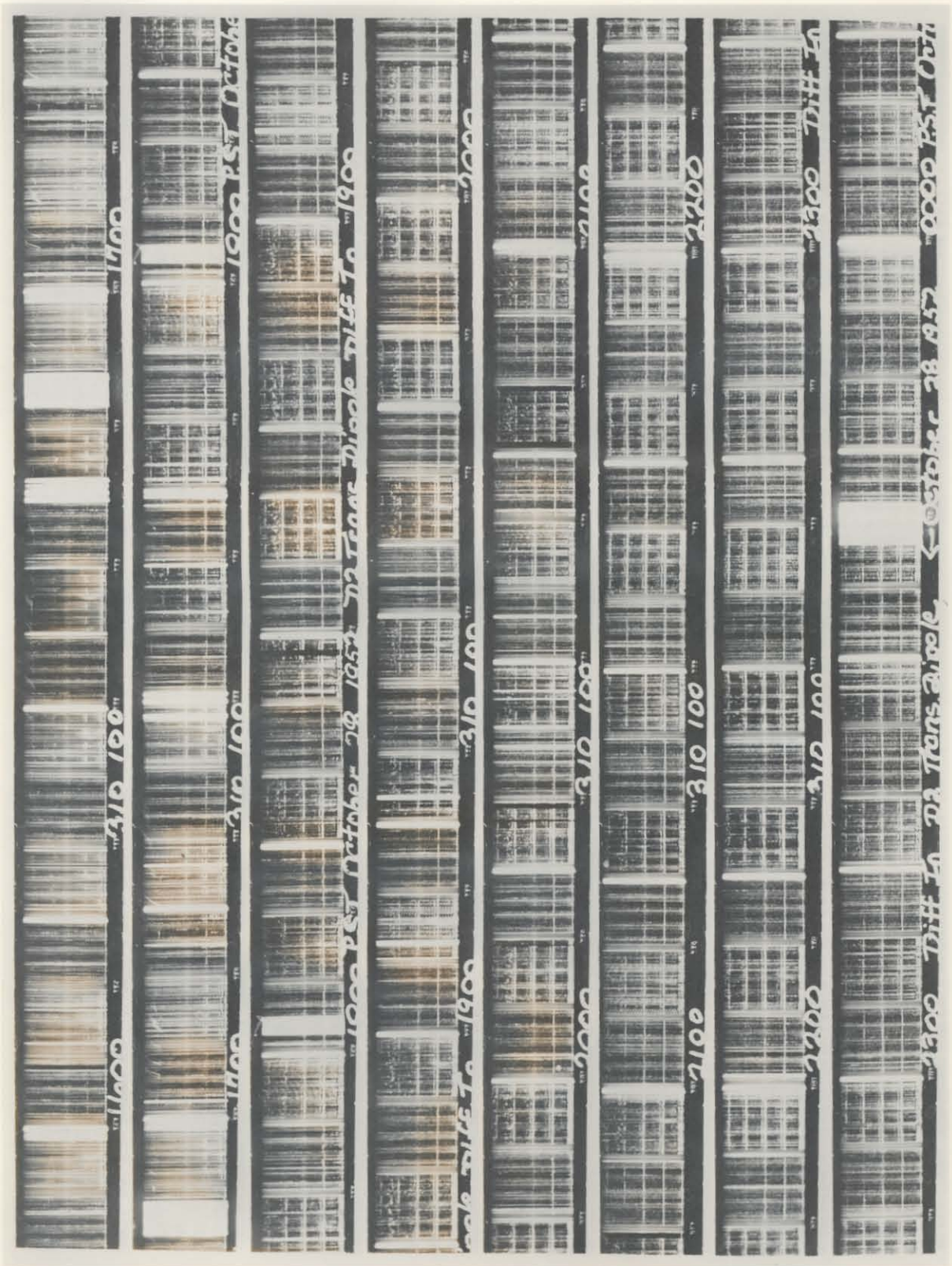

Figure 34. 100-kc/s and 310-kc/s Pulse Data

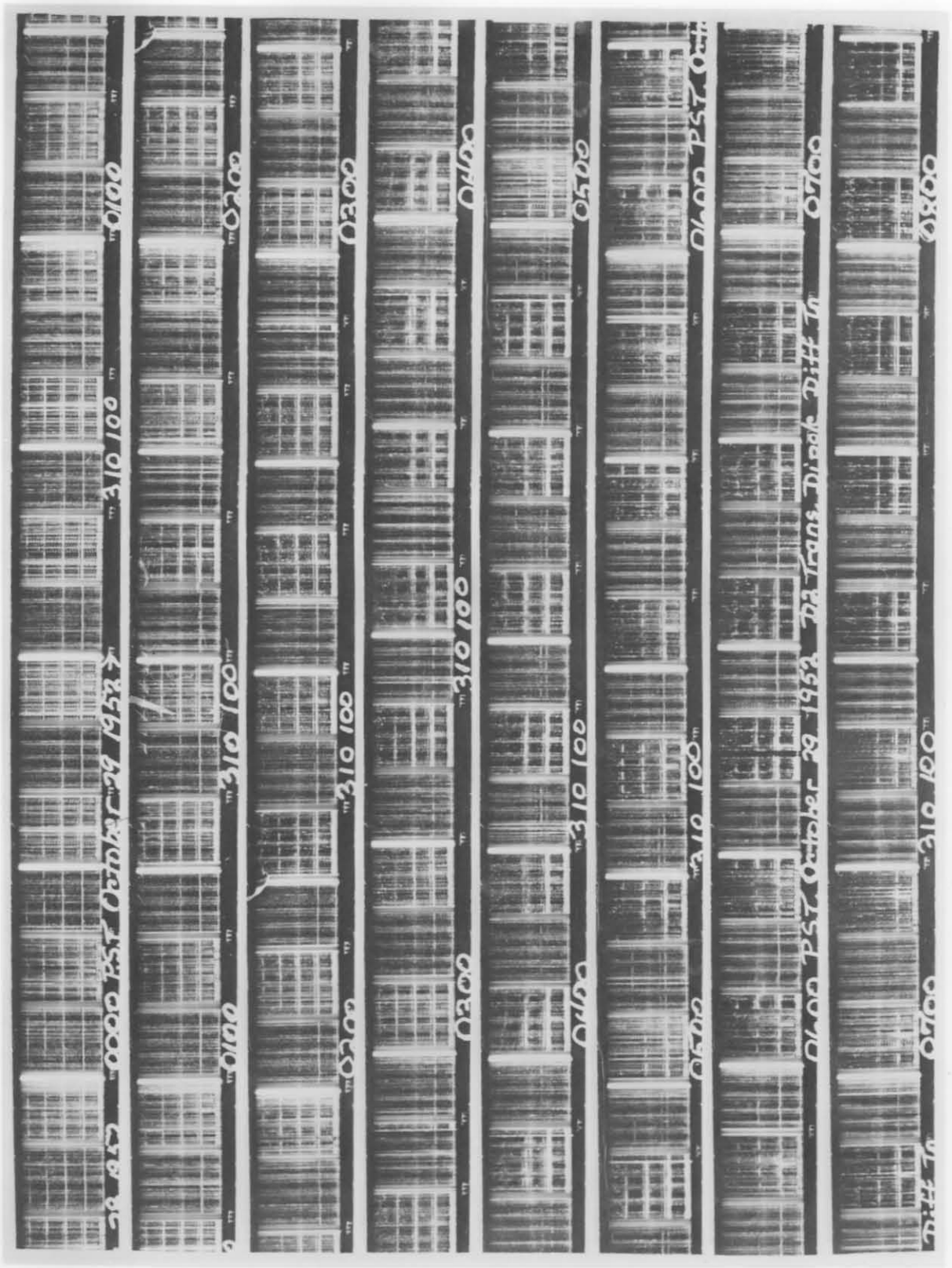

Figure 35. 100-kc/s and 310-kc/s Pulse Data

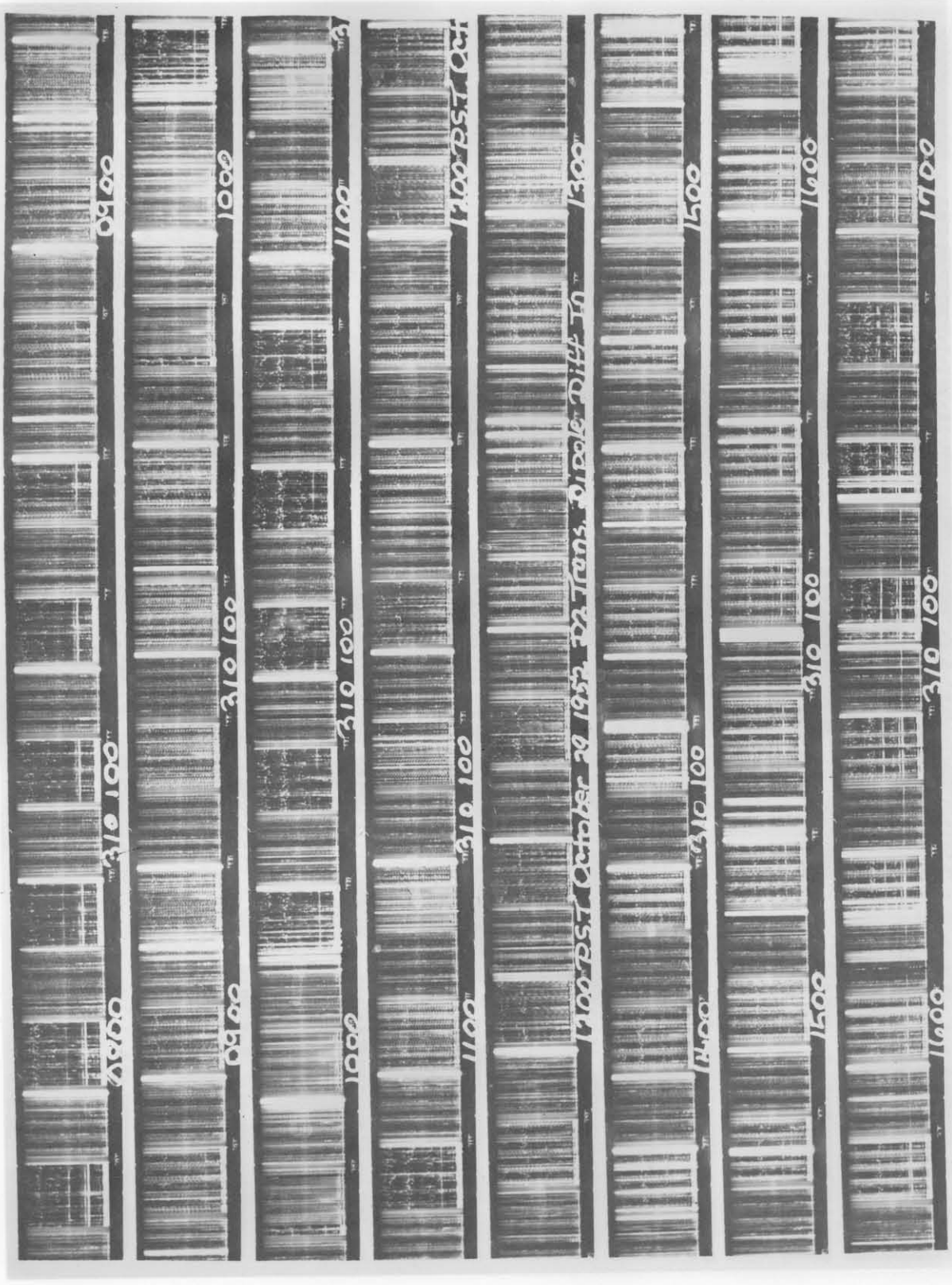

Figure 36. 100-kc/s and 310-kc/s Pulse Data

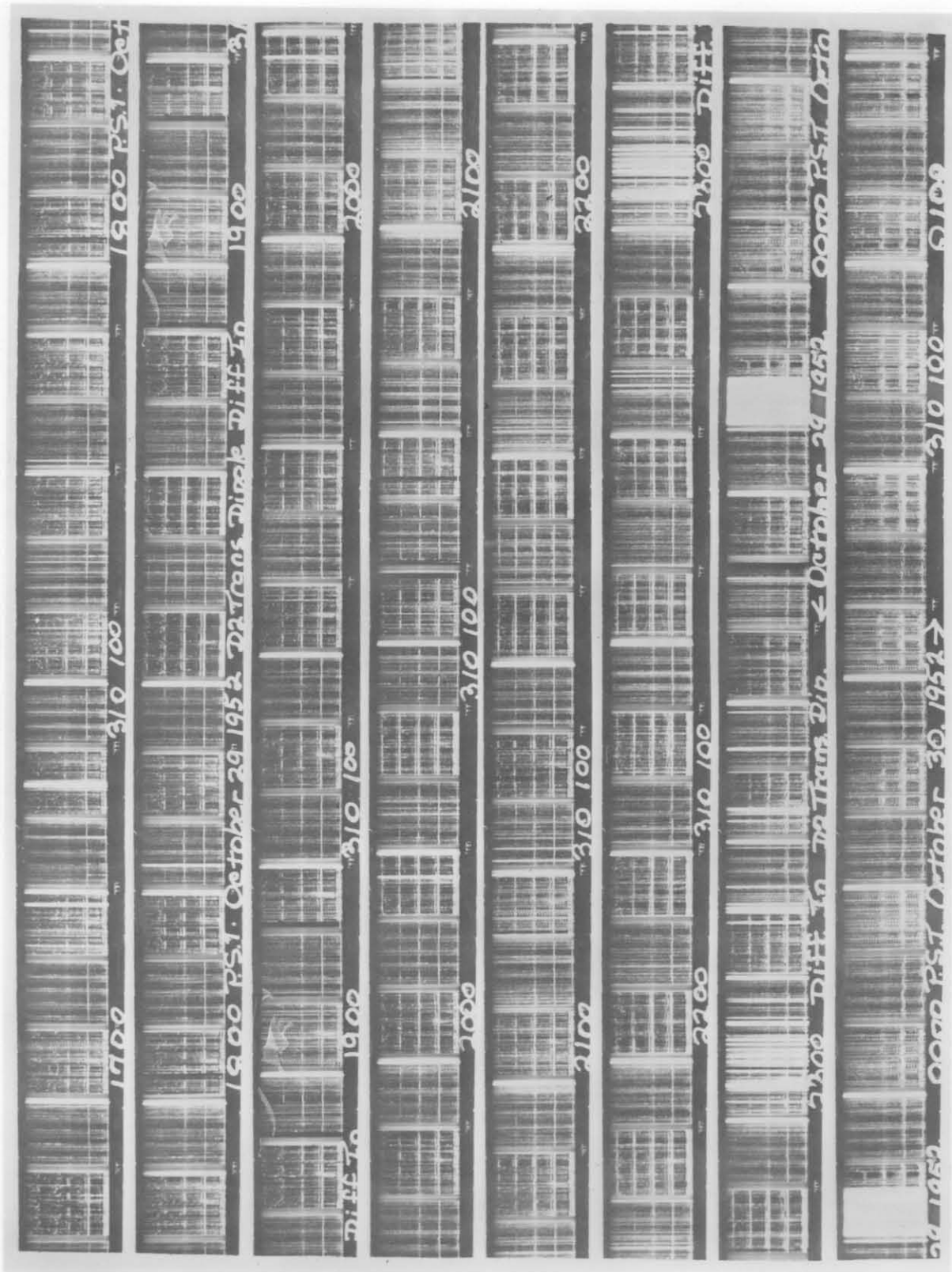

Figure 37. 100-kc/s and 310-kc/s Pulse Data

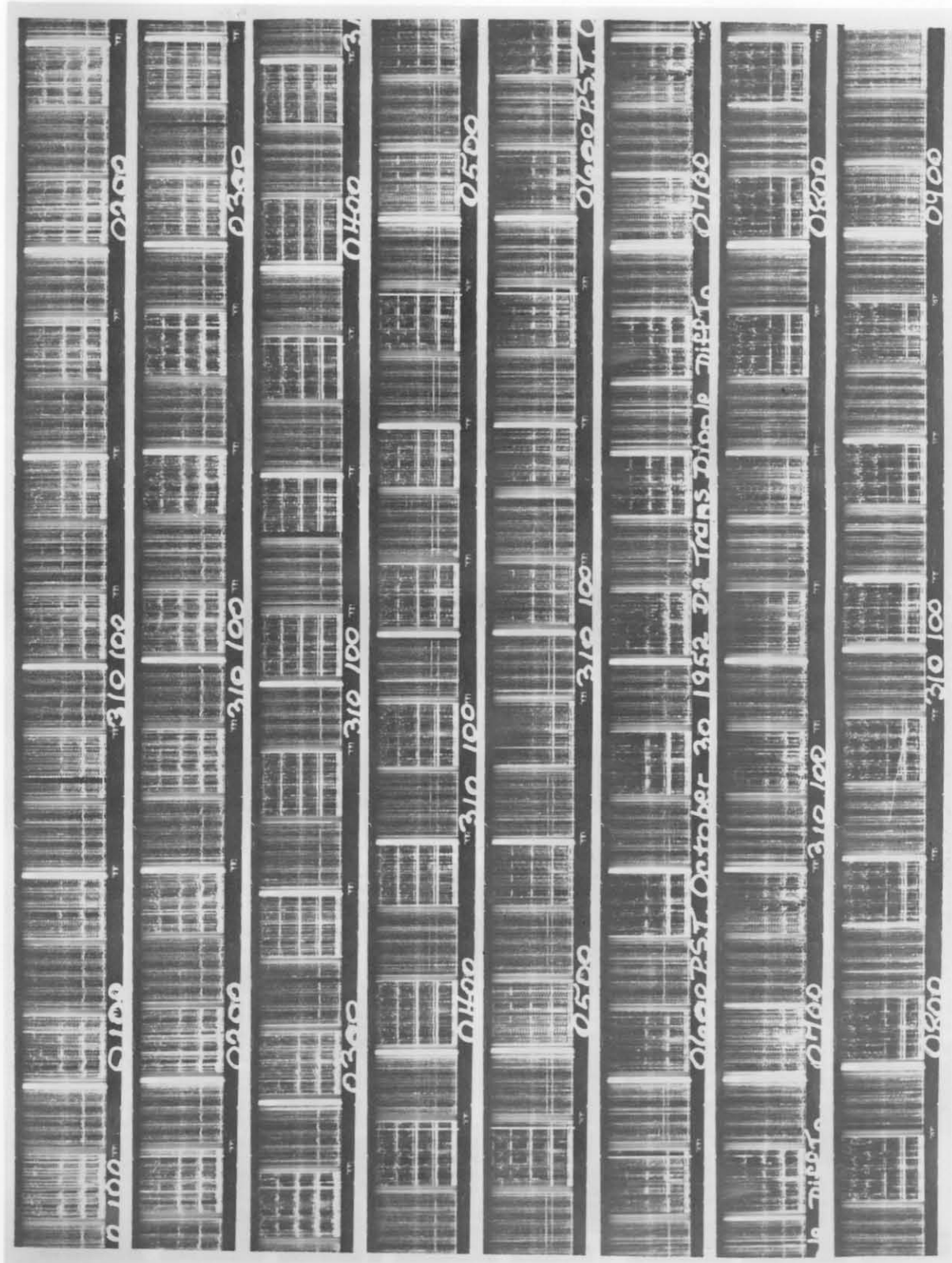

Figure 38. 100-kc/s and 310-kc/s Pulse Data

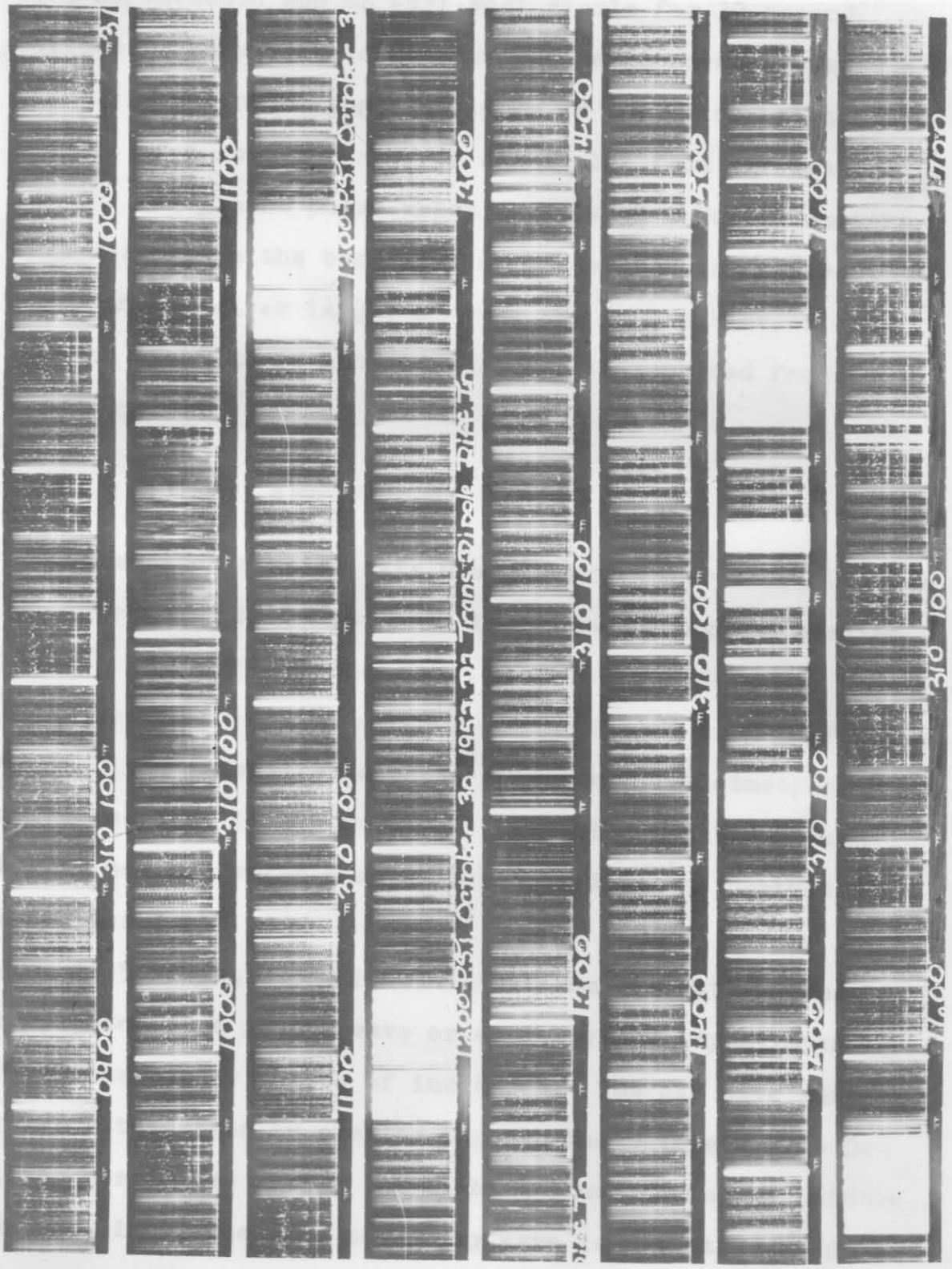

Figure 39. 100-kc/s and 310-kc/s Pulse Data

to a north-south and an east-west dipole for 30-second periods. The spacing of the height marks corresponds to a total virtual path length of 10 km or a virtual height difference of 5 km. The records are scaled from the leading edge of the ground pulse which is delayed a few kilometers with respect to the beginning of the oscilloscope sweep. Since the receiver is 3.7 km from the transmitter, a correction of +2 km is made to all heights measured from the ground pulse.

A. Atmospheric Noise Data

Atmospheric noise data are given in Figures 27, 29, and 31. The noise field strength increased during the evening hours. It reached its maximum value between 0030 and 0130 PST. During the early morning hours of 0300 to 0400 PST the noise field intensity began to decrease. The atmospheric noise received in the east-west direction reached a much higher maximum value than that received in the north-south direction.

At 50 kc/s, atmospheric noise from distant sources is propagated as a ground wave or as a sky wave by E-layer reflections at low angles of incidence. The sky wave suffers great attenuation in passing through the D-layer. The D-layer dissipates during the night. Thus, during the middle of the night, when the noise sky wave is not attenuated by the D-layer, the noise field strength reaches a maximum value. The author believes that the higher noise field

strengths received in the east-west direction are due to atmospheric noise from tropical storms located in the Gulf of Mexico and the Caribbean Sea.

B. Relative Virtual-Height Data and the Sunrise Effect

Changes in the virtual height of the E-layer may be computed from the changes in the phase angle of the sky wave. Absolute virtual-height measurements could be made by determining the total phase shift of the reference signal.

In Figure 40, the geometry of reflection from the E-layer is given. A nominal height of 90 km is assumed for the reflecting layer. At 50 kc/s, a change of 360° in the

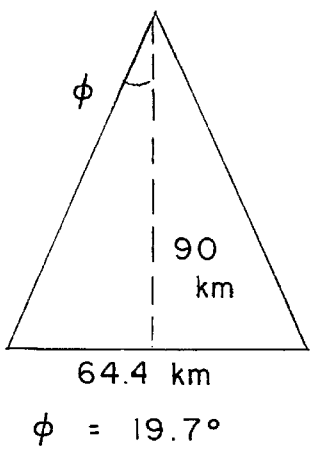

Figure 40. E-Layer Reflection Geometry

phase angle of the sky wave corresponds to a change of 2.83 km in the virtual height. A phase change of 5 or 6° can be easily resolved. Thus the resolution of the virtual-height measurements is approximately 0.05 km. The resolution of this continuous-wave system is much higher than

that of pulse systems. Pulse systems have an advantage in that two or more partially reflecting layers can be detected. However, pulse techniques are unsatisfactory for making vertical-incidence measurements at very-low frequencies.

During the night, the virtual height of the E-layer fluctuated by about 2 to 3 km. Helliwell's 100-kc/s data also show these fluctuations.

There is an apparent splitting in the 100-kc/s pulse data which is due to double pulsing of the transmitter. The separation is roughly 20 km and appears on multiple as well as first-order reflections. The 100-kc/s pulse data show evidence of ionospheric splitting during a major portion of the time. Thus it is possible that at times our signal was reflected from two or more partially reflecting layers rather than from a single layer.

The relative virtual-height measurements made with the two receiving antennae differ. At 0245 PST on 29 October, the difference in virtual-height measurements reached a maximum value of 1.9 km. This difference is interpreted as being evidence for strong magneto-ionic splitting. On entering the ionized region, the incident wave must have been split into two parts, presumably the magneto-ionic components. These two wave components travel different paths and are reflected from different heights. This effect would give rise to the phase difference that is observed on the two receiving dipoles.

During the late afternoon and early evening (the sunset period), the height of the layer increased by about 7.5 km, and during the morning (the sunrise period), the layer lowered by about 7.5 km. This height change agrees very well with the average values observed in October. Ground sunrise occurred at 0608 PST on 29 October. No significant change in height was observed prior to ground sunrise. This fact is a little surprising in that Helliwell observes the beginning of the sunrise effect as much as 50 minutes prior to ground sunrise. However, it will be necessary to accumulate more data before we can regard our results as being typical or representative.

The light that reaches the E-layer before ground sunrise passes through the atmosphere at grazing incidence. All but the red light is filtered out by N_2, O_2, O, ozone, haze, and fog. This red light does not have enough energy to produce direct ionization in the E-region. The E-layer effects occurring before ground sunrise are attributed to the detachment of electrons from O^- ions by the red light. This process has a very low detachment potential.

C. Sky-Wave, Field-Strength Data and Relative Reflection Coefficients

Sky-wave, field-strength data are presented in Figures 27, 28, and 30. All measurements were made with a constant input power of 625 watts at the transmitting antenna terminals. The sky-wave field strength is a measure of the E-

layer reflection coefficient. The data give the relative changes in the reflection coefficients. By suitably calibrating the system, absolute reflection-coefficient measurements could be made.

Data for two reflection coefficients $_{\perp}R_{\perp}$ and $_{\perp}R_{\parallel}$ were taken. $_{\perp}R_{\perp}$ is measured when the antennae are oriented so that the transmitted signal and received signal are polarized normal to the plane of incidence. $_{\perp}R_{\parallel}$ is a conversion coefficient. It is measured when the antennae are oriented so that the transmitted signal is polarized normal to the plane of incidence and the received signal is polarized parallel to the plane of incidence. By selecting a receiving site in a direction off the end of the transmitting dipole, an additional coefficient $_{\parallel}R_{\perp}$ could be measured. The 50-kc/s ground wave would probably interfere with the measurement of the $_{\parallel}R_{\parallel}$ reflection coefficient.

The 50-kc/s sky wave is attenuated by the D-layer. Thus the field strength is a maximum during the night when the D-layer has dissipated. Between 1100 and 1300 PST (the period of maximum D-layer ionization) the field strength was so low that it could not be measured.

The field-strength data show severe and rapid fluctuations. This is evidence of strong magneto-ionic splitting. The phenomenon of rapid fading during strong magneto-ionic splitting has been observed before (Ref. 27). Several factors possibly contributed to this effect. First, the virtual height was varying considerably. This fact is prob-

ably indicative of large fluctuations in the ionization gradients which would cause variations in the reflection coefficients. There may be interference effects due to the presence of two or more partially reflecting layers. Also there may be partial interference between the two magneto-ionic components.

In Section VI-A it was shown that the ionization density required for reflection of the extraordinary component is approximately 29.3 times that necessary for reflection of the ordinary component. With a scale height of 0.7 km, this increase in ionization corresponds to a distance of 2.36 km. This distance is nearly equal to 3 km, the half-wavelength in free space at 50 kc/s. Thus interference effects between the split components should be important. With fluctuating ionization gradients, interference between the magneto-ionic components would give rise to variations in the polarization of the sky wave. The polarization of the sky wave is considered next.

D. Polarization of the Sky Wave

The phase-angle and field-strength data of Figure 28 give all of the information which is necessary for completely describing the polarization of the down-coming wave. The polarization of the sky wave may be described in terms of an electric-polarization ellipse. Let us calculate the ellipticity of this ellipse.

The sky wave is received on crossed dipole anten-

nae. Let the voltage induced in the north-south antenna be given by

$$x = E_{NS} \cos \omega t \tag{88}$$

and let the voltage induced in the east-west antenna be given by

$$y = E_{EW} \cos (\omega t + \delta) \tag{89}$$

where south and east are the $+x$ and $+y$ directions. E_{NS}, E_{EW}, and δ are quantities which are measured in the experiment. Equations 88 and 89 are the parametric equations for an ellipse. By eliminating t in these equations, we obtain

$$\frac{x^2}{E_{NS}^2} + \frac{y^2}{E_{EW}^2} - \frac{2xy}{E_{NS}\, E_{EW}} \cos \delta = \sin^2 \delta \tag{90a}$$

or

$$E_{EW}^2 x^2 - 2(E_{EW}\, E_{NS} \cos\delta)\, xy + E_{NS}^2 y^2 = E_{EW}^2\, E_{NS}^2 \sin^2 \delta \tag{90b}$$

The term containing xy in Equation 90b can be eliminated by rotating the coordinate system through an angle ϕ, where ϕ is given by the expression

$$\phi = \tfrac{1}{2} \tan^{-1} \left(\frac{-2 E_{EW}\, E_{NS} \cos \delta}{E_{EW}^2 - E_{NS}^2} \right) \tag{91}$$

If this coordinate transformation is performed, it is easy to show that the ellipticity of the polarization ellipse is given by the equation

$$\epsilon_\ell = \left(\frac{A - \sqrt{B}}{A + \sqrt{B}} \right)^{\frac{1}{2}} \tag{92}$$

where

$$A = E_{EW}^2 + E_{NS}^2 \tag{93}$$

$$B = E_{EW}^4 - 2 E_{EW}^2 E_{NS}^2 (1 - 2\cos^2\delta) + E_{NS}^4 \tag{94}$$

The ellipticity ϵ_ℓ is defined as the ratio of the minor axis to the major axis of the ellipse. Equation 92 was used in calculating the ellipticity of the polarization ellipse. These data are shown in Figure 41.

The angle ϕ gives the orientation of the minor axis of the electric-polarization ellipse with respect to the x-y coordinate system. By referring to Figure 10, we see that Θ, the angle of the major axis with respect to the geomagnetic coordinates, is given by the expression

$$\Theta = \phi - 90° - 56° = \phi - 146° \tag{95}$$

A curve of Θ as a function of time is given in Figure 42.

Both the ellipticity and orientation of the major axis of the ellipse varied during the night. This fact is to be expected under conditions of strong splitting and fluctuating ionization gradients. However, it is interesting to note that, during most of the night, the major axis was oriented approximately either magnetic east-west or magnetic north-south.

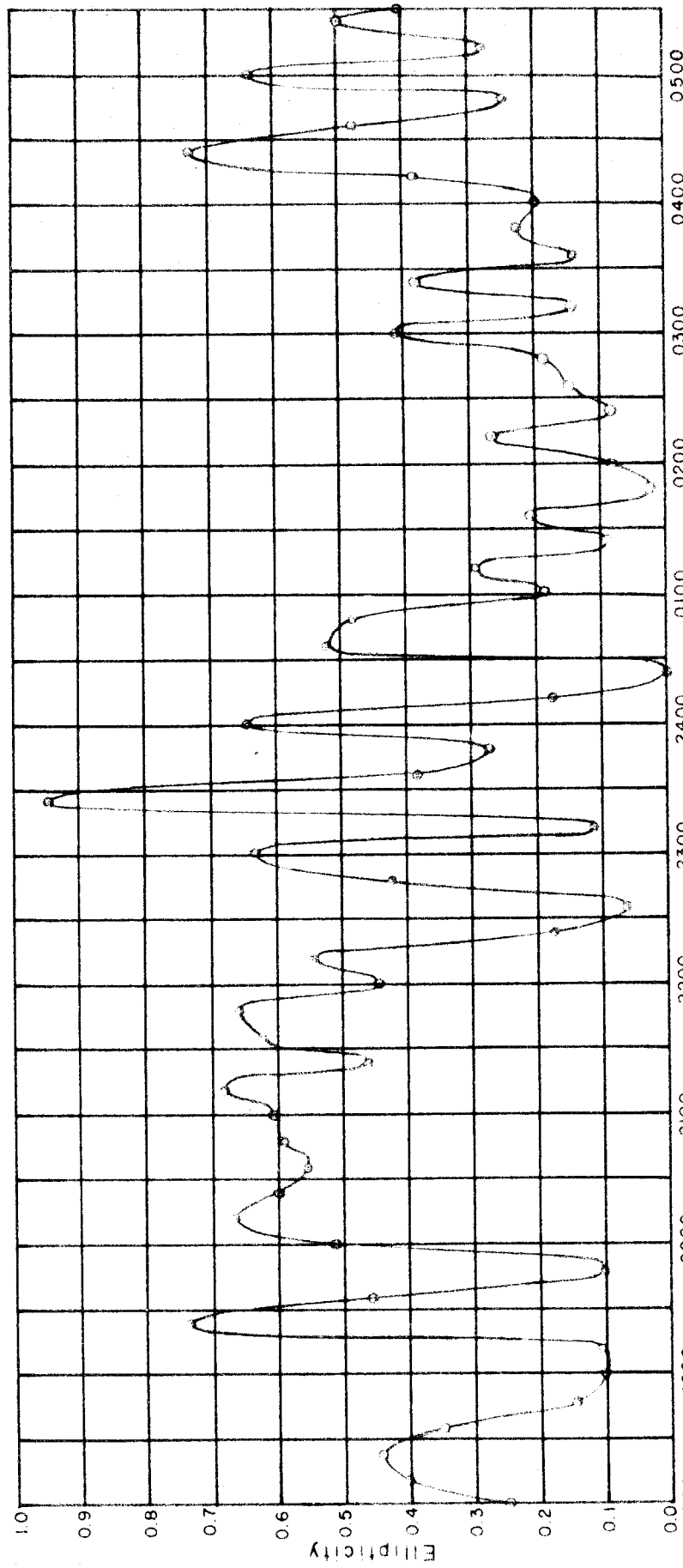

Figure 41. Ellipticity of the Polarization Ellipse October 28–29, 1952

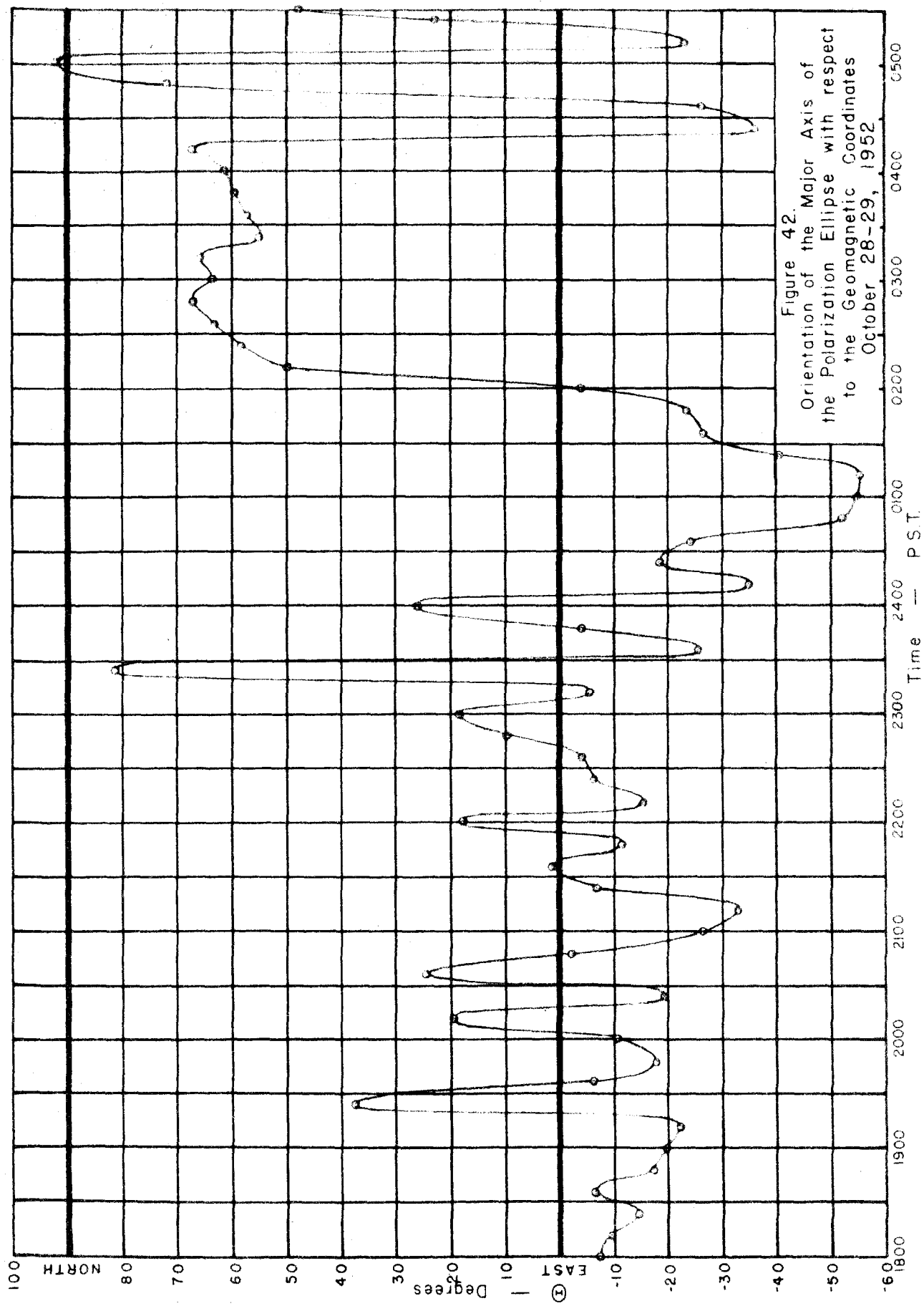

Figure 42.
Orientation of the Major Axis of the Polarization Ellipse with respect to the Geomagnetic Coordinates October 28-29, 1952

It is interesting to calculate the limiting polarization from Equation 38. The limiting polarization is the polarization that the magneto-ionic components possess on emergence from the ionosphere. A plane-polarized wave incident on the ionosphere is split into the two magneto-ionic components. These components, if they could retrace their original paths, would on emergence have the same polarization which they possessed on entry into the ionosphere. Thus the limiting polarization may be calculated by letting the ionization density N approach zero in Equation 38. With $N \longrightarrow 0$, Equation 38 becomes

$$R|_{N\to 0} = \frac{j}{\mu_v H_L}\left[\frac{\mu_v^2 H_T^2}{\left(-\frac{\omega m}{e} + j\frac{m\upsilon}{e}\right)} \pm \sqrt{\frac{\mu_v^4 H_T^4}{\left(-\frac{\omega m}{e} + j\frac{\omega\nu}{e}\right)^2} + \mu_v^2 H_L^2}\right] \qquad (96)$$

By substituting in Equation 96 the values

$H_L = 0.44$ gauss

$H_T = 0.25$ gauss

$\upsilon = 1.56 \times 10^6$ per second (electronic collisional frequency for nighttime at 90 km)

$\omega = \pi \times 10^5$ radians/sec

we obtain for the ordinary wave

$$R_O\Big|_{N=0} = 0.794\, e^{-j\,138.4} \qquad (97)$$

and for the extraordinary wave

$$R_X\Big|_{N=0} = 1.26\, e^{+j\,138.4} \qquad (98)$$

If the collisions of the electrons with other particles are neglected, we obtain for the ordinary wave

$$R_O\Big|_{\substack{N=0\\ \nu=0}} = 0.124\, e^{-j\,90} \tag{99}$$

and for the extraordinary wave

$$R_X\Big|_{\substack{N=0\\ \nu=0}} = 8.06\, e^{+j\,90} \tag{100}$$

Equations 99 and 100 show that, in the absence of collisions, the ordinary wave is elliptically polarized with the major axis of the electric polarization ellipse magnetic north-south, and the extraordinary wave is elliptically polarized with the major axis of the electric polarization ellipse magnetic east-west. As a result of the electron collisions, the ellipticity of the polarization ellipses is increased, and the major axes are rotated symmetrically toward the northeast-southwest direction. By referring to Equation 91, we find that the major axes are rotated through an angle of 36.4^{o}.

It is somewhat difficult to interpret the polarization data of Figure 42, because the two magneto-ionic components cannot be separated. At any time the two components add together, or partially interfere with one another, to give the resultant signal. However, the data seem to indicate that the ordinary and extraordinary ellipses are symmetric about the north-south direction. This result is not in agreement with the predictions of the quasi-homogeneous, magneto-ionic theory, but it is in agreement with Morgan's observations (Ref. 28) at high frequencies (2.8 to 6.6 mc/s).

VIII. PROPOSALS FOR FURTHER RESEARCH

The work that has been accomplished has demonstrated the value and flexibility of our new technique for studying the ionosphere at low frequencies. We have shown that the ground antenna operates as predicted. This antenna has high radiation efficiency; it is easy and inexpensive to construct; it is resonant and readily tunable; and it has an ideal radiation pattern for vertical-incidence ionospheric studies. It should be profitable to carry out both theoretical and experimental work to determine whether or not some antenna of this general nature would be useful for low-frequency communication purposes.

In Northern Canada there is a great need for dependable communication systems. High-frequency and very-high-frequency sky-wave propagation is unreliable, because at these high latitudes there is insufficient ionization in the upper atmosphere. Since most of the atmospheric noise originates in the tropical latitudes, the low-frequency radio noise level is very low. Thus low-frequency, ground-wave propagation should provide a most satisfactory means of communication. Conventional low-frequency antenna systems have the disadvantage of being expensive to construct. Our ground-dipole antenna radiates a large ground-wave field. Thus a ground dipole or some modification of it might prove very satisfactory for communication purposes in northern lati-

tudes.

Ground antennae should be useful in oblique-incidence ionospheric studies. The present antenna radiates the major part of its energy vertically upward, a fact which is ideal for vertical-incidence experiments. However, for oblique-incidence experiments, the radiation should be at a moderate angle with the horizon. This type of radiation pattern may be achieved by using an array of two parallel dipole antennae or by arranging the antennae in the form of a resonant loop. As a result of the interest expressed by the Air Force Cambridge Research Center, we are considering the making of some oblique-incidence measurements. These experiments would be conducted jointly with Helliwell. For these studies, it is proposed to transmit a low-frequency signal between Palo Alto, California, and our desert site. It is expected that this work would provide valuable information regarding the nature and structure of the lower regions of the ionosphere.

It is difficult to draw any definite conclusions from the 50-kc/s data we have taken, because, statistically, they cannot be regarded as typical or representative. More of the same type of data should be taken both at 50 kc/s and at lower frequencies. The system should be calibrated so that absolute measurements of virtual height and reflection coefficients could be made. It would be of interest to attempt to correlate very-low-frequency ionospheric data with terrestrial magnetic activity and the occurrence of solar flares. The Mount Wilson Laboratories have expressed

a desire to cooperate in this type of program.

With a moderate amount of additional equipment, the transmitting antenna could be pulsed. It would be of great interest to compare pulse data and continuous-wave data taken under the same conditions and during the same periods of time.

There are no simple methods for separating the two magneto-ionic wave components at the receiving site. However, the polarization of the transmitted signal could be controlled at the transmitter. It is proposed to use crossed transmitting dipoles. By controlling the phase and amplitudes of the currents in the dipoles, either a signal polarized in a manner similar to that of the ordinary component or the extraordinary component could be transmitted. The data obtained would be for the purpose of attempting to understand more fully the mechanism of the interaction of low- and very-low-frequency radio waves with the ionosphere.

The experiments mentioned are but a few of the many that could be performed. Ground antennae and the system described have many outstanding features for use in ionospheric research. It is expected that a continuation of the research program will result in valuable contributions to the fields of ionospheric physics and radio propagation.

REFERENCES

1. Mitra, S. K., "The Upper Atmosphere," 2nd ed., Calcutta, India: The Asiatic Society (1952).

2. Gerson, N. C., and R. J. Donaldson, Proceedings of the Conference on Ionospheric Physics, Geophysical Research Papers (No. 11), Cambridge, Massachusetts: Air Force Cambridge Research Center (July, 1950).

3. Fleming, J. A., "Terrestrial Magnetism and Electricity," New York: Dover Publications, Inc. (1949).

4. Sheppard, P. A., Science Progress, vol. 37, p. 488 (1949).

5. White, F. W. G., "Electromagnetic Waves," 4th ed., New York: John Wiley & Sons, Inc. (1950).

6. Helliwell, R. A., Unpublished lecture notes for a series of lectures given at Stanford University, Stanford, California.

7. Chapman, F. W., Proceedings of the Physical Society of London, vol. 44, p. 246 (1932).

8. Appleton, E. V., "Wireless Studies of the Ionosphere," Journal of the Institution of Electrical Engineers, p. 642 (1932).

9. Mitra, S. K., J. N. Bahr, and S. P. Ghosh, Indian Journal of Physics, vol. 12, p. 455 (1938).

10. Nicolet, M., Mixed Commission on the Ionosphere, Brussels, Belgium: International Scientific Radio Union, p. 50 (1948).

11. Budden, K. G., J. A. Ratcliffe, and M. V. Wilkes, Proceedings of the Royal Society, vol. A-171, p. 188 (1939).

12. Mitra, A. P., "The D-Layer of the Ionosphere," Journal of Geophysical Research, vol. 56 (No. 3), pp. 373-402 (1951).

13. Nicolet, M., Journal of Geophysical Research, vol. 54, p. 373 (1949).

14. George, E. F., "Electronic Collisional Frequency in the Upper Atmosphere," Proceedings of the Institute of Radio Engineers, vol. 35, pp. 249-252 (1947).

15. Sommerfeld, A., and F. Renner, "Strahlungsenergie und Erde Absorption bei Dipole Antennen," Annalen der Physik, vol. 41 (No. 1), pp. 1-36 (1942).

16. Sommerfeld, A., "Partial Differential Equations in Physics," New York: Academic Press Inc. (1949).

17. Hertz, "Die Krafte elektrischer Schwingungen," Collected Works II, p. 147.

18. Booker, H. G., "Some General Properties of the Formulae of the Magneto-Ionic Theory," Proceedings of the Royal Society, vol. 147, pp. 325-382 (1934).

19. Helliwell, R. A., A. J. Mallinckrodt, F. W. Kruse, and B. A. Wambsganss, Pulse Studies of the Ionosphere at Low Frequencies, Stanford, California: Stanford University, Electronics Research Laboratory (March, 1950).

20. Mott, N. F., "Elements of Wave Mechanics," Cambridge at the University Press (1952).

21. Eckersley, T. L., Proceedings of the Physical Society of London, vol. B-63, p. 49 (1950).

22. Booker, H. G., Proceedings of the Royal Society, vol. A-155, p. 235 (1936).

23. Försterling, H., Hochfrequenz und Elektrotechnik, vol. 59, p. 10 (1942).

24. Wilkes, M. V., Proceedings of the Royal Society, vol. A-189, p. 130 (1947).

25. Feinstein, J., "Ionospheric Wave Propagation at Low Frequencies," IXth General Assembly, Document A. G. 1950/No. 60/Commission III, Zurich, Switzerland: International Scientific Radio Union (1950).

26. Helliwell, R. A., A. J. Mallinckrodt, et al., Interim Progress Report, Ionospheric Research, Stanford, California: Stanford University, Electronics Research Laboratory (March, 1951).

27. Hutchinson, H. P., "Short Period Sky-Wave Fading of CW Emissions," Transactions of the Institute of Radio Engineers, Professional Group on Antennas and Propagation (No. 3), pp. 12-18 (1952).

28. Morgan, M. G., "Polarization Observations at Dartmouth College, with Twin-Channel Transmitting and Receiving Equipment, of HF Ionospherically Reflected Pulse Signals at Vertical Incidence," Paper presented at the joint meeting of the International Scientific Radio Union and the Institute of Radio Engineers. Washington, D. C. (April, 1953).

APPENDIX

Electronic Circuit Diagrams for the Transmitting and Receiving Equipment

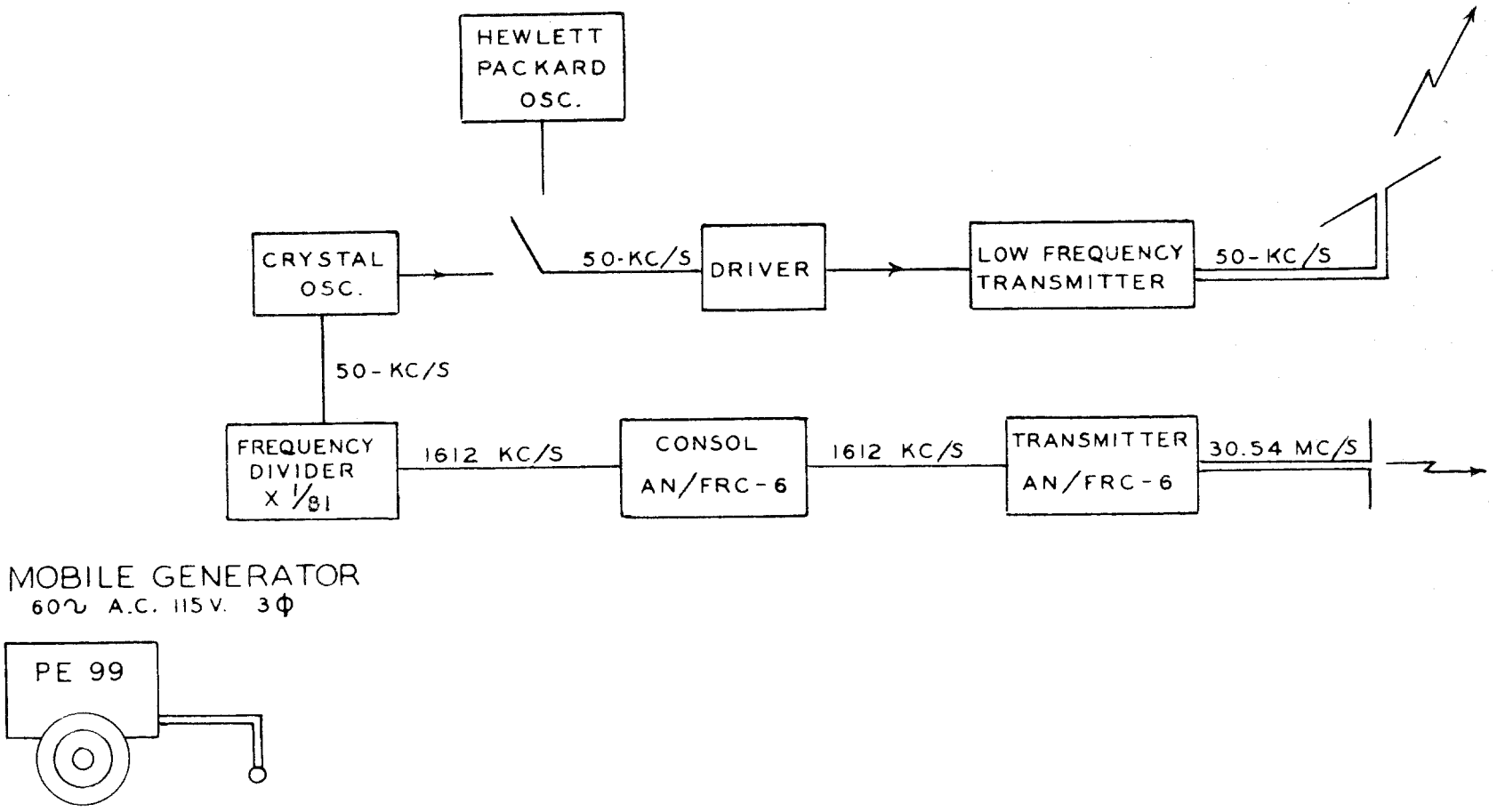

FIGURE 43.

BLOCK DIAGRAM OF TRANSMITTING STATION.

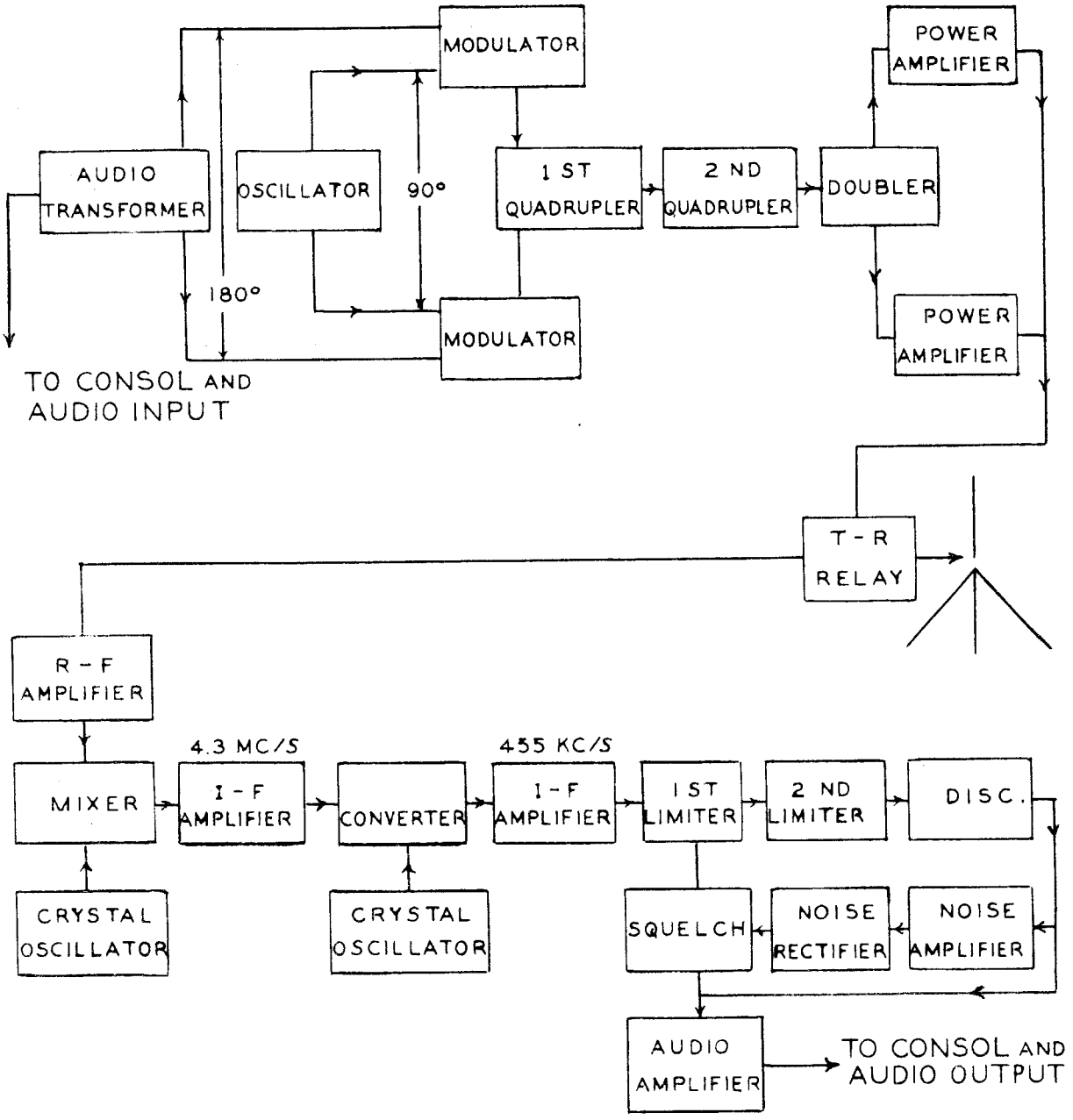

FIGURE 44.

BLOCK DIAGRAM OF AN/FRC-6 30-Mc/s FM TRANSMITTER.

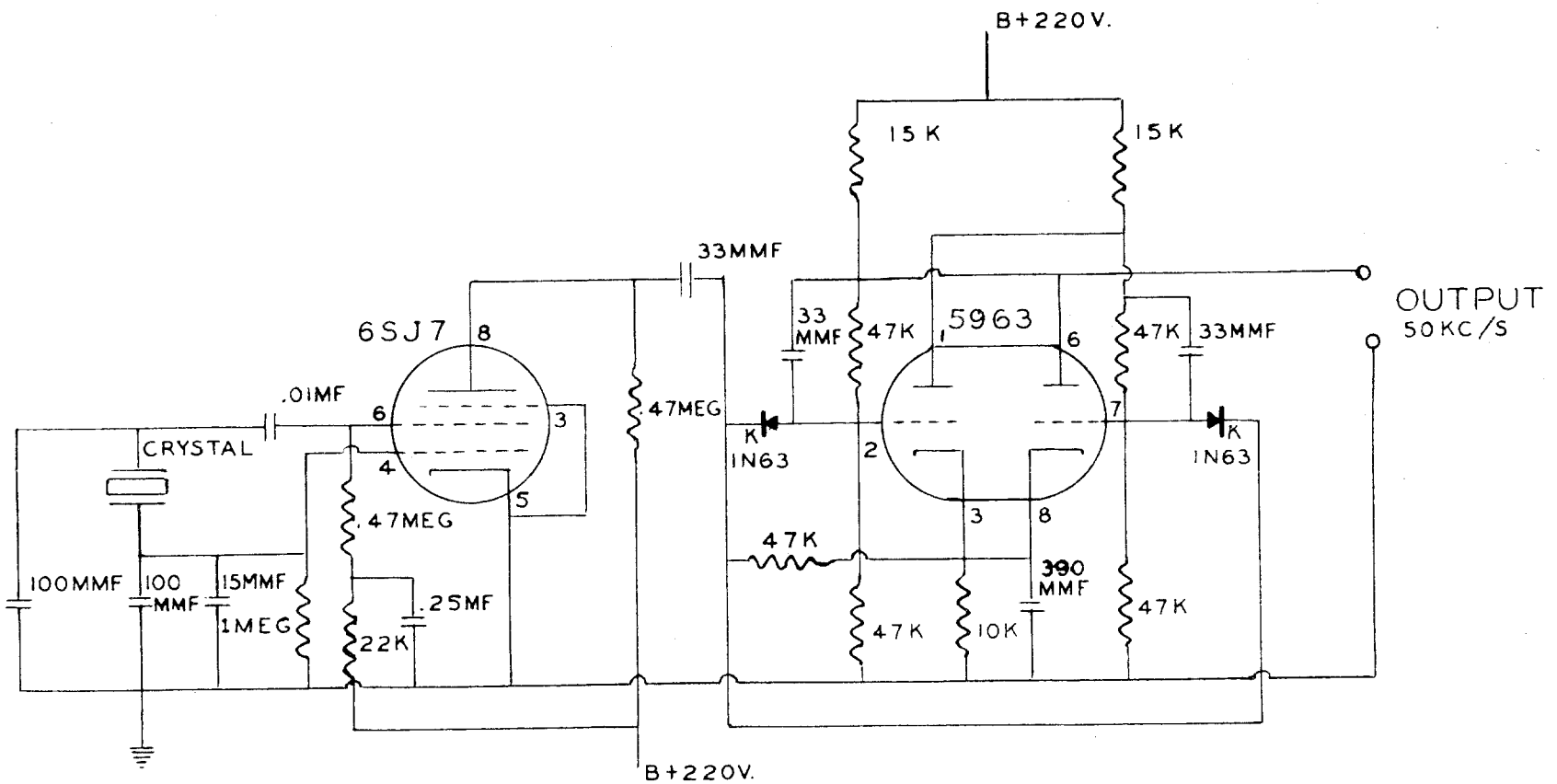

FIGURE 45.

100-KC/S CRYSTAL OSCILLATOR AND SCALER CIRCUIT.

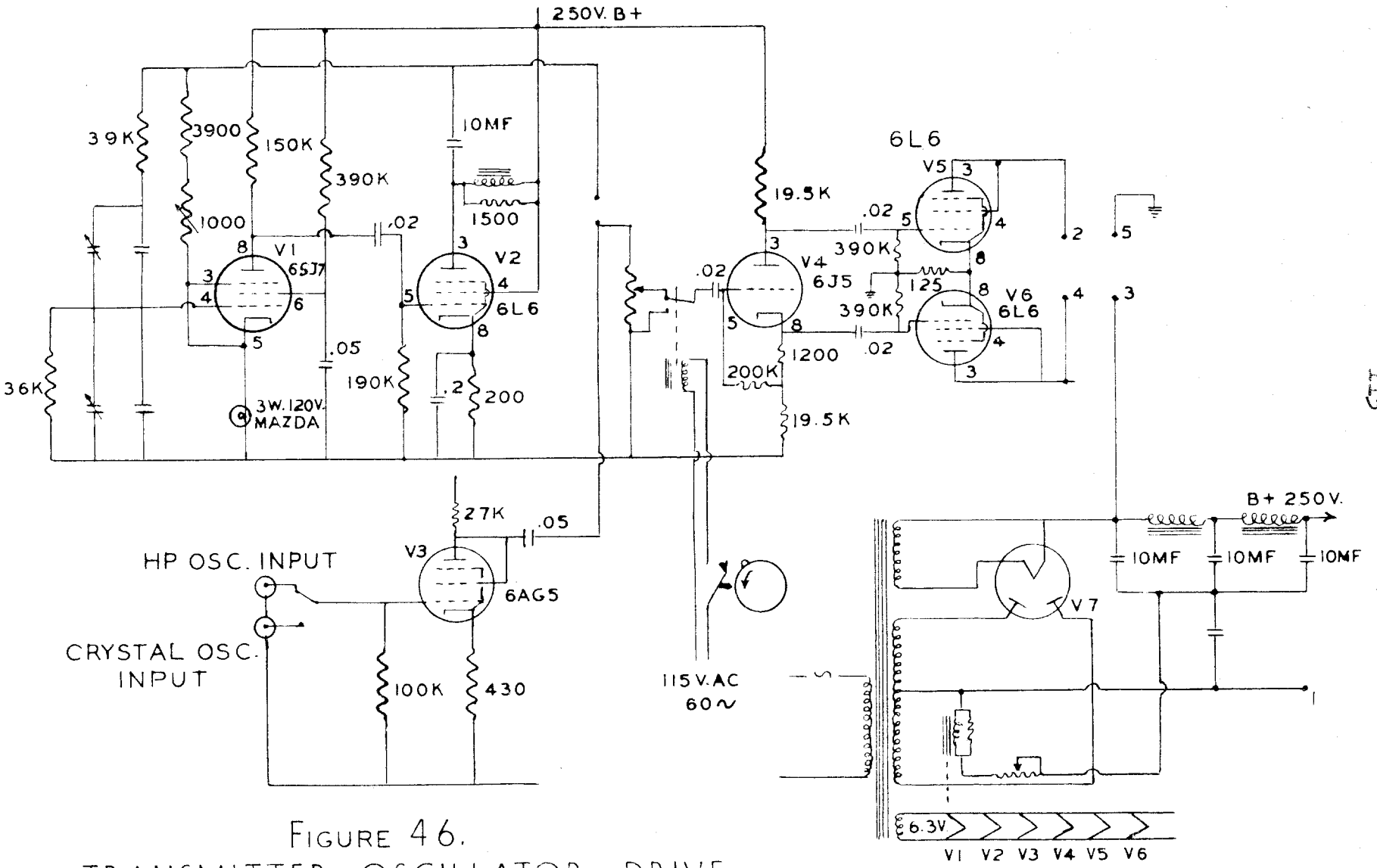

FIGURE 46.

TRANSMITTER OSCILLATOR DRIVE.

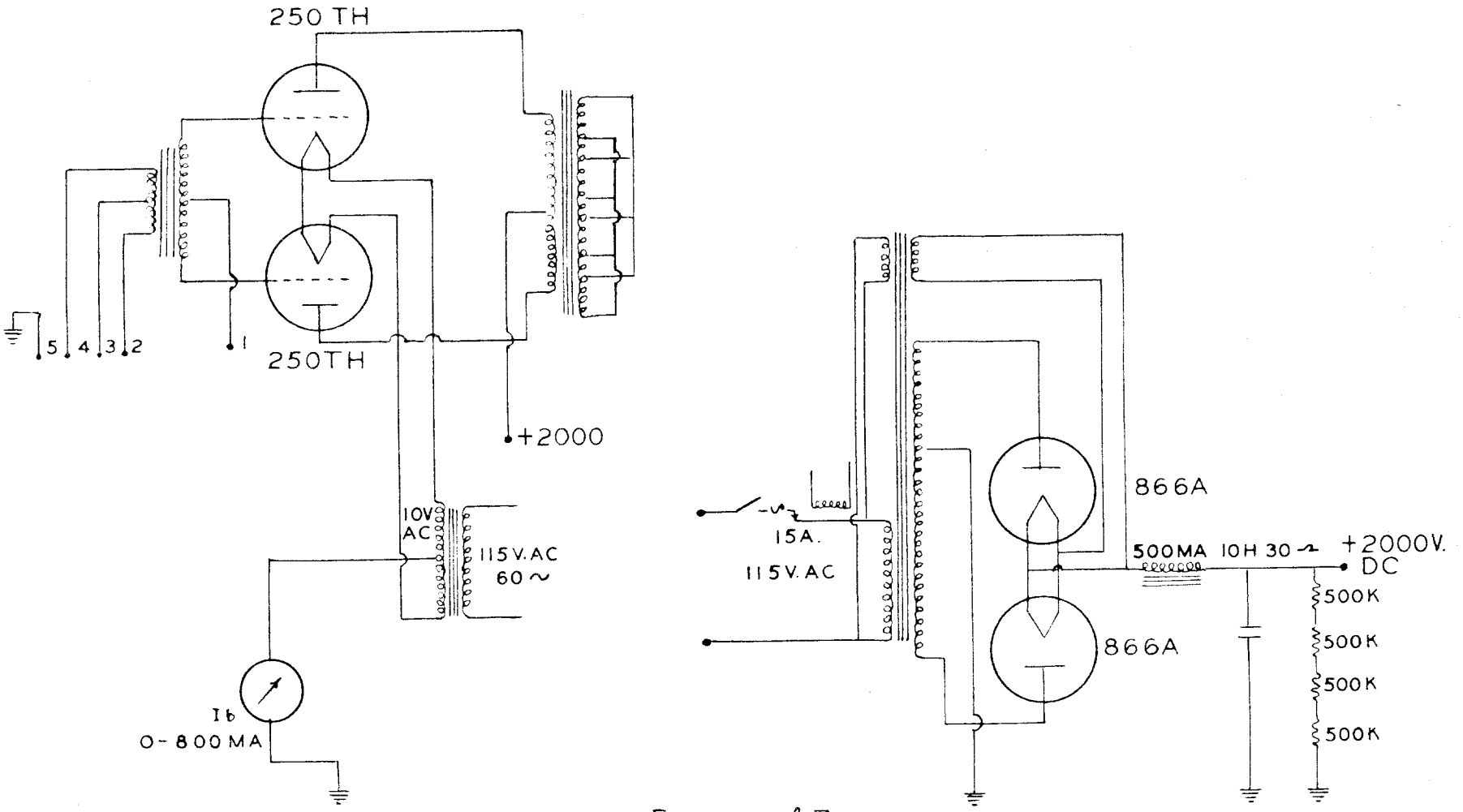

FIGURE 47.

50-KC/S TRANSMITTER OUTPUT STAGE AND HIGH VOLTAGE POWER SUPPLY.

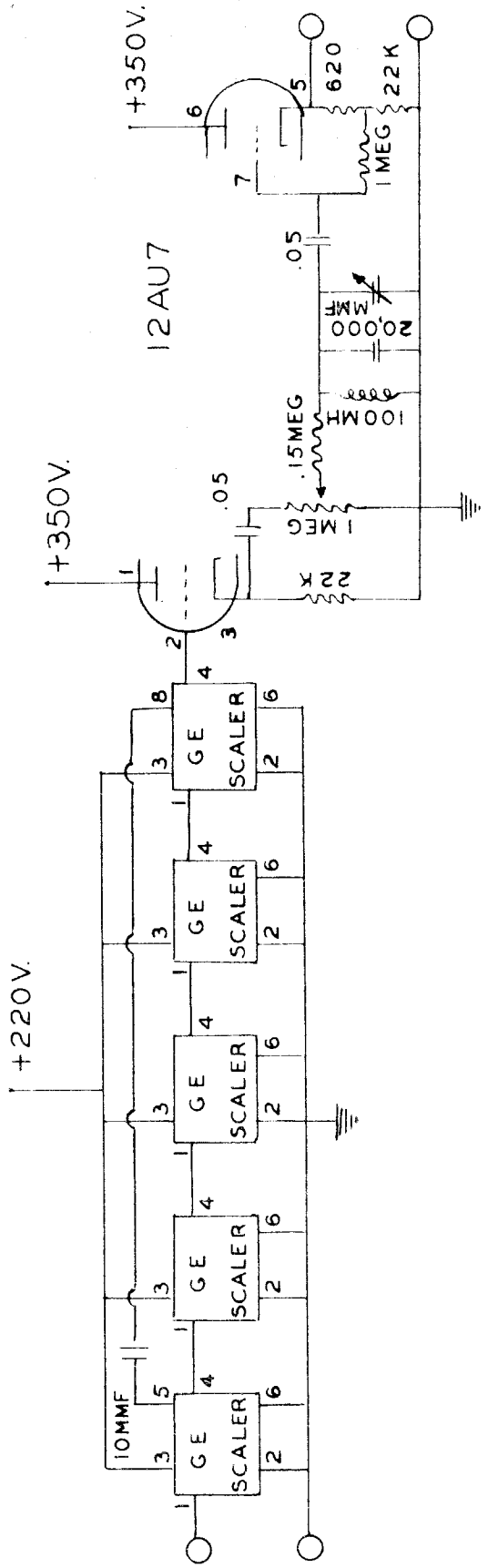

FIGURE 48.

FREQUENCY DIVIDING CIRCUIT.

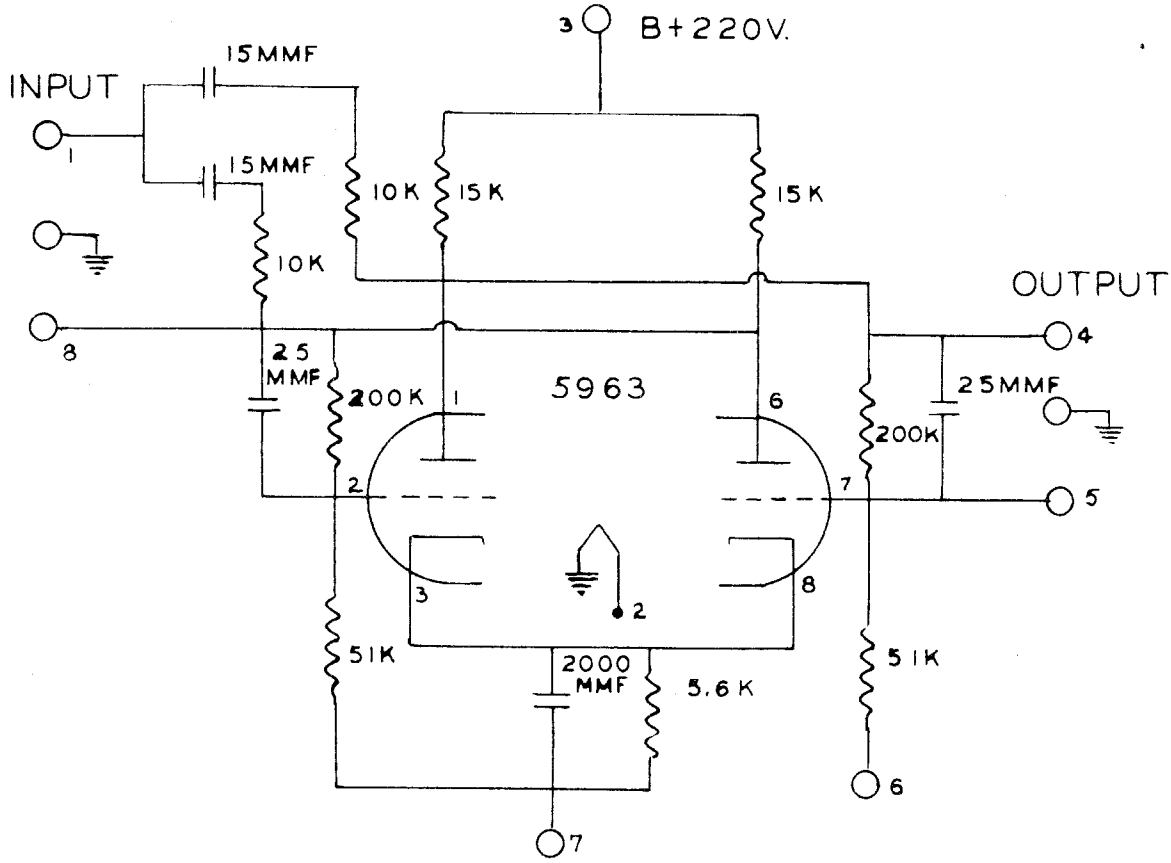

FIGURE 49.
G.E. BINARY SCALER.

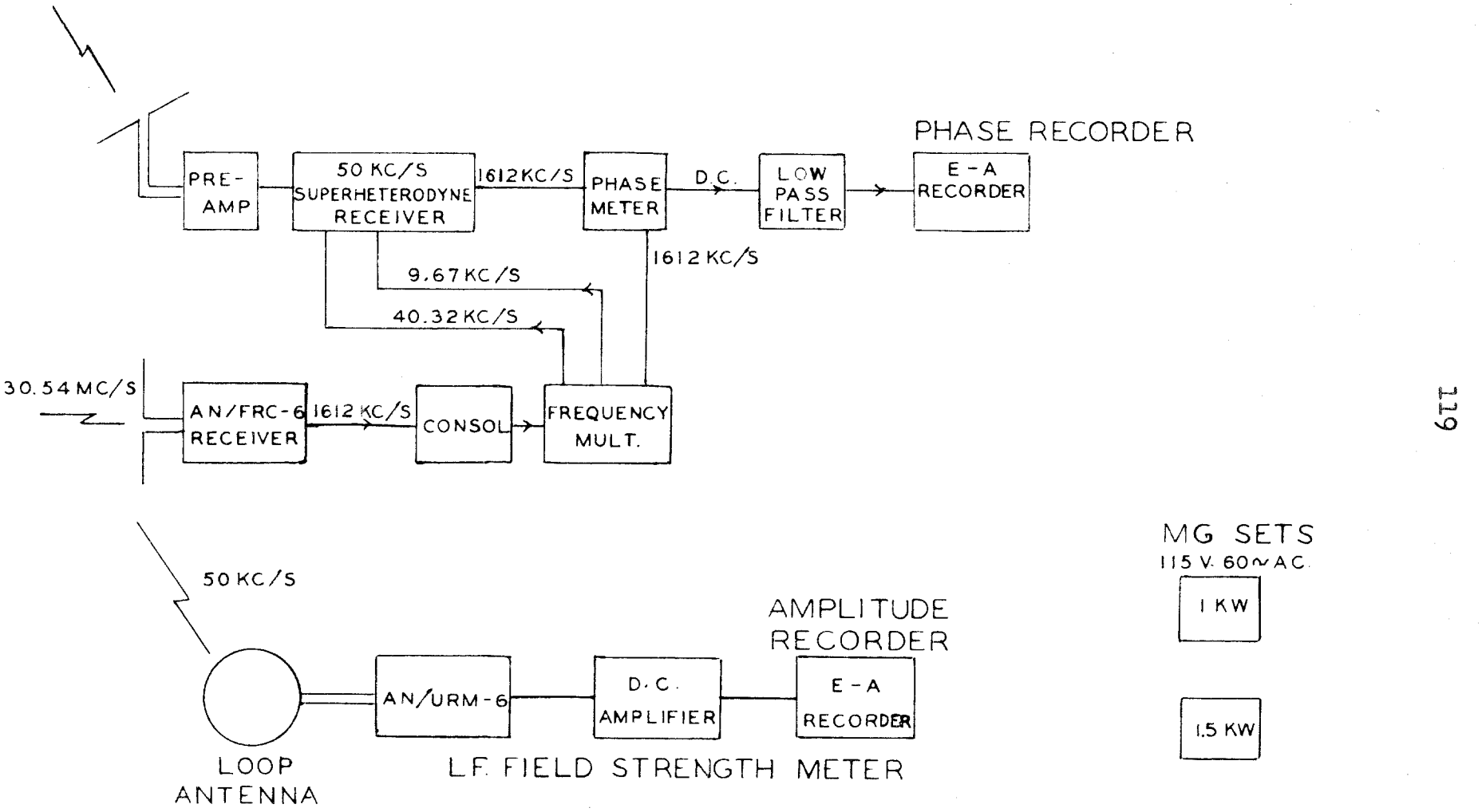

FIGURE 50.

BLOCK DIAGRAM OF RECEIVING STATION.

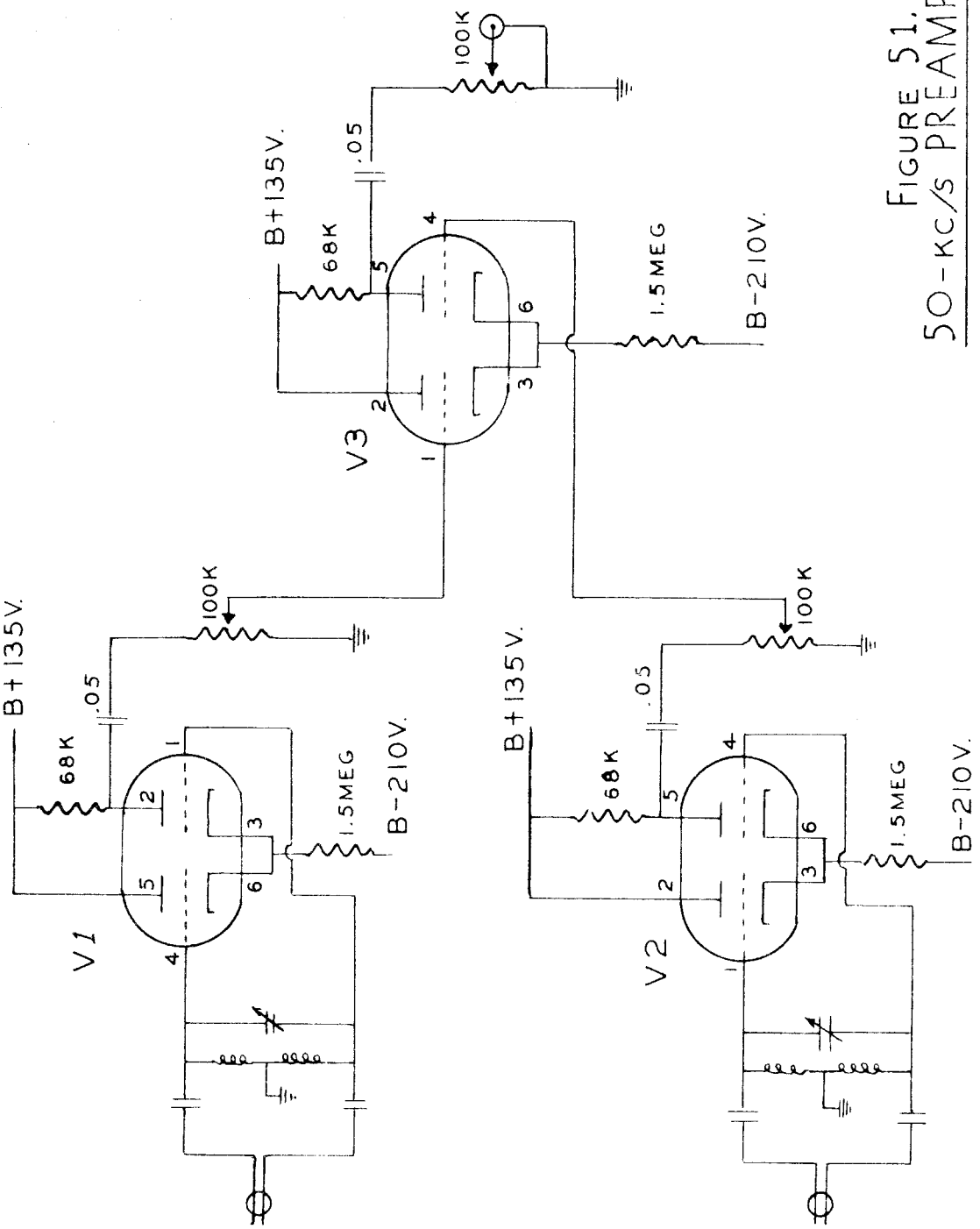

FIGURE 51.
50-KC/S PREAMPLIFIER.

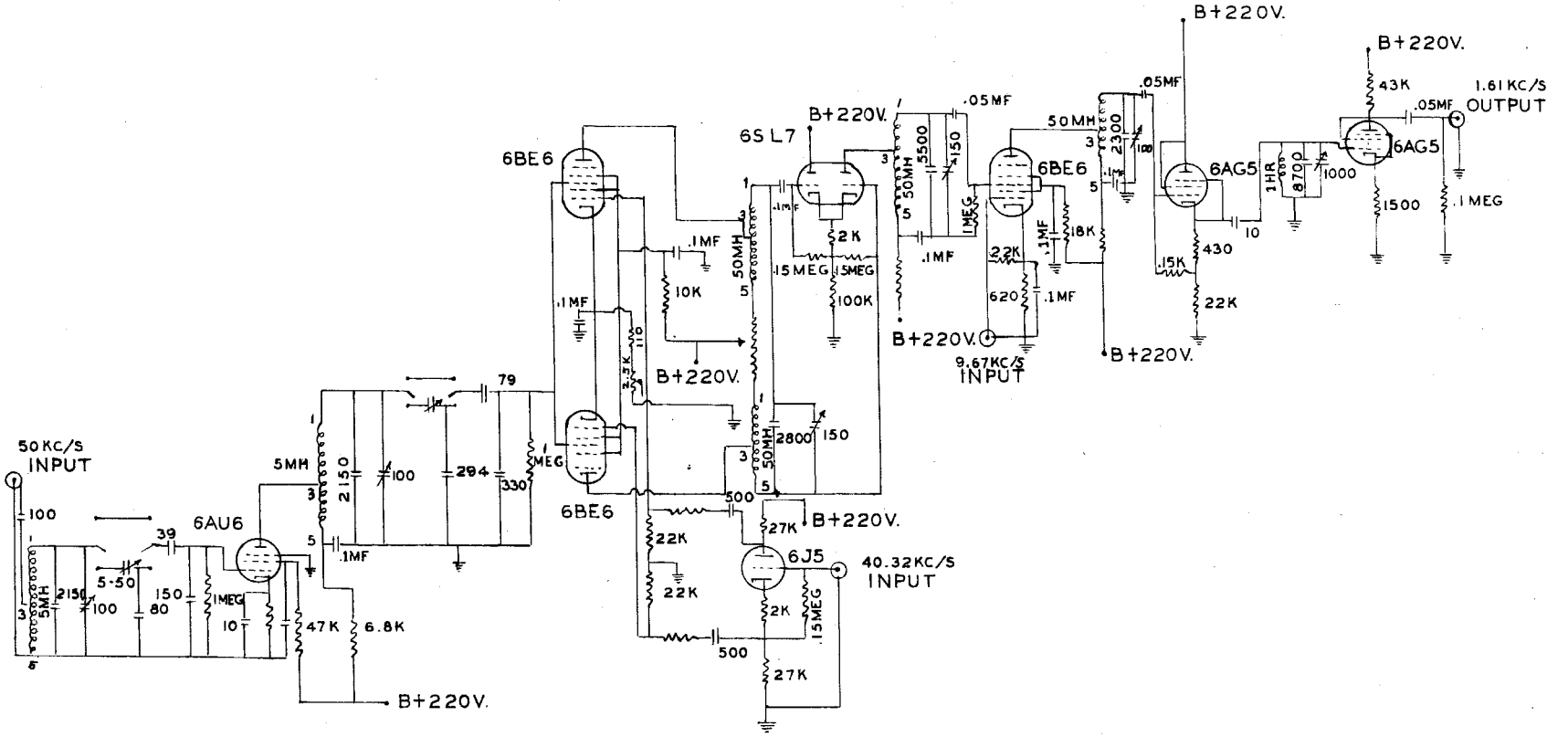

FIGURE 52.

50-KC/S SUPERHETERODYNE RECEIVER.

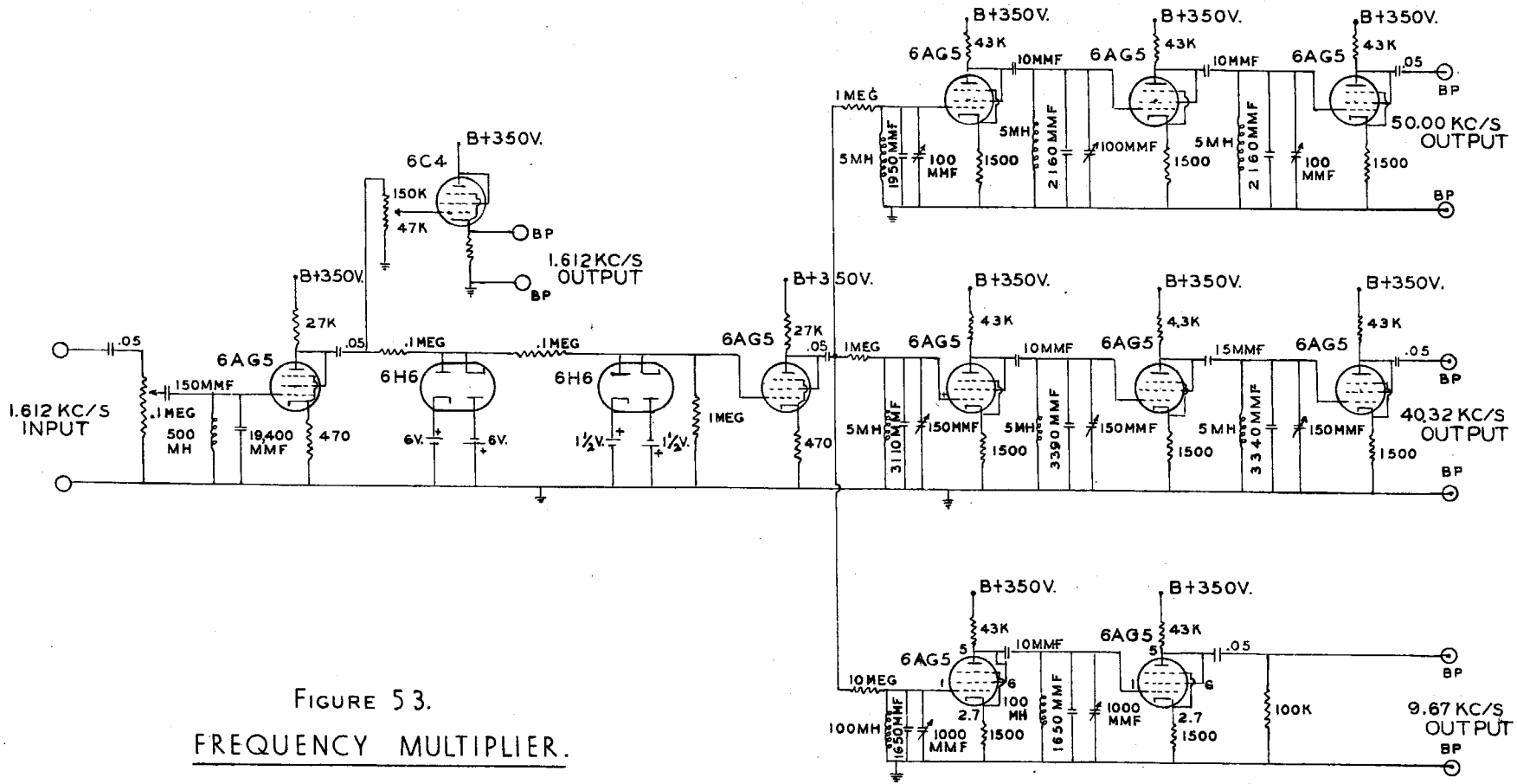

FIGURE 53.

FREQUENCY MULTIPLIER.